Investigation of Composites of Carbon Black and Metallocycles, and Functionalized Transition-Metal Nanoparticles as Chemiresistive Vapor Sensors

Thesis by

Edgardo García-Berríos

In Partial Fulfillment of the Requirements

for the Degree of

Doctor of Philosophy

California Institute of Technology

Pasadena, California

2011

(Defended May 23, 2011)

A María, Edgardo, Enid, Zulma, Tregenna, Sarah y Carmela.

Acknowledgments

Thank you Tregenna for all your support and care. I must thank my parents María and Edgardo, who taught me how to be respectful, disciplined and committed, among many other values. From baseball to science, after been accepted to Caltech, I will always remember my parents words, "*Who knows if you could make it to the Major Leagues of Baseball, but what we do know is that you made it to the Major Leagues of Science!*". My sisters, Enid and Zulma, show me how to be loyal and to love unconditionally. Thank you Zulma for showing me the field of chemistry. I must thank my friends Rafi, Poma, Jimmy, Fufi, Juanmi, Michael and Pica for 22 years (and counting!) of support, and to my California family, Jehoshua ("*Shuki*"), Anat, Gal, Or, Marc, Andrew, Manuel, Juanse, Luca, Samuel, Dani, Victor and Ubaldo.

I would like to thank my advisor, Prof. Nathan S. Lewis, for giving me the opportunity to be part of his research group and to allow me to expand my knowledge to other scientific areas. I also would like to thank Dr. Bruce Brunschwig for constantly being there to answer silly questions and correcting thoughts. I also must extend thanks to my thesis committee, Prof. Harry B. Gray, Prof. Sarah Reisman and Prof. John Bercaw.

Many people have helped me in a great variety of ways, and I would like to render my heartfelt thanks to the following people: Dr. Marc Woodka, Prof. Stephen Maldonado, Dr. Ting Gao, Dr. Brian Sisk, Dr. Anna B. Folinsky, Heather McCaig, Jordan C. Theriot, Dr. Don Walker, Nathan O. Hodas, Jean Li, José L. Mendoza, Chad Schmutzer, Dr. Brian Leigh, Dr. Ricardo Moncho, Dr. Cristina de Zan, Sue Chiarchiaro, Felicia Hunt, Prof. Wilfredo Otaño, Prof. Raúl Castro, and Prof. John N. DiNardo.

Abstract

An electronic nose is a man-made implementation of an olfactory system that is comprised of an array of broadly cross-reactive sensors. Electronic noses are used in the food industry, environmental monitoring, explosive detection and medical diagnosis. Our laboratory has focused in the development and implementation of arrays of low power, inexpensive chemiresistive thin films, that are able to identify and quantify a diverse collection of vapors and mixtures of vapors. Novel bioinspired sensors, and array chamber architectures are constantly been developed and improved to fulfill the desired performance of such arrays in different applications. This work details the development and the sensing performance of novel sensor materials based on composites of carbon black and metalloporphyrins, and organically-functionalized gold (Au) and titanium (IV) dioxide (TiO_2) nanoparticles.

Composites of carbon black and metalloporphyrin complexes were developed and optimized to sensitively detect and classify a series of organic vapors. Such sensors films also exhibited a high sensitivity towards trace levels of ammonia (NH_3(g)) and 2,4,6-trinitrotoluene (TNT) in air. Such composites thus broaden the types of materials that can be used for this type of low-power chemiresistive vapor sensing, and broaden the types of analytes that can be sensitively detected to include inorganic gases and explosives, as well as organic vapors.

Au and TiO_2 nanoparticles were synthesized and functionalized with a variety of ligands. These materials allowed for molecular control of the interparticle physicochemical properties such as electron transfer. Details about the performance of each unique functionalized Au or TiO_2 nanoparticle film upon exposure to a variety of organic vapors was described as a function of ligand length, structure and other physicochemical properties. The discrimination performance for arrays of such sensors was also evaluated.

Contents

List of Figures

List of Tables

Chapter 1

Introduction

1.1 Electronic Noses

No man-made sensor array system combines the low-power, rapid response, sensitivity, selectivity and ability to track an odorant to its source that is characteristic of the olfactory system of a canine. Mammals contain a broad class of trans-membrane receptors called G-protein-coupled receptors (GPCRs) that are used in many physiological processes, such as visual transduction, hormonal regulation, and stimulation and inhibition of various processes.[1] The mammalian genome possess approximately 1,000 olfactory receptor genes that are part of the broader GPCRs class.[2] These genes can encode up to 1,000 different functional odor receptors and are able to detect over 10,000 different odors. Thus, such receptors must be broadly cross responsive, which means that a each receptor can be triggered by more than one odorant, and an odorant, in turn, will produce a response from more than one receptor.[3] These olfactory receptors produce a response pattern to the brain, where such response pattern is used to identify, classify, and quantify the odor of interest.

Bioinspired man-made artificial olfactory systems, often called electronic noses, also perform vapor detection through use of an array of cross responsive sensors, and in con-

junction with pattern recognition methods, they are able to identify, classify, and quantify vapors.[4] The difference among existent electronic noses, is the transduction mechanism performed. Sensor modalities include surface acoustic wave devices,[5] bulk resonating quartz crystal devices,[6] conducting polymers,[7] polymeric coated capacitors,[8] semiconducting metal oxide resistors,[9] and transistors.[10] Pattern recognition algorithms include statistically-based methods, such as principal component analysis, neural-network-based methods and linear discriminants.[11]

Our approach utilizes composites comprised of insulating organic materials such as polymers or non-polymeric/non-volatile organic molecules and conducting particles such as carbon black (CB).[12] When a vapor of interest is presented to the composite sensor, the analyte is sorbed into the insulating organic matrix, producing a volume increase or swelling of the film. The sorption-induced swelling increases the dc resistance of the film, providing a low-power method for transducing the presence of an analyte into a readily detectable electrical signal. An array of such sensors, each containing a chemically different insulating matrix and a common conducting phase, produces a response fingerprint that used for identification, classification, and quantification of various analytes. Physicochemical properties of the analyte such as molecular structure, molecular weight, volume, dipole moment and polarity are able to induce differentiable response signatures for different analytes.

Like the human nose, the electronic nose devices are change-detection systems and cannot readily break down a complex mixture (i.e., wine) into its hundreds of different chemical components. However, arrays of broadly cross-reactive sensors can readily probe

changes in complex analyte mixtures either over time or over a collection of samples. Accordingly, such sensor arrays are well-mated to probing time-dependent changes in the environment, such as in the cabin air of the U. S. Space Shuttle, or for use in quality control applications in the food, beverage, chemical, and medical industries. Novel bioinspired sensor materials and array chamber architectures are constantly been developed and improved to fulfill the desired performance of such arrays for such different applications.

The development of materials with a wide range detection capability is of interest. This work presents the development of two novel sensor materials, and details about their transduction mechanism are explored in response to multiple vapors with different physicochemical properties. The development and sensing performance of composites of CB and metalloporhyrins is described. Such materials allowed for the detection of organic vapors, inorganic gases and explosives. A second class of sensor materials comprised of organic ligand-functionalized gold (Au) and titanium (IV) dioxide (TiO_2) nanoparticles is studied. The transduction mechanism of such functionalized metal nanoparticles is described as a function of ligand length and polarity in response to a library of organic vapors.

1.2 Thesis Outline

1.2.1 Composites of Carbon Black and Metalloporphyrins

This work details the development and the sensing performance of sensor films comprised of composites of CB and metalloporhyrins (Chapters 2 and 3). Composites of CB and metalloporphyrin complexes were developed and optimized to sensitively detect and classify a

series of organic vapors, trace levels of NH_3(g) (Chapters 2 and 3) and 2,4,6-trinitrotoluene in air (Chapter 3), without the use of an electric bias or elevated temperatures. With this sensor design, metalloporphyrin-based CB composite sensors function as conventional sorption chemiresistors for the detection and discrimination of various organic vapors. This work highlights the pertinent features of the metalloporphyrin/CB signal transduction modes, demonstrating that these sensors are capable of both volumetric expansion and adsorptive conductance changes because the CB fraction, rather than the metalloporphyrin fraction, supports the film conductance. The findings reported here expand the potential applications for inexpensive composite thin-film chemiresistor arrays.

1.2.2 Functionalized Transition Metal Nanoparticles

Information about the transduction mechanism of CB-based chemiresistive sensors is limited due to the wide size distribution of the CB particles, and the inability to describe the degree of swelling between CB particles and/or organic matrix upon exposure to a chemical vapor. Such lack of information thus limits the ability to optimize the performance, and fine tune the selectivity and sensitivity of such sensor films at the molecular level. This work explores the development of composite films comprised of transition metal nanoparticles functionalized with organic ligands such as organothiol-capped Au nanoparticles and carboxylate-capped TiO_2 nanoparticles. The synthetic procedure for the development of such materials allows for control of the metal core size and the chemical functionality of the passivating self-assembled monolayer. Thus, such procedure allows for control over the interparticle physicochemical properties such as electron transfer.

This work investigates the effect of changing the length of the nanoparticle organic ligands on the performance of such films as chemical vapor sensors by investigating the response sensitivity to a variety of vapors (Chapters 4 and 6). This work also investigates the influence of the physicochemical properties of sorbed analyte on the relative differential resistance response of the nanoparticle film (Chapters 4, 5 and 6). The discrimination performance of arrays of such sensor films has been evaluated in response to a variety of test vapors (Chapters 5 and 6). The analytes were chosen to have similar physicochemical properties, because vapor classification becomes more difficult as the vapor properties become increasingly mutually similar. Vapor discrimination was also evaluated as a function of the array size (i.e., number of sensors) and the average sensitivity of the array (Chapter 5). The discrimination analysis was explored using principal components analysis to visualize the array response clustering, and using Fishers linear discriminant to determine the resolution factor of binary combination of analyte responses.

Bibliography

[1] Stryer, L.; Bourne, H. R. *Annu. Rev. Cell Biol.* **1986**, *2*, 391–419.

[2] Buck, L.; Axel, R. *Cell* **1991**, *65*(1), 175–187.

[3] Axel, R. *Sci. Am.* **1995**, *273*(4), 154–159.

[4] Lewis, N. S. *Acc. Chem. Res.* **2004**, *37*(9), 663–672.

[5] Wohltjen, H.; Dessey, R. *Anal. Chem.* **1979**, *51*(9), 1458–1470.

[6] Janghorb.M.; Freund, H. *Anal. Chem.* **1973**, *45*(2), 325–332.

[7] Talaie, A.; Romagnoli, J. *Iran. Polym. J.* **1997**, *6*(1), 53–61.

[8] Ozturk, Z. Z.; Zhou, R.; Ahsen, V.; Bekaroglu, O.; Gopel, W. *Sens. Actuators B* **1996**, *36*(1-3), 404–408.

[9] Vlasov, Y. G. *Microchim. Acta* **1991**, *2*(1-6), 363–77.

[10] Sundgren, H.; Lundstrom, I.; Winquist, F.; Lukkari, I.; Carlsson, R.; Wold, S. *Sens. Actuators B* **1990**, *B2*(2), 115–23.

[11] Duda, R.; Hart, P. *Pattern Classification and Scene Analysis;* John Wiley Sons: New York, 1973.

[12] Freund, M. S.; Lewis, N. S. *Proc. Natl. Acad. Sci. U.S.A.* **1995**, *92*(7), 2652–2656.

Chapter 2

Detection of Organic Vapors and NH_3(g) Using Thin Film Chemiresistive Composites of Carbon Black and Metallophthalocyanines

2.1 Abstract

Thin-film chemiresistive vapor sensors have been fabricated using composites of carbon black (CB) and metallophthalocyanines. The resulting sensors exhibited large, rapid, and reversible relative differential resistance changes upon exposure to a series of test organic vapors. The individual sensor responses, and collective sensor array properties for classification of a series of test organic vapors, were comparable to those of chemiresistor arrays made from composites of conductors and insulating organic polymers. In addition to displaying resistance responses to volatile organic compounds, the CB/metallophthalocyanine composite sensors exhibited a high sensitivity towards trace levels of NH_3(g) under ambient temperature and pressure conditions. No degradation in sensor response was observed after nearly 12 h of repeated exposure to 30 parts per million of NH_3(g) in air. Chemiresis-

Reproduced in part with permission from *Sens. Actuators B*, 134, **2008**, 521-531.

tors formed from composites of CB and zinc phthalocyanines demonstrated responses that were comparable to those of commercial NH_3(g) sensors. The CB/metallophthalocyanine composites thus broaden the types of materials that can be used for this type of low-power chemiresistive gas sensing, and broaden the types of analytes that can be sensitively detected to include inorganic gases as well as organic vapors.

2.2 Introduction

Chemiresistive materials have been used as detectors for gaseous analytes for several decades.[1] A principal advantage that chemiresistors have is their comparatively simple and compact design. In their simplest form, chemiresistive sensing systems are naturally low power (0.1-1 mW) devices aptly suited for miniaturization and portability.[2] Our laboratory has focused on the development and implementation of low-power, inexpensive chemiresistive materials. We have previously reported on composite chemiresistive thin films comprised of insulating organic material and electronically conductive carbon black that function as vapor detectors under ambient conditions.[3–5] Chemiresistive films composed of carbon black and insulating polymers (CB/IP) operate via a volumetric sensing modality, i.e. concomitant analyte(s) absorption and volumetric-expansion render a reversible change in total DC film resistance.[4] For carbon black loadings above the percolation threshold,[6] the observed resistance changes are proportional to the volume of absorbed analyte.[7] Accordingly, these composite materials generally exhibit excellent sensor response characteristics towards organic vapors at low absolute concentrations, readily allowing the detection, identification, and discrimination of chemical warfare agent simulants and trace vapor signatures of ex-

plosives.[5,8]

A constraint of volumetric signal transduction is the inverse dependence of the detector sensitivity on the vapor pressure, P°, of the gaseous analyte of interest[9,10]

$$K = \frac{\rho RT}{\gamma M P^{\circ}} \tag{2.1}$$

where K is the partition coefficient of the gaseous analyte into the sensor material, T is the system temperature (K), ρ is the sensor material density (g cm^{-3}), R is the ideal gas constant (atm mol^{1} dm^{3} K^{-1}), γ is the activity coefficient of the analyte within the sensor material, and M is the molar mass of the analyte (mol dm^{-3}). For analytes with high-vapor pressures ($P^{\circ} > 1$ atm), low absolute vapor concentrations will consequently generate small signals, because the equilibrium driving force favors keeping the analyte largely in the gas phase rather than in the solid phase. Hence, these sorption-based chemiresistors are relatively insensitive to extremely low absolute concentrations of inorganic gases. Many toxic inorganic gases, e.g. Cl_2, HCN, SO_2, NO_2, and NH_3 , are hazardous even at trace (parts per million, ppm) concentrations,[11] so an ongoing effort in our group is to increase the sensitivity of composite chemiresistors films without sacrificing their inherent low-power consumption, thereby increasing the sensing capacity without compromising the utility of these chemiresistor arrays.

We have previously demonstrated that specific chemical interactions between the analyte and insulating organic material can improve certain responses the sensors. For example, the sensitivity of carbon black-polyethyleneimine sensors towards carboxylic acid vapors is 103 times larger than that of other carbon black-polymer composite chemiresistive

thin films.[12,13] We have recently described functional composite chemiresistors that consist of carbon black and non-polymeric organic (CB/NPOM) materials.[14,15] Non-polymeric organic materials allow a greater density of chemical functional groups relative to that in a comparable functionalized polymer. Further, CB/NPOM sensors are not limited in composition by materials that are solely available as polymers.[14] Hence, one potential approach for increasing the sensitivity of composite chemiresistive thin films towards inorganic gases is to choose a non-polymeric insulating material that has strong interaction with the gaseous analyte.

Organometallic compounds have often been used as sensor materials for the detection of gaseous analytes and are thus an interesting class of materials for the sorptive fraction of CB/NPOM sensors.[16–19] In particular, the conductance of crystalline metallophthalocyanine films can be particularly sensitive to reducing and oxidizing gases.[18,20–25] The modulation of the electrical properties of these materials by exposure to oxidizing or reducing gases is known to arise from their semiconductor behavior.[25–27] While neat metallophthalocyanine thin films can, under controlled conditions, function as responsive chemiresistors, they have important operational drawbacks as standalone sensors. Metallophthalocyanines generally require both a high temperature (80-170 °C),[28] as well as a large applied electric field to function as chemiresistors.[17] Further, metallophthalocyanine sensors are generally insensitive towards common organic vapors.[17]

In this work, we describe the use of metallophthalocyanine-based CB/NPOM sensors for the analysis of gaseous analytes under ambient operating conditions. With this sensor design, we demonstrate that metallophthalocyanine-based CB/NPOM sensors can function

as conventional sorption chemiresistors for the detection and discrimination of various organic vapors. Importantly, this same array of sensors, under the same operating conditions (i.e. no field effect conductivity or elevated temperature), can also identify and detect low levels of an inorganic gas. We demonstrate that metallophthalocyanine CB/NPOM sensors can respond to trace levels of NH_3(g) (P° = 8.69 atm at T = 25 °C), i.e. levels below the 8 h recommended permissible exposure level, PEL, of NH_3(g). The more sensitive metallophthalocyanine CB/NPOM sensors showed no reduction in response after nearly 12 h of periodic exposure to 30 ppm of NH_3(g) in air, with a signal-to-noise ratio of $\sim$300:1. We highlight the pertinent features of the metallophthalocyanine CB/NPOM signal transduction modes, demonstrating that these sensors are capable of both volumetric expansion and adsorptive conductance changes because the carbon black fraction, rather than the metallophthalocyanine fraction, supports the film conductance. The findings reported here expand the potential applications for inexpensive composite thin-film chemiresistor arrays.

2.3 Experimental

2.3.1 Sensor Preparation

Sensor films were spray cast from suspensions that contained Black Pearls 2000 carbon black (Cabot Co.), and the desired nonconductive component of the composite (Table 2.1). The solvent was 50 mL of tetrahydrofuran (THF, reagent grade, EM Science). After preparation, the suspensions were sonicated for 2 h and then immediately used for fabrication of sensor films. The weight fractions of CB used for the CB/metallophthalocyanine sen-

Sensor Material	Abbreviation	Source	Amount (mg) Sorbent	CB
Phthalocyanine	H_2Pc	Fluka	30	90
Co(II) phthalocyanine	CoPc	Fluka	30	90
Cu(II) phthalocyanine	CuPc	Aldrich	30	90
Fe(II) phthalocyanine	FePc	Strem	30	90
Sn(II) phthalocyanine	SnPc	Aldrich	30	90
Zn(II) phthalocyanine	ZnPc	Aldrich	30	90
Zn(II) tetranitrophthalocyanine	ZnPc-*t*-NO_2	Aldrich	30	90
Zn(II) 2,9,16,23-tetra-tert-butyl-29H,31 H-phthalocyanine	ZnPc-*t*-tb	Aldrich	30	90
Zn(II) 2,3,9,10,16,17,23,24-octakis(octyloxy)-29H,31H-phthalocyanine	ZnPc-*op*-OC_8	Aldrich	30	90
Cu(II) 2,3,9,10,16,17,23,24-octakis(octyloxy)-29H,31H-phthalocyanine	CuPc-*op*-OC_8	Aldrich	30	90
Tetracosane	Tetracosane	Aldrich	30	90
Poly(ethylene-co-vinyl acetate)	PEVA	Polymer Science	72	48

Table 2.1: Sorption materials used in CB/NPOM and CB/polymer composite sensors

sors were chosen based upon prior optimization of signal-to-noise and response linearity of related CB/NPOM chemiresistive films.[14]

Substrates for the sensors were prepared by sequentially evaporating 20 nm of Cr, followed by 70 nm of Au, onto masked glass slides. The Cr underlayer was necessary to improve the adhesion of the Au film to the glass substrate. This process produced two metallic electrodes, separated by a 0.2 cm gap, on each slide. The sensor films were spray cast onto the substrates using an airbrush (CM-C Plus, Iwata Inc.) that was connected to filtered laboratory air, pressurized at 1 atm. The composite suspension was sprayed through a 0.3 cm long $\times$ 0.45 cm wide mask until a nominal resistance of 5 kΩ was measured between the electrodes. Following preparation, the sensors were dried under vacuum ($\sim 10^{-1}$ Torr) for at least 30 min and/or presented with 200 exposures (60 s background; 80 s hexane; 70 s background purge) of hexane at P/P° = 0.0050. This preconditioning was not necessary for sensor activity but did eliminate spurious initial sensor variability.

2.3.2 Scanning Electron Microscopy

Scanning electron microscopy data were obtained using a LEO1550 VP field emission scanning electron microscope operating at 10 kV with an InLens detector (30 μm aperture). Cross-sectional film images were obtained on films that had been deposited on oxidized, 1 Ω cm resistivity, p-type Si(1 1 1) substrates, with the Si scored on the underside and fractured immediately prior to microscopy.

2.3.3 Vapor Measurement System

NH_3(g) was obtained as a diluted mixture (Scott Specialty Gas) at a concentration of 3000 ppm ($\pm$ 0.1 %) in dry air. Organic vapors were generated by sparging filtered laboratory air ($\leq$ 10 parts per thousand of water vapor) through 45 cm tall bubblers that had been filled with ethanol, ethyl acetate, toluene, n-hexane, cyclohexane, n-heptane, n-octane, or iso-octane (Aldrich). Laboratory air was used as the background gas for organic vapor exposures. Use of laboratory air as the background gas for NH_3(g) exposures did not change the magnitude, temporal character, or recovery behavior of the sensor responses, but dry ($<$ 10 ppm of H_2O, Industrial Air Inc.), compressed air was chosen as the background gas for NH_3(g) exposures to match the composition of the dilute NH_3(g) mixture provided by Scott Specialty Gas. The pure-phase vapor pressures were calculated according to a modified Clapeyron equation,[29] using tabulated coefficients and a temperature, T, of 298 K.[30] The concentrations of each of the analytes were controlled by modulating the volumetric mixing ratio of the concentrated analyte and the background gases.

The flow rates of the background and foreground gases were regulated under computer

control using either Omega, MKS, or UNIT mass flow controllers. The analyte vapors were diluted by addition to a constant flow of 5000 standard cubic centimeters per minute (sccm) of background gas, to produce the desired concentration of analyte for exposure to the sensors. The total flow rate passed over the sensors varied between 5000 and 5500 sccm, depending on the mixing ratios necessary to produce the desired analyte concentration. These flow rates were sufficiently rapid to ensure that no accumulation of analyte vapor/gas within the sensor chamber occurred. The small variation (< 10 %) in flow rate did not noticeably change the time behavior of the sensor responses to NH_3(g). Unless noted otherwise, exposures consisted of 70 s of pure background gas, 80 s of dilute analyte, and then 60 s of background gas.

The sensors were loaded into a rectangular, 40-slot chamber, with sensor film replicates randomly positioned. No dependence was observed on the performance of a given sensor on its spatial position in the array. The 45.5 cm long $\times$ 3.0 cm wide $\times$ 1.5 cm deep chamber was connected by Teflon tubing to the gas delivery system. The resistance of each of the 40 sensors in the array was measured sequentially by a Keithley 2002 multimeter coupled to a Keithley 7001 multiplexer, with $\sim$ 6 s between measurements on the same sensor. The measurement electronics were interfaced to a computer via a GPIB connection and were controlled with LabVIEW software.

2.3.4 Partition Coefficient Measurements

Measurements of partition coefficients were performed as described previously.[31] Briefly, quartz crystal microbalance (QCM) measurements were made in a modified, dual sensor

chamber (8.5 cm $\times$ 6.0 cm $\times$ 3.0 cm) that contained a chemiresistive sensor and a commercial 10 MHz QCM (ICM) that had been coated with the desired sensor film material. The total vapor flow rates through the sensor chamber were between 4000 and 4200 sccm, depending on the mixing ratio used to attain the desired analyte concentration. The changes in the crystal frequency upon presentation of analyte were monitored using a frequency counter (53181A, Hewlet Packard) that had been interfaced with a computer. The same airbrush-spray protocol used for sensor fabrication was used for deposition of neat and composite sorption films on QCM crystals. All measured thin films were prepared so that they produced frequency shifts in the quartz crystal resonators which were < 10 % of the natural crystal resonance, ensuring that the frequency changes could be reliably ascribed to mass changes due to analyte sorption onto the coated QCMs.[31] For each of the eight organic vapor analytes, five film responses were recorded at each of four partial pressures, P (P/P° = 0.012, 0.024, 0.036, and 0.048), of analyte vapor. The order of vapor exposures was randomized with respect to concentration and analyte. The measured changes were referenced to the frequency recorded in background air to produce plots of the frequency change, Δf, vs. the absolute analyte concentration at $T = 23 \pm 2$ °C. For all analyte-vapor combinations, the Δf vs. concentration plots were linear. All 20 measurements for a given analyte were used for linear least-squares fitting of the steady-state change in frequency vs. analyte concentration, to determine the sensitivity of a given film/analyte combination. All fits were forced through zero for the *y*-axis intercept.

The partition coefficients, K, for the film/vapor combinations were determined from

the QCM measurements according to the following equation:[31,32]

$$K = \frac{\rho_s RT}{M_w(\Delta f_\circ)} s \tag{2.2}$$

where ρ_s is the density of the sorption material (g cm^{-3}), T is the temperature (K), s is the slope of the observed QCM response vs. partial pressure of analyte (Hz atm^{-1}), M_w is the molecular weight of the vapor analyte (g mol^{-1}), and $\Delta f_\circ$ is the initial frequency change of the crystal after coating with the sorption material (Hz). The densities of the composite films were taken to be the average of the densities of the individual components, weighted by the mass fractions of carbon black and non-conductive material, respectively, in each film. Density values of 2, 0.87, and 0.97 g cm^{-3} were used for Black Pearls 2000 carbon black, PEVA (18 wt. % acetate, M_w= 105 g mol^{-1}), and tetracosane,[33] respectively. An average value of 1.5 g cm^{-3} was assumed for the densities of the unsubstituted phthalocyanines.[34–36] Hence, the reported K values of the pure and composite CB/Pc films are weighted to the mass fraction of the respective components.

2.3.5 Signal Processing

The response of a sensor to an analyte was expressed as $\Delta R_{max}/R_b$, where R_b is the baseline-corrected resistance of the sensor and ΔR_{max} is the maximum baseline-corrected resistance change observed during exposure of the sensor to the analyte. Baseline correction was performed by fitting a line to the first five resistance measurements immediately before analyte exposure. The slope of this line was then used to correct for drift in baseline resistance by extrapolating to the end of the exposure and subtracting the extrapolated value

from the measured value. For organic vapors, ΔR_{max} was determined by averaging the last five film resistances before the end of the exposure. For responses to NH_3(g), the last film resistance before the end of the exposure was used to calculate R_{max}. Signal-to-noise ratios (SNR) ratios were calculated through the following relationship:

$$SNR = \frac{\Delta R_{max}}{\sigma_{baseline}} \tag{2.3}$$

where $\sigma_{baseline}$ is the standard deviation in the baseline-corrected resistance prior to the analyte exposure, calculated over five data points. All signal processing was performed using scripts written in MATLAB (Mathworks, Natick, MA).

2.3.6 Array Responses Processing

Each individual sensor response was first sum-normalized by the total array response in that exposure, to create a concentration independent unit-vector response.[14] The normalization was performed to ensure that any observed differences in patterns were due to the array response fingerprint and not due to differences in perceived analyte concentration.[37] Principal components analysis (PCA) was then performed to facilitate visual inspection of the discrimination capabilities of the sensor array towards all tested organic vapors.[3,37] In this approach, linear combinations of the sensor array response matrix were determined across n orthogonal vectors so as to maximize the variance between the data. In this analysis, the first PC vector contains the most variation in response data, and the subsequent PC vectors capture progressively smaller fractions of the total variance. For ease of visualization, the array responses were plotted using the first two PCs.

To quantitatively assess the sensor array discrimination performance between pairs of organic vapors, a supervised pattern recognition algorithm, the Fisher linear discriminant (FLD), was applied to the sensor array responses.[14] For each binary task, a train/test approach was employed in which the FLD algorithm was trained on 25 randomized exposures to each of the analytes. During this training, the single dimension and associated transformation vectors maximizing the separation between the 25 training exposures of the two gaseous analytes were calculated. These transformation vectors were then used to project the testing data onto the single optimized separator dimensions. Results from the FLD testing analysis are reported as resolution factors (rf), which describe the confidence level of the binary discrimination task of interest.

2.4 Results

2.4.1 Film Structure

Figure 2.1 displays scanning electron micrographs of cross-sectional views of carbon black composites of either PEVA (40 wt % CB), tetracosane (75 wt % CB), or ZnPc (75 wt % CB). For comparison, Figure 2.1d depicts an image of a film comprised only of CB, without any deliberately added other sorbent phase. The CB/PEVA films depict prototypical morphologies of CB/insulating organic polymer composites,[4,7] while the CB/tetracosane composites are indicative of the morphologies of CB/NPOM sensors.[14] The CB/ZnPc films represent the new sub-class of CB/NPOM sensors described herein that utilize organometallic materials as the complement to the CB conductor in chemiresistor films.

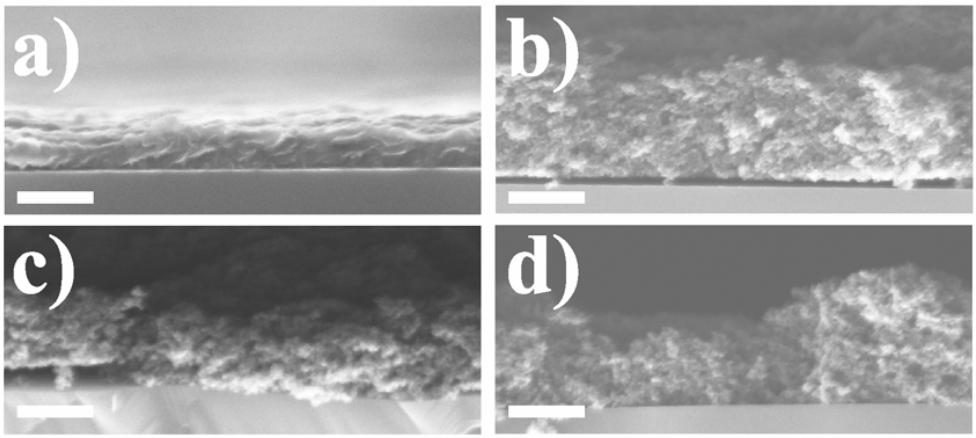

Figure 2.1: Cross-sectional electron micrographs of (a) CB/PEVA, (b) CB/tetracosane, (c) CB/ZnPc and (d) pure CB fractured chemiresistor films. Scale bar = 500 nm.

The morphologies of the CB/tetracosane, CB/ZnPc, and pure CB films were uneven, porous, and grainy (Figure 2.1b-d). In higher resolution micrographs, individual constituent CB particles/aggregates, with diameters less than 20 nm, were clearly visible in all three film types. These grains are consistent with the known grain size of Black Pearls 2000 CB.[38] In contrast, the carbon black/PEVA film (Figure 2.1a) was noticeably smoother, more compact, and denser, and showed much larger aggregates and grains ($\sim$60 nm). The structure of the CB/PEVA film was uniform throughout the entire film, and had minimal apparent void spaces. In general, the CB/PEVA film had CB particles embedded in an organic matrix. In contrast, the sorption material component could not be readily differentiated from the CB in the CB/NPOM sensor films.

2.4.2 Response to Organic Vapors

Table 2.2 lists the logarithmic values of the apparent film/vapor partition coefficients, K, for a series of test organic vapors into thin films of either PEVA, tetracosane, H_2Pc, FePc, or ZnPc, as measured from QCM data. The K values trended towards larger values for

analytes that had lower pure-phase vapor pressures. Single component films of tetracosane or of the organometallic compounds generally exhibited lower K values than PEVA (except for H_2Pc, which gave slightly higher values for all but toluene and ethanol), but the values were within an order of magnitude of each other for a given analyte. Conversely, films composed of only CB exhibited K values that were much larger, by as much as two orders of magnitude, than those of pure metallophthalocyanine, PEVA, or tetracosane films.

The CB/PEVA composite exhibited K values for all tested analytes that were nominally equivalent (within a factor of 2 or less) to the values obtained with the pure PEVA film, indicating that the total sorptive capacity of the CB/PEVA composite was dictated by that of the PEVA. In contrast, CB/tetracosane, CB/H2Pc, CB/ZnPc, and CB/FePc composites exhibited K values that were much higher than those observed for the corresponding materials that did not contain CB. In fact, the overall sorptive properties of the CB/Pc films were close to, but slightly smaller than, the apparent K values of the pure Black Pearls 2000 CB. The partition coefficients for these materials were therefore dominated by the properties of the CB, modified by the presence of the Pc phases, as opposed to being dominated by the sorption properties of the pure Pc materials.

Table 2.3 displays the sensor responses ($\Delta R_{max}/R_b$) and SNR values of selected CB/Pc sensors upon exposure to some test organic vapors at P/P° = 0.0050. The errors in the values listed in Table 2.3 describe the variability between nominally identical sensors, and not the variability of an individual sensors responses. The response magnitudes of the six different types of CB/Pc sensors varied significantly across the eight test organic vapors. The SNR values for the CB/Pc sensors were similar to those of CB/organic polymer com-

	log K							
Sensor Film	n-hexane (0.174 atm)	toluene (0.0317 atm)	ethanol (0.0650 atm)	ethyl acetate (0.105 atm)	cyclohexane (0.113 atm)	n-heptane (0.051 atm)	n-octane (0.0154 atm)	iso-octane (0.0558 atm)
CB/PEVA	2.26	3.31	2.32	2.57	2.49	2.72	3.18	2.56
PEVA	2.23	3.05	2.18	2.23	2.49	2.70	3.16	2.61
CB/tetracosane	2.45	3.49	2.32	2.46	2.56	2.95	3.45	2.90
Tetracosane	1.85	2.62	2.00	1.85	2.11	2.34	2.79	2.26
CB/ZnPc	3.02	3.86	3.34	3.22	3.05	3.57	4.09	3.51
ZnPc	1.70	2.68	2.78	1.70	2.18	2.26	2.74	2.30
CB/FePc	2.95	3.73	2.99	3.12	2.92	3.52	4.04	3.45
FePc	1.81	2.48	1.44	2.13	2.22	2.39	2.40	2.30
CB/H2Pc	3.45	4.21	3.46	3.55	3.49	3.99	4.50	3.91
H2Pc	2.53	2.76	2.11	2.36	2.60	2.98	3.42	2.81
CB	3.47	4.35	3.50	3.55	3.56	4.03	4.55	3.97

Table 2.2: Apparent equilibrium sorption partition coefficients, K, for selected organic vapors at T = 298 $\pm$ 2 K and P = 1 atm. The vapor pressures, P°, of each analyte vapor are presented in parentheses.

posites exposed to these same concentrations of test organic vapors.

PCA was used to evaluate the discrimination ability of an array of the six different types of CB/Pc sensors (Table 2.3) towards the organic test vapors delivered at P/P° = 0.0050. Figure 2.2 displays a graphical representation of the first two PC vectors, which contained 86 % of the total variance in the six-sensor array response data. In general, the array of six CB/Pc sensors produced a reasonable separation between the responses for polar and non-polar analytes. The response data for the nonpolar analytes were clearly separated from those of ethyl acetate and ethanol, respectively. The separation among the non-polar analytes was less visually pronounced using only two PC vectors, as expected for an array with limited chemical diversity.

To quantify the array discrimination performance, the normalized resistance changes of the six-sensor film types listed in Table 2.3 were recorded for 25 training exposures to each of the test organic vapor analytes at P/P° = 0.0050. The rf values for pairwise analyte classification were determined and tabulated in Table 2.4, with rf = 1 implying a correct

	n-hexane	toluene	ethanol	ethyl acetate	cyclohexane	n-heptane	n-octane	iso-octane
$(\Delta R_{max}/R_b) \times 10^3$								
H2Pc	0.9±0.2	1.0±0.2	0.9±0.2	1.1±0.2	0.4±0.1	0.9±0.2	0.7±0.1	0.8±0.2
CoPc	0.7±0.1	0.8±0.1	0.2±0.1	0.52±0.05	0.20±0.08	0.9±0.2	0.9±0.1	0.7±0.2
CuPc	2.1±0.3	2.8±0.2	1.9±0.2	2.5±0.2	0.9±0.1	2.4±0.3	2.4±0.3	1.5±0.2
FePc	0.2±0.2	2.0±0.2	4.4±0.3	4.1±0.4	0.3±0.2	0.2±0.3	-0.3±0.3	0.2±0.4
SnPc	0.89±0.09	0.9±0.1	1.8±0.2	1.6±0.1	0.3±0.1	1.21±0.07	1.23±0.08	1.1±0.1
ZnPc	1.3±0.3	2.7±0.6	0.26±0.06	0.6±0.1	0.7±0.1	1.7±0.4	1.8±0.5	1.7±0.5
SNR								
H2Pc	264±183	359±208	256±151	323±179	125±82	282±183	228±137	242±146
CoPc	325±208	436±199	142±66	257±119	99±60	464±214	464±219	374±189
CuPc	402±200	617±382	386±242	499±267	177±78	527±293	522±276	277±120
FePc	25±63	311±206	773±579	732±559	35±42	22±82	69±80	-39±120
SnPc	350±200	402±242	689±409	656±348	128±85	523±324	491±283	456±86
ZnPc	545±268	1270±648	101±54	255±128	321±185	780±433	851±539	750±256

Table 2.3: Phthalocyanine CB/NPOM mean signal responses for exposure to organic vapors (P/P° = 0.0050). Values are averages from 50 exposures to four replicate sensors. Means and standard deviations are given for each sensor type (mean ± standard deviation).

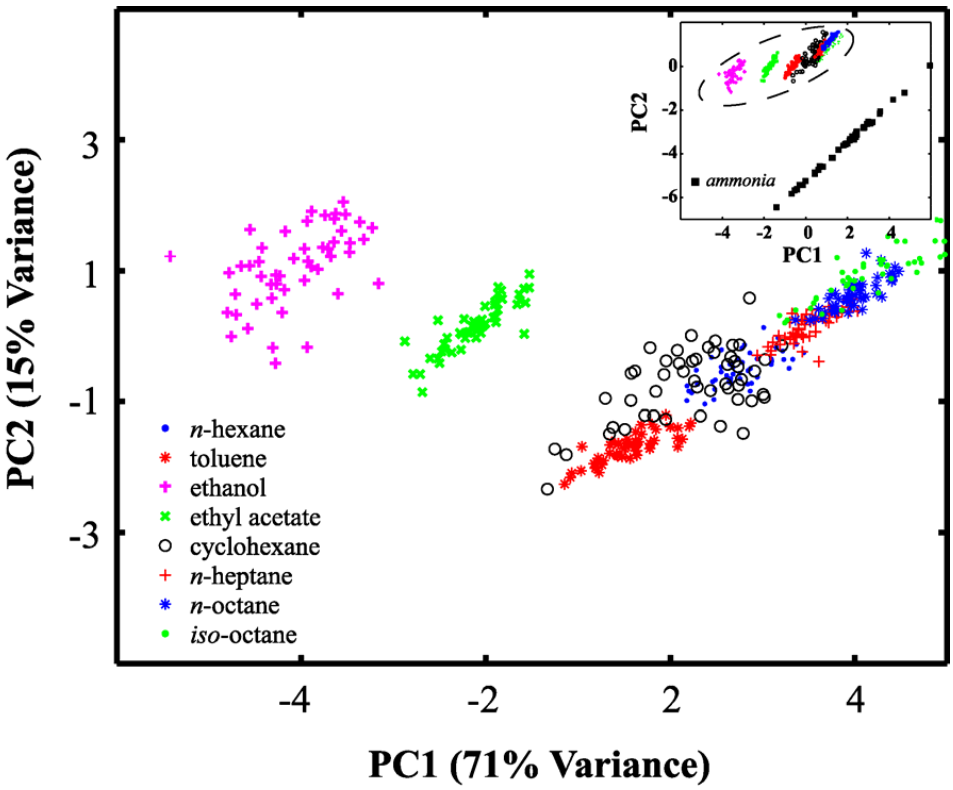

Figure 2.2: Principal components analysis of the response of an array composed of the metallophthalocyanine materials listed in Table 2.1. Principal components 1 and 2 from the normalized sensor array response data are shown for the same analytes listed in Table 2.2. Inset: Principal components analysis of the same array including the response data for NH_3(g). The encircled analytes are the same organic vapors and the solid black squares are the response data for NH_3(g).

Analytes	toluene	ethanol	ethyl acetate	cyclohexane	n-heptane	n-octane	iso-octane
n-hexane	13.4(16.3)	24.4(30.3)	26.1(32.7)	3.3(13.4)	3.6(11.7)	6.4(18.2)	10.3(15.0)
toluene		15(36.0)	16.9(32.6)	10.4(14.5)	15.2(28.9)	19.7(35.6)	21(35.7)
ethanol			11.5(17.0)	16.4(27.1)	23.8(29.9)	24.6(28.5)	24(30.1)
ethyl acetate				14.9(27.4)	24.4(29.8)	21.8(25.2)	20.4(27.4)
cyclohexane					5.2(20.8)	5.5(26.0)	7.9(22.3)
n-heptane						2.5(11.3)	9.3(10.4)
n-octane							8.4(16.2)

Table 2.4: Resolution factors of a CB/unsubstituted metallophthalocyanine array for pairwise discrimination between organic vapors presented at P/P° = 0.0050. The array consisted of CB composites of the same six metallophthalocyanines listed in Table 2.3. Values in parentheses correspond to a seven-sensor array that included a CB/tetracosane sensor.

classification at the 72 % confidence level, rf = 2 indicating a classification at the 92 % confidence level, and rf = 3 implying a classification at the 98 % confidence level. These rf values indicate that accurate pairwise analyte differentiation for all tasks was observed at $>$ 92 % confidence levels, with most of the differentiation tasks being performed at 98 % confidence levels. While the rf values in Table 2.4 are somewhat lower, in general, than those of a CB/NPOM array with increased chemical diversity,[14] the rf values are comparable to those observed for a typical CB/organic polymer array.[14]

2.4.3 Response to NH_3(g)

Figure 2.3 depicts representative responses of CB/organic polymer, CB/NPOM, and CB/Pc sensors to NH_3(g) at P/P° = 3.4$\times 10^6$ (30 ppm) in air. The CB/PEVA and CB/tetracosane sensors exhibited no detectable response to this concentration of NH_3(g), with $\Delta R_{max}/R_b$ values $\leq 10^{-5}$ and SNR values < 10 (Table 2.5). Responses were, however, evident for CB/Pc composites that contained H_2Pc, CoPc, CuPc, FePc, SnPc, or CuPc-*op*-OC_8, with $\Delta R/R_b$ values $< 10^{-3}$ and SNR values between 60 and 150 at 30 ppm of NH_3(g) (Table 2.5). In contrast, the CB/ZnPc composite sensors showed larger, more rapid, more

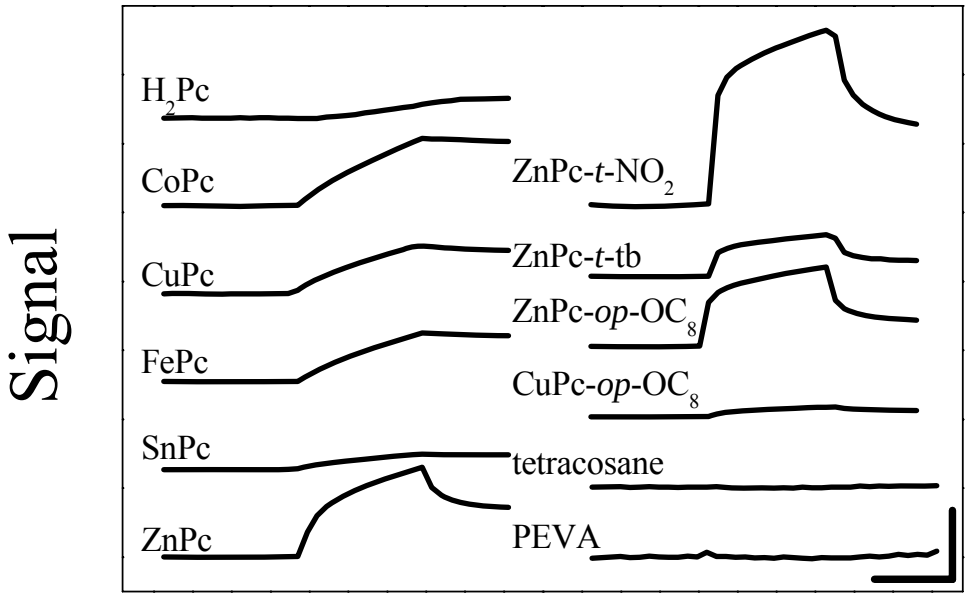

Figure 2.3: Representative relative differential resistance responses of various CB composite sensors to NH_3(g) at $P/P^\circ = 3.4\times10^{-6}$ (30 ppm) in air. The *y*-axis scale bar is $\Delta R/R_b$ = 0.001 and the *x*-axis scale bar is 50 s.

reversible, and more reproducible responses than those produced by composites with the other metallophthalocyanines. In fact, CB composites that contained either ZnPc, ZnPc-*op*-OC_8, or ZnPc-*t*-NO_2 exhibited average R_{max}/R_b and SNR values of $> 1\times10^{-3}$ and $\geq$ 280, respectively, at 30 ppm of NH_3(g) in air. Among the substituted ZnPc materials, CB/ZnPc-*t*-NO_2 composites showed the largest maximum differential resistance change, composites with ZnPc-*op*-OC_8 and CuPc-*op*-OC_8 gave nominally identical responses as compared to the corresponding unsubstituted metal phthalocyanine materials, and the observed responses of CB composites with ZnPc-*t*-tb were nearly half that of CB/ZnPc composites. For all metallophthalocyanine sensors, the film resistance did not return completely to the pre-exposure baseline value.

The effects of changes in carbon black loading of the CB/Pc sensors were also investigated. Minimal change in sensor response was observed for compositions having 25-50

Sensor Material	$\Delta R_{max}/R_b(\times 10^3)$	SNR
H_2Pc	0.4±0.4	61±51
CoPc	0.9±0.3	153±37
CuPc	0.3±0.3	65±54
FePc	0.7±0.2	147±66
SnPc	0.2±0.1	47±40
ZnPc	1.1±0.1	340±30
ZnPc-*t*-NO_2	3.0±0.6	330±40
ZnPc-*t*-tb	0.60±0.08	290±40
ZnPc-*op*-OC_8	1.0±0.1	280±60
CuPc-*op*-OC_8	0.12±0.04	66±24
Tetracosane	0.05±0.06	26±32
PEVA	-0.03±0.03	3±3

Table 2.5: Figures of merit of CB/NPOM sensors for NH_3(g) detection. Values are averages from 200 exposures at four replicate sensors. $P/P^\circ = 3.4\times10^{-6}$ (30 ppm), 80 s exposures.

wt % of the phthalocyanine component, but the SNR values decreased significantly for other mass loading values. For lower mass loadings of CB, phthalocyanine contents > 50 wt % produced an increase in baseline noise but no significant increase in $\Delta R_{max}/R_b$. Additionally, the resistances of such films could not be made lower than 10^6 Ω. Conversely, for higher CB mass loadings, such as those having phthalocyanine contents < 25 wt %, $\Delta R_{max}/R_b$ values decreased substantially.

Figure 2.4 displays the shape and magnitude of the raw, uncorrected responses for a CB/ZnPc sensor upon repeated exposure to NH_3(g). Neither the magnitude nor the form of the sensor response changed appreciably during 200 successive exposures to 30 ppm NH_3(g) over a 12 h period. The initial response for all sensors was slightly larger than the response observed during subsequent exposures. The change in sensor response from the first exposure to the tenth exposure was less than 30 % and the variability in subsequent sensor responses was less than 5 %. This behavior is in contrast to the rapid degradation in sensor response that is generally observed for conducting-polymer sensors during repeated exposures to NH_3(g).[39] Changes in the CB/metallophthalocyanine sensor responses did not

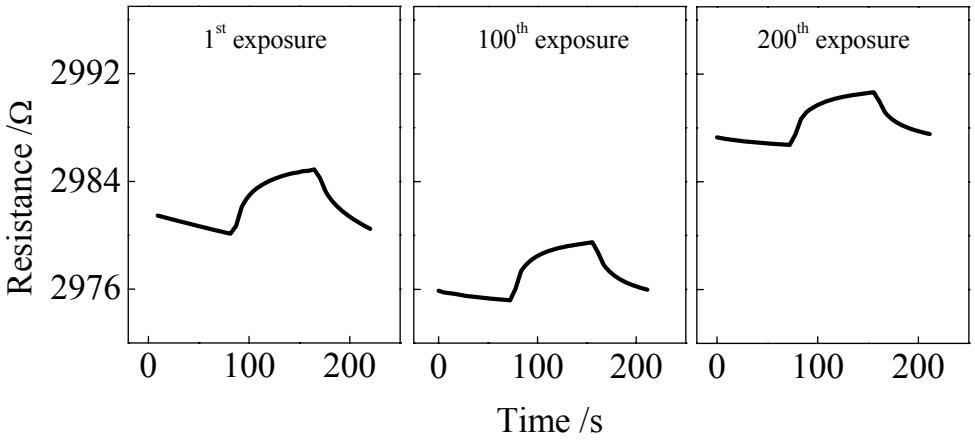

Figure 2.4: Representative resistance responses of a CB/ZnPc chemiresistor to NH_3(g) as a function of the number of exposures at P/P° = 3.4×10^{-6} (30 ppm) in air.

arise from physical degradation of the film. Throughout the course of these studies, we did not observe any visible cracking or delamination during, or arising from, any of the testing protocols.

For the CB/ZnPc sensors, the responses did not reach an apparent saturation after 80 s of exposure to NH_3(g) (Figures 2.3 and 2.4). Figure 2.5 shows overlays of the responses, as a function of exposure time, of CB/ZnPc and CB/H2Pc sensors towards 30 ppm NH_3(g). The response profiles for the two different types of composites were similar,with neither exhibiting an apparent steady-state resistance response even after 600 s of exposure to NH_3(g). The maximum $\Delta R/R_b$ for both sensors was clearly dependent on the time exposed to NH_3(g), but the majority of the change in signal magnitude was observed during the first $\sim$ 60 s of exposure.

Figure 2.6 shows the response profiles of a CB/ZnPc film as a function of the concentration of NH_3(g). Figure 2.6a shows an overlay of representative differential resistance responses, demonstrating that the time-dependent form of the response was not a function of concentration and that the maximum $\Delta R/R_b$ value increased with higher concentrations

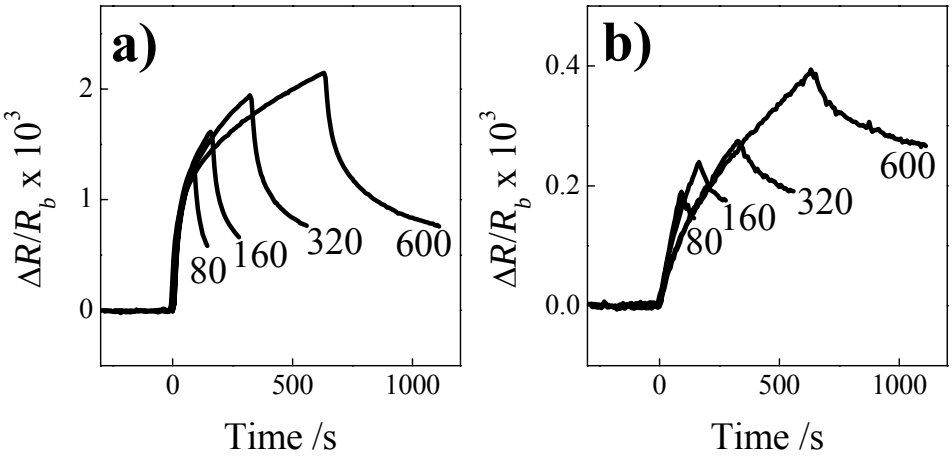

Figure 2.5: Relative differential resistance responses of (a) CB/ZnPc and (b) CB/H_2Pc chemiresistors as a function of exposure times to NH_3(g) at P/P° = 3.4×10^{-6} (30 ppm) in air.

of NH_3(g). Figure 2.6b shows a representative profile of ΔR_{max} as a function of the NH_3(g) concentration. The sensor responses were clearly not a linear function of NH_3(g) concentration, tending towards saturation at concentrations $>$ 100ppm of NH_3(g) in air. The data in Figure 2.6b could be moderately well fit assuming a Langmuir-type of adsorption of NH_3 onto the sensor film.

Figure 2.7 compares the measured analyte mass uptake of CB/ZnPc films during exposures to ethanol and NH_3(g), respectively. The raw quartz crystal microbalance frequency changes, and the uncorrected resistance changes, are shown for both analytes, using the same set of CB/ZnPc sensors and corresponding CB/ZnPc-coated QCM crystals. Raw responses, rather than data normalized by Δf or $\Delta R/R_b$, are shown for clarity to fully depict the unprocessed response of the sensors. A $+9\ \Omega$ increase in the film resistance was observed during exposure of the CB/ZnPc composite to ethanol at P/P° = 0.0050 (325 ppm, Figure 2.7a). The same exposure conditions produced a -70 Hz decrease in the resonant frequency of the CB/ZnPc-coated quartz crystal. In contrast, Figure 2.7c and d shows

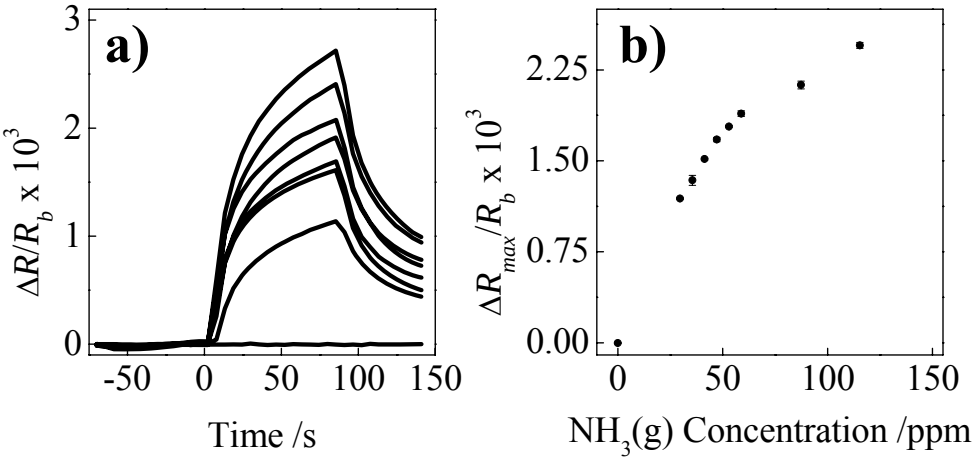

Figure 2.6: Representative relative differential resistance responses of a CB/ZnPc sensor towards various concentrations of NH_3(g). (a) Time-dependent relative differential resistance profiles for the NH_3(g) concentrations shown in (b). (b) Relative differential resistance changes recorded at t = 80 s as a function of NH_3(g) concentration. Each data point represents the average of 10 randomized exposures. The error bars represent the standard deviation in the response magnitudes over 10 exposures.

the response of the same sensor/QCM set to presentation of NH_3(g) at $P/P^\circ = 3.4\times10^{-6}$ (30 ppm). The observed maximum resistance change was $+6\ \Omega$ (Figure 2.7c), approximately the same as that for exposure to 325 ppm of ethanol (Figure 2.7a). However, the time-dependent sensor response to NH_3(g) (Figure 2.7c) was noticeably different than the response to ethanol (Figure 2.7a). Specifically, a steady-state resistance was not reached for NH_3(g), while the maximum $\Delta R/R_b$ was obtained within 10 s for ethanol. Figure 2.7d shows that negligible mass uptake was observed during exposure to NH_3(g). For repeated NH_3(g) exposures on numerous CB/ZnPc films, the frequency shift of the coated QCM was always $\leq |5$ Hz$|$, which was much less than that observed for any of the test organic vapor analytes at the same vapor phase partial pressure and at the same relative differential resistance response magnitude (Figure 2.7b).

The difference between the response magnitudes for NH_3(g) of the CB/Pc sensors that

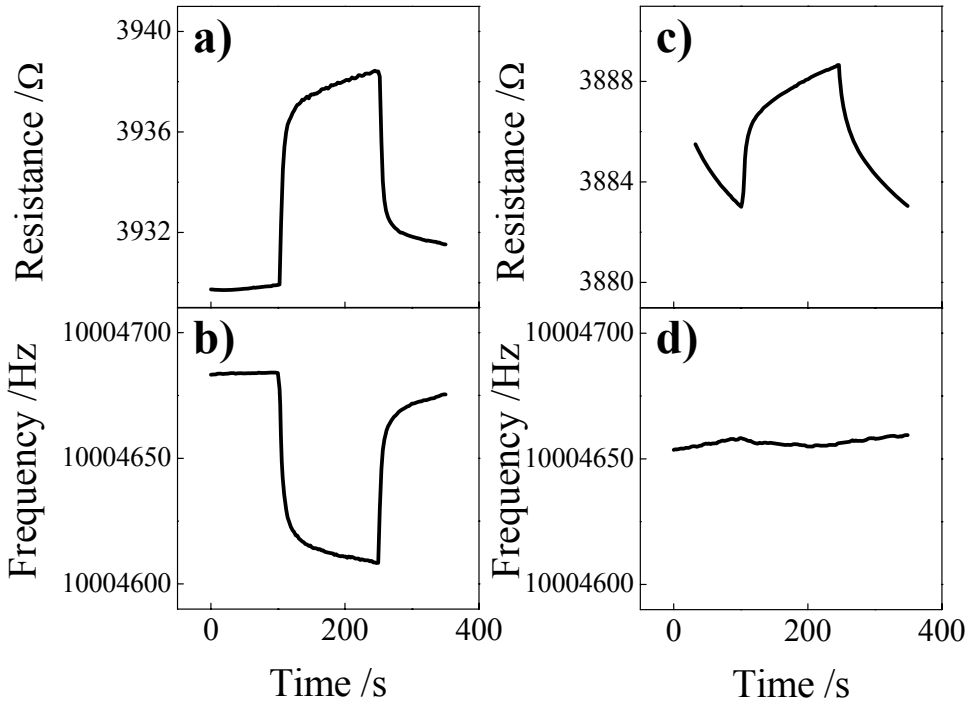

Figure 2.7: Resistance and mass changes of CB/ZnPc films upon exposure to analyte. (a) Resistance change for a chemiresistor exposed to 325 ppm of ethanol. (b) Mass uptake during a 150 s exposure to 325 ppm of ethanol. (c) Resistance change for the same chemiresistor as in (a) during a 150 s exposure to 30 ppm of NH_3(g). (d) Mass uptake of the same film as in (b) during a 150 s exposure to 30 ppm of NH_3(g).

contained unsubstituted phthalocyanines was investigated further. XPS analysis on each of the six unsubstituted CB/Pc sensor types was conducted to determine if the sensor responses were a function of subtle variations in concentration of metallophthalocyanine. The elemental abundances of the metal centers were used to gauge the composition of the composite films near the two gold contacts and in the center of the film. In all cases, the measured intensities of the corresponding metal-based $3d_{3/2}$ signal were observed to be spatially uniform across the surface of the sample. The phthalocyanine metal center abundances were nominally the same for each of the six unsubstituted phthalocyanine CB/Pc films, ranging from 0.5 to 0.8 at. %. Comparison of these values with the respective NH_3(g) responses for these sensors showed no direct correlation between the phthalocyanine abundance and the sensor response. For example, in the presented sample set, the CB/SnPc sensor showed the highest phthalocyanine content while possessing the poorest NH_3(g) signal, while the CB/ZnPc sensor had a slightly lower measured phthalocyanine content yet demonstrated the strongest signal response.

The responses towards NH_3(g) at P/P° = 3.4×10^{-6} for the CB/unsubstituted metallophthalocyanine sensors were included with the response data for the organic vapors for additional principal components analysis. The inset of Figure 2.2 clearly demonstrates a marked and distinct separation between the NH_3(g) responses and those observed for all of the organic vapor analytes. The data in Figure 2.2 thus demonstrate that the chemiresistive array was capable of clear, rapid separation of trace organic and inorganic vapor analytes.

2.5 Discussion

The CB/Pc sensors individually responded well to the selected organic vapor analytes, with SNR values similar to those reported previously for CB/NPOM films.[14] Interestingly, variations in the coordinated metal center were sufficient to effect measurable differences in the relative sensor responses of the CB/Pc sensors. An array of CB composites of six unsubstituted metallophthalocyanines contained enough sensor-element diversity that concentration-normalized pairwise discrimination tasks were performed at > 98 % confidence levels. Addition of a single CB-organic (CB/tetracosane) composite to the same array augmented the differentiation capability to levels equal to, or surpassing that of, previously reported CB/organic polymer or CB/NPOM arrays.[14,40] Hence, for the sensing/discrimination tasks of common organic vapors, the CB/Pc sensors could be used as sensor elements in any of these previously reported CB chemiresistive vapor detection arrays.

The metallophthalocyanine CB/Pc sensors, however, demonstrated an advantage over conventional CB/organic polymer and CB/NPOM sensors for the detection of trace levels of NH_3(g). Specifically, CB/PEVA and CB/tetracosane sensors were unresponsive to ppm levels of NH_3(g) while the metallophthalocyanine CB/Pc sensors showed good responses. Taking the limit-of-detection (LOD) to be the concentration for which the SNR = 3, the most sensitive CB/metallophthalocyanine sensor type (CB/ZnPc-*t*-NO_2) demonstrated a LOD of $\sim$ 300 ppb, well below both the 30 min immediately dangerous to life or health concentration (IDLH) and the 8 h PEL (permissible exposure level) for NH_3(g).[41,42] Further, these CB/metallophthalocyanine sensors exhibited minimal degradation in sensor

response upon repeated exposure to NH_3(g), and showed a clear sensitivity to changes in NH_3(g) concentration, making these sensors potentially interesting for onsite, first warning sensor applications such as airplane cabin-air monitoring, livestock air-quality assessment, and breath analysis for medical diagnostics.[42]

Three principal observations suggest that the signal transduction mechanism for CB/ metallophthalocyanine sensors towards NH_3(g) is not the same as the response mechanism towards the organic vapors. For the organic vapors, the QCM responses of CB/Pc and of organic CB/NPOM[14] films are consistent with a concomitant volumetric-expansion/resistance-increase signal transduction mechanism, as is well-documented for CB/polymer films.[4,43] For NH_3(g), the QCM response of a CB/ZnPc film indicated that a negligible mass of NH_3(g) sorbed into/onto the sensor film during 30 ppm NH_3(g) exposure as compared to the mass change observed upon exposure to 325 ppm ethanol, yet both analytes elicited nominally equivalent relative differential resistance changes. For short and long exposure times, the CB/ metallophthalocyanine composites did not reach a steady-state differential resistance change for NH_3(g), whereas plateau-type responses were generally observed for the organic vapor analytes. The large chamber headspace above the sensors, and the fast gas flow rates through the sensor chamber, have been optimized for fast equilibration and analyte partitioning into the sensor film,[31] so the time-dependent features of the responses to NH_3(g) are not artifacts of the vapor presentation system. Instead, they suggest that the NH_3(g)-Pc sensor film interaction is inherently slow, proceeding on the time scale of tens of seconds. Finally, the metallophthalocyanine composite sensor responses were decidedly non-linear with NH_3(g) concentration, whereas the CB/Pc sensors exhibited linear signal

responses for the tested organic vapor analytes.

Hence a simple absorption/volumetric-expansion signal transduction mechanism is unlikely to be operative for the responses towards low absolute concentrations of NH_3(g). Instead, the response data of the CB/metallophthalocyanine sensors (particularly the time-dependent $\Delta R_{max}/R_b$, the sensor response concentration isotherm, and the observed QCM response of the CB/ZnPc film) are consistent with NH_3(g) adsorption being a controlling feature. Interestingly, the temporal response characteristics of these CB/Pc sensors strongly resemble the responses of ligand stabilized metal nanoparticle (Au or Pt) composite sensor films.[44] For those films, Vossmeyer and co-workers suggested that NH_3 adsorption strongly affected the contact resistance between particulates in the films. A similar effect may be operative for the behavior of the CB/metallophthalocyanine sensors towards NH_3(g).

NH_3(g), a strongly reducing gas, is known to adsorb substantially on CBs[45,46] and on phthalocyanines,[20,28,47,48] with strong influences on the conductivity of thin films of the latter. However, a simple interaction with either just the CB or just the phthalocyanine is insufficient to account for the observed phenomena. CB/NPOM sensors consisting of tetracosane showed no response towards NH_3(g), indicating that the CB is not inherently active towards NH_3(g) nor is the CB sensitized towards NH_3(g) as an indirect result of the sensor fabrication process. Similarly, thin films prepared with only CB showed erratic, very small, and inconsistent exposure responses, indicating that the as-received material itself did not produce viable sensors for NH_3(g). Correspondingly, CB/Pc films consisting either mostly or entirely of just the phthalocyanine component did not show any enhanced sensor response to NH_3(g). Although metallophthalocyanines are prototypical examples of

organic semiconductors, the phthalocyanine fraction was not responsible for a significant fraction of the film conductance. The electronic conductivity at room temperature of amorphous metallophthalocyanine films is several orders of magnitude less than that of Black Pearls 2000 CB. In fact, thin films of only the phthalocyanine materials applied between the 2 mm electrode gap possessed resistances $> 10^9\Omega$, consistent with the known low inherent conductivities of phthalocyanines under ambient conditions (10^{-12} S cm^{-1}).[28,49,50] Useful current-voltage measurements with metallophthalocyanine films are typically only obtained with large external electrical fields of $\sim 10^6$ V cm^{-1}.[28] Accordingly, pure metallophthalocyanine films were insufficiently conductive and therefore unusable as spray-deposited chemiresistive gas sensors in our low power, room temperature sensor readout approach. Moreover, since reducing gases such as NH_3(g) are known to increase the resistivity of metallophthalocyanines,[18,19,28,48,51,52] it seems unlikely that a resistance increase in solely the metallophthalocyanine fraction of the composite films would independently measurably alter the overall film conductivity.

Rather, the data presented herein suggest a cooperative interaction between the CB and metallophthalocyanine fractions that results in a measurable response towards NH_3(g). The sorptive properties of the composite CB/phthalocyanine films, as indicated by measured K values, are different than the pure forms of the respective two film components. As indicated by the SEM and partition coefficient analyses, the general physical character of the CB/Pc films suggests that the CB particles are not embedded in a coherent organic matrix, as is the case with the CB/organic polymer composites (e.g. CB/PEVA), but rather that the non-polymeric materials coat the constituent CB particles as a thin layer and there by

modulate the sorptive properties of the CB. The metallophthalocyanines appear to increase the sensitivity of electronic conduction across adjacent CB particles, akin to the action of thin oxide layers on the conduction across silver nanoparticle films exposed to NH_3(g).[53–55] Moreover, the strong resemblance of the time-dependent sensor response behavior of the CB/Pc sensors to that of the precious-metal nanoparticle films reported by Vossmeyer and co-workers[44] further support the possibility that NH_3(g) adsorption modulates the contact resistance between CB particulates. Such a scenario suggests that the signal-to-noise ratios and corresponding detection sensitivities could potentially be enhanced through the use of form factors that limit the possible conduction pathways across the sensor film.[53] In this work, we have made no attempt to vary the form factor of the metallophthalocyanine-based sensors to optimize their capacity for NH_3(g) detection. Further work will be directed towards elucidating more fully the signal transduction mechanism of these composite materials, improving their sensitivity and response times, and determining whether similar sensitivities can be obtained for other high-vapor pressure gaseous analytes of interest.

2.6 Conclusions

Composite films of CB and metallophthalocyanines have demonstrated reasonable response times, good signal-to-noise, stability, and sensitivity towards assorted organic vapors. An array of chemiresistive vapor sensors comprised of metallophthalocyanine-based CB composites exhibited excellent pairwise discrimination of the tested organic vapor analytes. Moreover, these sensors showed reversible responses towards NH_3(g) at concentrations below the 8 h permissible exposure level while operating under ambient conditions. The

behavior of the thin-film CB/metallophthalocyanine sensors depended on the metal center and/or the peripheral substituents, with coordinated zinc centers yielding sensor responses comparable to state-of-the-art NH_3(g) sensors.

Bibliography

[1] Seiyama, T.; Kato, A.; Fujiishi, K.; Nagatani, M. *Anal. Chem.* **1962**, *34*(11), 1502–.

[2] Kim, Y. S.; Yang, Y. S.; Ha, S. C.; Pyo, H. B.; Choi, C. A. *ETRI* **2005**, *27*(5), 585–594.

[3] Freund, M. S.; Lewis, N. S. *Proc. Natl. Acad. Sci. U.S.A.* **1995**, *92*(7), 2652–2656.

[4] Severin, E. J.; Lewis, N. S. *Anal. Chem.* **2000**, *72*(9), 2008–2015.

[5] Hopkins, A. R.; Lewis, N. S. *Anal. Chem.* **2001**, *73*(5), 884–892.

[6] Sisk, B. C.; Lewis, N. S. *Langmuir* **2006**, *22*(18), 7928–7935.

[7] Severin, E.; Doleman, B.; Lewis, N. *Anal. Chem.* **2000**, *72*(4), 658–668.

[8] Briglin, S.; Burl, M. C.; Freund, M. S.; Lewis, N. S.; Matzger, A.; Ortiz, N. D.; Tokumaru, P. *Proc. SPIE* **2000**, pages 530–538.

[9] Janghorb.M.; Freund, H. *Anal. Chem.* **1973**, *45*(2), 325–332.

[10] Doleman, B. J.; Severin, E. J.; Lewis, N. S. *Proc. Natl. Acad. Sci. U.S.A.* **1998**, *95*(10), 5442–5447.

[11] Saltzman, B. E. *Anal. Chem.* **1961**, *33*, 1100–1112.

[12] Tillman, E.; Koscho, M.; Grubbs, R.; Lewis, N. *Anal. Chem.* **2003**, *75*(7), 1748–1753.

[13] Gao, T.; Tillman, E. S.; Lewis, N. S. *Chem. Mater.* **2005**, *17*(11), 2904–2911.

[14] Gao, T.; Woodka, M. D.; Brunschwig, B. S.; Lewis, N. S. *Chem. Mater.* **2006**, *18*(22), 5193–5202.

[15] Woodka, M. D.; Brunschwig, B. S.; Lewis, N. S. *Langmuir* **2007**, *23*(26), 13232–13241.

[16] Janzen, M. C.; Ponder, J. B.; Bailey, D. P.; Ingison, C. K.; Suslick, K. S. *Anal. Chem.* **2006**, *78*(11), 3591–3600.

[17] Bora, M.; Schut, D.; Baldo, M. A. *Anal. Chem.* **2007**, *79*(9), 3298–3303.

[18] Jones, T. A.; Bott, B. *Sens. Actuators* **1986**, *9*(1), 27–37.

[19] Waite, S.; Pankow, J.; Collins, G.; Lee, P.; Armstrong, N. R. *Langmuir* **1989**, *5*(3), 797–805.

[20] Brina, R.; Collins, G. E.; Lee, P. A.; Armstrong, N. R. *Anal. Chem.* **1990**, *62*(21), 2357–2365.

[21] Roisin, P.; Wright, J. D.; Nolte, R. J. M.; Sielcken, O. E.; Thorpe, S. C. *J. Mater. Chem.* **1992**, *2*(1), 131–137.

[22] Germain, J. P.; Pauly, A.; Maleysson, C.; Blanc, J. P.; Schollhorn, B. *Thin Solid Films* **1998**, *333*(1-2), 235–239.

[23] Schollhorn, B.; Germain, J. P.; Pauly, A.; Maleysson, C.; Blanc, J. P. *Thin Solid Films* **1998**, *326*(1-2), 245–250.

[24] Valli, L. *Adv. Colloid Interface Sci.* **2005**, *116*(1-3), 13–44.

[25] Fielding, P. E.; Gutman, F. *J. Chem. Phys.* **1957**, *26*(2), 411–419.

[26] Kaufhold, J.; Hauffe, K. *Berich. Bunsen. Gesell.* **1965**, *69*(2), 168–.

[27] Tachikawa, H.; Faulkner, L. R. *J. Am. Chem. Soc.* **1978**, *100*(14), 4379–4385.

[28] Leznoff, C. C.; Lever, A. B. P. *Phthalocyanines: Properties and Applications;* VCH Publishers Inc.: New York, 1989.

[29] Smith, J. M.; Van Ness, H. C.; Abbott, M. *Introduction to Chemical Engineering Thermodynamics;* McGraw-Hill: New York, 1996.

[30] Perry, R. H. *Perry's Chemical Engineer's Handook;* McGraw-Hill: New York, 7th ed. ed., 1997.

[31] Briglin, S. M.; Lewis, N. S. *J. Phys. Chem. B* **2003**, *107*(40), 11031–11042.

[32] Grate, J. W.; Snow, A.; Ballantine, D. S.; Wohltjen, H.; Abraham, M. H.; Mcgill, R. A.; Sasson, P. *Anal. Chem.* **1988**, *60*(9), 869–875.

[33] Queimada, A. J.; Marrucho, I. M.; Coutinho, J. A. P.; Stenby, E. H. *J. Thermophys.* **2005**, *26*(1), 47–61.

[34] Zhang, L.; Peisert, H.; Biswas, I.; Knupfer, M.; Batchelor, D.; Chasse, T. *Surf. Sci.* **2005**, *596*(1-3), 98–107.

[35] Maennig, B.; Pfeiffer, M.; Nollau, A.; Zhou, X.; Leo, K.; Simon, P. *Phys. Rev. B* **2001**, *64*(19), art. no.–195208.

[36] Stenzel, O.; Wilbrandt, S.; Stendal, A.; Beckers, U.; Voigtsberger, K.; Vonborczyskowski, C. *J. Phys. D* **1995**, *28*(10), 2154–2162.

[37] Sisk, B. C.; Lewis, N. S. *Sens. Actuators B* **2005**, *104*(2), 249–268.

[38] D'Silva, A. P. *Carbon* **1998**, *36*(9), 1317–1325.

[39] Choi, J.; Hormes, J.; Kahol, P. K. *Appl. Phys. Lett.* **2003**, *83*(11), 2288–2290.

[40] Sotzing, G. A.; Briglin, S. M.; Grubbs, R. H.; Lewis, N. S. *Anal. Chem.* **2000**, *72*(14), 3181–3190.

[41] Brousseau, L. C.; Mallouk, T. E. *Anal. Chem.* **1997**, *69*(4), 679–687.

[42] Timmer, B.; Olthuis, W.; van den Berg, A. *Sens. Actuators B* **2005**, *107*(2), 666–677.

[43] Swann, M. J.; Glidle, A.; Cui, L.; Barker, J. R.; Cooper, J. M. *Chem. Commun.* **1998**, (24), 2753–2754.

[44] Joseph, Y.; Guse, B.; Yasuda, A.; Vossmeyer, T. *Sens. Actuators B* **2004**, *98*(2-3), 188–195.

[45] Anderson, R. B.; Emmett, P. H. *J. Phys. Chem.* **1952**, *56*(6), 756–761.

[46] Bomchil, G.; Harris, N.; Leslie, M.; Tabony, J.; White, J. W.; Gamlen, P. H.; Thomas, R. K.; Trewern, T. D. *J. Chem. Soc. Faraday Trans. I* **1979**, *75*, 1535–1541.

[47] Steinbach, F.; Zobel, M. *J. Chem. Soc. Faraday Trans. I* **1979**, *75*, 2587–2593.

[48] McKeown, N. B. *Phthalocyanine Materials: Synthesis, Structure, and Function;* Cambridge University Press: Cambridge, 1998.

[49] Batey, J.; Petty, M. C.; Roberts, G. G.; Wight, D. R. *Electron. Lett.* **1984**, *20*(12), 489–491.

[50] Hua, Y. L.; Jiang, D. P.; Shu, Z. Y.; Petty, M. C.; Roberts, G. G.; Ahmad, M. M. *Thin Solid Films* **1990**, *192*(2), 383–390.

[51] Sakaguchi, M.; Ohta, M. *J. Solid State Chem.* **1986**, *61*(1), 130–134.

[52] Piasecki, R.; Zabkowskawaclawek, M.; Waclawek, W. *Phys. Status Solidi A* **1988**, *108*(1), 331–335.

[53] Murray, B. J.; Walter, E. C.; Penner, R. M. *Nano Lett.* **2004**, *4*(4), 665–670.

[54] Murray, B. J.; Li, Q.; Newberg, J. T.; Hemminger, J. C.; Penner, R. M. *Chem. Mater.* **2005**, *17*(26), 6611–6618.

[55] Murray, B. J.; Newberg, J. T.; Walter, E. C.; Li, Q.; Hemminger, J. C.; Penner, R. M. *Anal. Chem.* **2005**, *77*(16), 5205–5214.

Chapter 3

Detection of Ammonia, 2,4,6-Trinitrotoluene, and Common Organic Vapors Using Thin Film Carbon Black-Metalloporphyrin Composite Chemiresistors

3.1 Abstract

Thin-film chemiresistive composites of octaethylporphine-based transition-metal complexes (Ph(M), M= Co, Cu and Zn) and carbon black (CB) have been fabricated and tested as chemical vapor sensors. The sensing performance of such sensor composites was compared to the sensing performance of composites of metallophthalocyanine (Phtc(M)) and CB. The relative differential resistance response of Ph(M)/CB sensor films upon exposure to organic vapors, such as n-hexane, n-heptane, n-octane, iso-octane, cyclohexane, toluene, ethyl acetate and ethanol, showed a minimal dependence on the on the nature of the metal center. An array of chemiresistive Ph(M)/CB vapor sensors provided discrimination between the organic vapor analytes that had different polarities, specifically classifying

Reproduced in part with permission from *Sens. Actuators B*, **2011**, In press.

non-polar vapors, aprotic polar vapors and protic polar vapors. However, discrimination was not observed for analytes that had mutually similar polarities. The Ph(M)/CB sensors showed reversible responses towards ammonia, NH_3(g), at concentrations below the 8 h permissible exposure level (50 ppm). Ph(M)/CB composites exhibited a slightly larger resistance response than Phtc(M)/CB composites, consistent with the Ph(M) species having less π-stacked molecular aggregates, resulting in an increase in the number of adsorption sites relative to the Phtc(M)/CB composites. Resistance responses with a signal-to-noise ratio value of $\sim$ 900 were obtained upon exposure to vapor pulses saturated with 2,4,6-trinitrotoluene.

3.2 Introduction

By use of bioinspired architectures that take advantage of spatiotemporally based vapor separation capabilities, arrays of chemiresistive sensor films have been used to detect and discriminate between a variety of vapors and/or gases, including organic vapors,[1,2] inorganic gases,[3] and organic vapor mixtures.[4] Composites of carbon black (CB) with polymeric or nonpolymeric organic materials (NPOM) are of interest as chemiresistors, due to the low operating power, as well as the inexpensive and reliable performance, of such materials. The use of NPOM-based sorption films has allowed the fabrication of sensors that have randomly oriented functional groups, providing excellent discrimination between common organic vapors. NPOM/CB composite sensors are capable of both volumetric expansion and adsorptive conductance changes.[3]

The vapor pressure, P° (atm), of the analyte plays an important role in determining

the sensitivity of sorption-based sensors. The value of P° is inversely proportional to the partition coefficient, K, of the vapor-sensor interaction:

$$K = \frac{\rho RT}{\gamma M_w P^{\circ}} \tag{3.1}$$

where ρ is the density of the sensor material (g cm^{-3}), R is the ideal gas constant (cm^3 atm K^{-1} mol^{-1}), T is temperature (K), γ is the activity coefficient within the sensor material and M_w is the molecular weight of the analyte (g mol^{-1}). Hence, the sensitive detection of toxic inorganic gases that have high vapor pressures ($P^{\circ} > 1$ atm), such as NH_3(g), is difficult with sorption-based detectors that primarily operate through van der Waals interactions, because the analyte is predominantly partitioned into the gas phase as opposed to being partitioned into the sorbent phase of the sensor film. One approach to circumventing this limitation is to incorporate specific binding sites for the toxic gases of interest into the sorbent film. For example, chemiresistive composites of CB and metallophthalocyanines (Phtc(M) (M = Co, Cu, Fe, Sn, or Zn) allow for the detection of common organic vapors as well as for sensitive detection of NH_3(g) under ambient conditions.[3] Within this series of complexes, Phtc(Zn)/CB composites were the most sensitive to NH_3(g), demonstrating a limit-of-detection (LOD) of $\sim$ 300 ppb.

One approach to improving further the sensitivity of chemiresistive films to gases such as NH_3(g) is to replace the aromatic phenyl rings of the phthalocyanines with polycyclic compounds that have functional groups which prevent molecular π-stacking.[5] Such an approach should increase the number of binding sites in the film that are available to sorb analyte. Hence, in this work, metalloporphyrins that have multiple ethyl substituents, such

as octaethylporphine transition-metal complexes (Ph(M)), have been investigated as the sorption component of CB composite chemiresistive sensor materials.

For analytes that have low vapor pressures, such as 2,4,6-trinitrotoulene (TNT, P° = 10 ppb at 25 °C), detection is challenging using sorption-based detectors, despite the large K values of such vapors into the sensor films, because of the small number molecules in the gas phase that are available for detection at any instant in time. Detection of explosives, such as TNT, has been performed with chemiresistors,[6] transistors,[7] and fluorescence/ absorption-based sensors.[8–16] As part of this work, the Phtc(M)/CB and Ph(M)/CB composite chemiresistors were also investigated for their sensing performance towards TNT vapor. Such chemiresistors exhibited good sensitivity towards TNT, further broadening the genus of vapors that can be sensitively detected using NPOM/CB chemiresistive sensors.

3.3 Experimental

3.3.1 Sensing Materials

Chemiresistive sensor films were deposited from suspensions that contained Black Pearls 2000 carbon black (Cabot Co.), and the desired NPOM of the composite (Table 3.1), dispersed in 50 mL of tetrahydrofuran (THF, EM Science). The suspensions were sonicated for 2 h and then immediately used for the fabrication of sensor films. The weight fractions of CB were selected to produce optimal signal-to-noise ratios (SNR) for each type of composite film, as described previously.[3]

The sensor substrates were prepared by sequentially evaporating 30 nm of Cr, followed

Sensor Material	M_w (g mol^{-1})	Abbreviation	Source	Amount (mg) Sorbent	CB
2,3,7,8,12,13,17,18-Octaethyl-21H,23H-porphine	534.78	Ph	Aldrich	30	90
2,3,7,8,12,13,17,18-Octaethyl-21H,23H-porphine Co(II)	591.69	Ph(Co)	Aldrich	30	90
2,3,7,8,12,13,17,18-Octaethyl-21H,23H-porphine Cu(II)	596.31	Ph(Cu)	Aldrich	30	90
2,3,7,8,12,13,17,18-Octaethyl-21H,23H-porphine Zn(II)	598.15	Ph(Zn)	Aldrich	30	90
Phthalocyanine	514.54	Phtc	Aldrich	30	90
Co (II) phthalocyanine	571.46	Phtc(Co)	Fluka	30	90
Cu (II) phthalocyanine	576.07	Phtc(Cu)	Aldrich	30	90
Zn (II) phthalocyanine	577.91	Phtc(Zn)	Aldrich	30	90

Table 3.1: Sorption materials used in CB/NPOM composite sensors. The amount values denote the composition of each suspension used for sensor preparation.

by 70 nm of Au, onto masked glass slides. This process produced two metallic electrodes that were separated by a 0.2 cm gap. The sensor films were spray cast onto the substrates using an airbrush (CM-C Plus, Iwata Inc.) that was connected to filtered laboratory air at 1 atm of pressure. Figure 3.1 shows a top-view of the as-prepared Ph(M)/CB films. The composite suspension was sprayed until a nominal resistance of 5 kΩ was measured between the electrodes. Following preparation, the sensors were dried under vacuum for 30 min and were conditioned by exposure for 24 h to pulses of various solvent vapors.

3.3.2 Sensing Measurements

Organic vapors were generated by sparging N_2(g) through 45 cm tall bubblers that had been filled with n-hexane (Hex), n-heptane (Hept), n-octane (Oct), iso-octane (iOct), ethyl acetate (EtOAc) or ethanol (EtOH) (Aldrich). NH_3(g) was obtained as a diluted mixture (Scott Specialty Gas) at a concentration of 3000 ppm in N_2(g). The analyte concentration presented to the sensors was controlled by adjusting the volumetric mixing ratio of the saturated analyte stream to the background N_2(g) stream. The flow rates of the background and foreground gases were regulated under computer control using UNIT mass flow controllers.

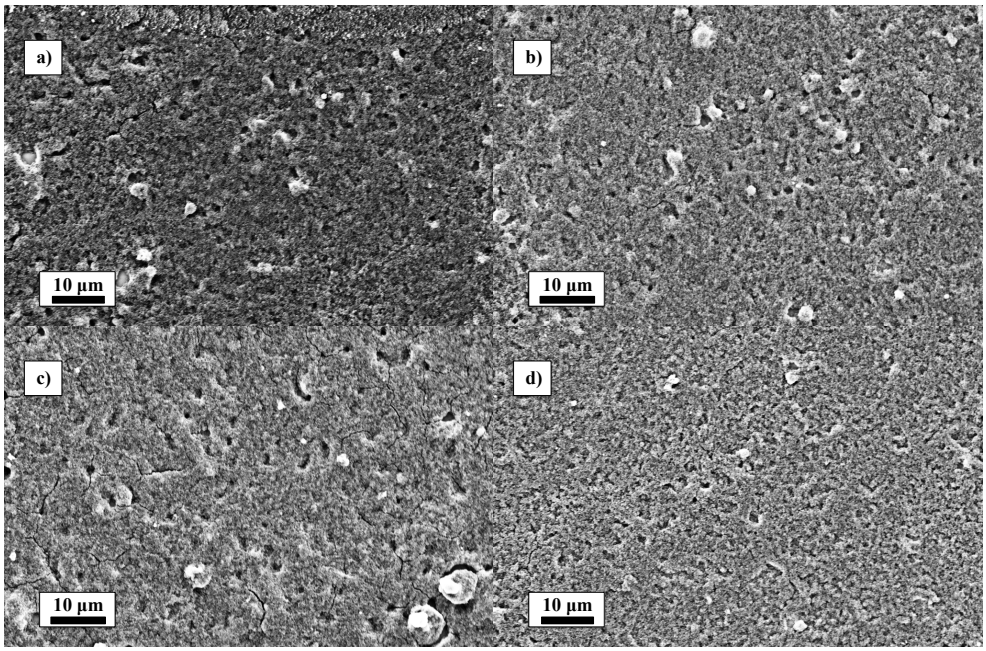

Figure 3.1: Top-view scanning electron micrograph of the as-prepared sensor films, a) Ph/CB, b) Ph(Co)/CB, c) Ph(Cu)/CB and d) Ph(Zn)/CB.

The total flow rate for the entire experiment was maintained at 5 L min^{-1}. Each analyte exposure consisted of 100 s of pure background gas, 100 s of diluted analyte, and then 100 s of background gas to purge the system. The sensors were loaded into a rectangular, 40-slot chamber, with sensor film replicates positioned randomly in the chamber. No dependence was observed on the performance of a given sensor on its spatial position in the array. The 45.5 cm long $\times$ 3.0 cm wide $\times$ 1.5 cm deep chamber was connected by Teflon tubing to the gas delivery system. The resistance of each of the sensors in the array was measured sequentially by a Keithley 2002 multimeter coupled to a Keithley 7001 multiplexer, with $\sim$ 7 s between measurements on the same sensor. The measurement electronics were interfaced to a computer via a GPIB connection and were controlled with LabVIEW software.

A custom vapor delivery system was built (Figure 3.2) to allow for TNT exposures. First, a sealed 450 mL glass container that contained $\sim$ 5 g of TNT was connected by teflon

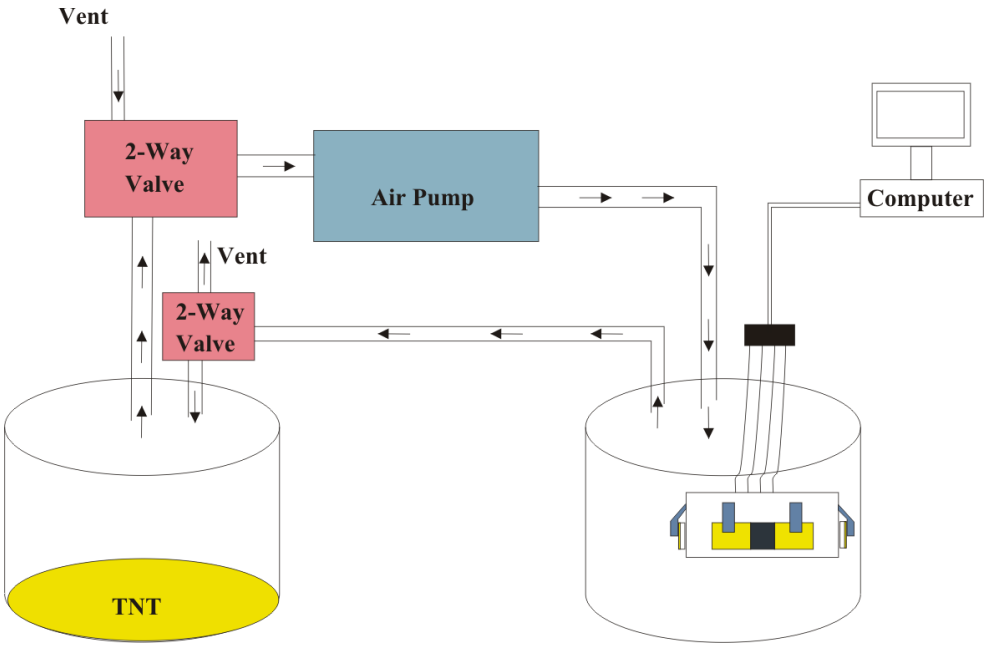

Figure 3.2: Vapor delivery system for 2,4,6-trinitrotoluene (TNT).

tubing to two-way valves. One of the valves was connected to an air pump that circulated air at a constant flow rate of 150 mL min^{-1}. A secondary 450 mL glass container that enclosed an array of 4 sensors was connected to the output of the pump space. The valves were computer-controlled using LabVIEW to deliver 200 s saturated pulses of TNT vapor. To purge the system, the valves were opened to air.

3.3.3 Signal Processing

All data processing was carried out using custom-written routines in MATLAB. The resistance-based response of a vapor sensor to a particular analyte was calculated as $\Delta R_{max}/R_b$, where R_b is the baseline-corrected resistance of the sensor in the absence of analyte, and ΔR_{max} is the baseline-corrected maximum resistance change upon exposure of the sensor to the analyte of interest. A spline was fitted to the baseline data obtained during the pre-exposure period, and values of $\Delta R_{max}/R_b$ were calculated by subtracting the values of the spline,

extrapolated over the time of the exposure, from the observed sensor resistance during the exposure period.[2] For organic vapors, the sensitivity of a resistance-based vapor sensor film, s_R, was calculated using a linear least-squares fit to determine the slope of $\Delta R_{max}/R_b$ vs. P/P°. SNR values were calculated by use of $SNR = \Delta R_{max}/s_{baseline}$, where $s_{baseline}$ is the standard deviation of R_b.

3.3.4 Discrimination Performance

To remove any systematic variation in the data that might have been produced by changes in the concentration of analyte eminating from the vapor delivery system, the $\Delta R_{max}/R_b$ responses were sum-normalized prior to analysis:[17]

$$S'_{ij} = S_{ij} \left(\sum_{j=1}^{n} S_{ij}^2) \right)^{-1/2} \tag{3.2}$$

where S_{ij} is the $\Delta R_{max}/R_b$ sensor response signal of the j^{th} sensor (out of n total sensors) to the i^{th} analyte exposure, and S'_{ij} represents the sum-normalized analog of S_{ij}.

Differences in the sensor response data were visualized using principal components analysis (PCA). The normalized data were mean-centered, and diagonalization of the covariance matrix of the data set provided a transformed set of dimensions that best described the data in terms of principal components (PCs). The 1st PC captured the largest amount of variance in the data; the 2nd PC captured the second most variance in the data (subject to being orthogonal to the 1st PC), etc. The mean-centered data were then projected onto the first, second and third PCs, and the data were plotted with respect to these coordinate vectors to observe the natural clustering of the data points. The eigenvalues of the

mean-centered covariance matrix provided the relative amounts of variance in each of the corresponding eigenvectors, allowing quantification of the amount of the variance that was captured in the 3-dimensional PC space.

3.4 Results

3.4.1 Detection of Organic Vapors

Figure 3.3 displays the resistance response sensitivities, s_R, for the Ph(M)/CB sensors and for Phtc(Zn)/CB obtained upon exposure to eight analyte vapors. Similar values of s_R were obtained for the different types of Ph(M)/CB and Phtc(Zn)/CB sensors in response to a given vapor. The lowest s_R values were obtained for the Ph/CB and Ph(Co)/CB sensor films, whereas Ph(Cu)/CB, Ph(Zn)/CB and Phtc(Zn)/CB produced slightly higher s_R values. The average SNR value obtained upon exposure to the eight vapors analytes were 420 $\pm$ 232 for Phtc(M) (i.e. Phtc, Phtc(Co), Phtc(Cu) and Phtc(Zn)) and 425 $\pm$ 199 for Ph(M) (i.e. Ph, Ph(Co), Ph(Cu) and Ph(Zn)).

3.4.2 Detection of NH_3(g)

Figure 3.4 displays the average $\Delta R_{max}/R_b$ values for the Ph(M)/CB and Phtc(M)/CB composite sensors obtained upon exposure to 25 pulses of 30 ppm of NH_3(g). The unmetallated Ph/CB sensor exhibited a 2-fold $\Delta R_{max}/R_b$ higher response than the Phtc/CB sensor. For metallated films, the Ph(Co)/CB films yielded a 50 % increase in response relative to that of the Phtc(Co)/CB sensors, whereas the Ph(Cu)/CB films yielded a 3-fold increase in re-

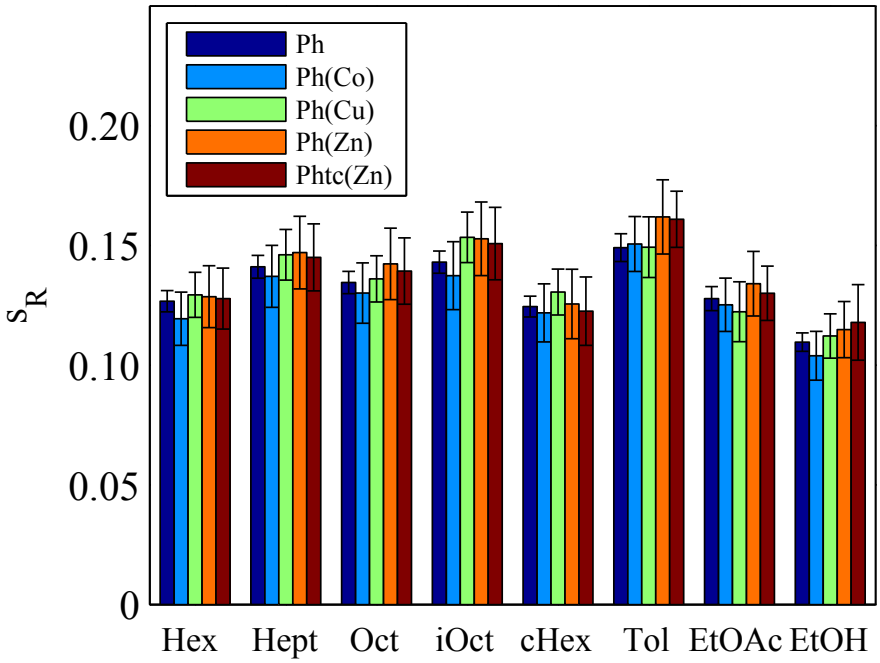

Figure 3.3: Resistance response sensitivity, s_R, for all Ph(M)/CB and Phtc(Zn)/CB sensors. Each s_R value represents the average over three sensor replicates for every sensor type upon exposure to eight chemical vapors.

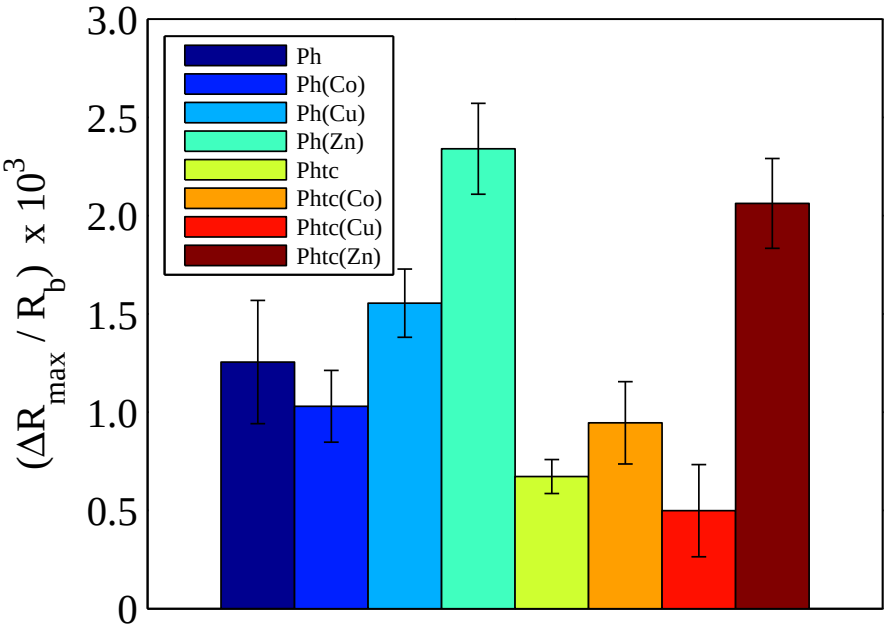

Figure 3.4: Maximum differential resistance response, $\Delta R_{max}/R_b$, values for the Ph(M) and Phtc(M) /CB sensors upon exposure to 30 ppm of NH_3(g).

sponse relative to that of the Phtc(Cu) sensors. In contrast, the Ph(Zn)/CB films produced only a slightly higher $\Delta R_{max}/R_b$ value than did the Phtc(Zn)/CB films. Figure 3.5 displays the response of the sensors as a function of exposure time. For all sensors, upon exposure to 30 ppm of NH_3(g), after 30-40 s, the $\Delta R_{max}/R_b$ response plateaued, and thereafter only increase slowly, at a rate $\delta(\Delta R_{max}/R_b)$ / $\delta t \approx 1 \times 10^{-3}$ s^{-1}, where t is time in s. Among the Ph(M)/CB sensors, Ph(Zn)/CB produced the highest $\Delta R_{max}/R_b$ value at any t. All of the sensors displayed a reversible response to NH_3(g) and to the tested organic vapors. Figure 3.6 displays the $\Delta R_{max}/R_b$ value as a function NH_3(g) concentration, for the Ph(M)/CB sensors and for Phtc(Zn)/CB. The response of all of the sensors clearly saturated as the NH_3(g) concentration increased. The data were well-fit by a Langmuir adsorption isotherm type of response.

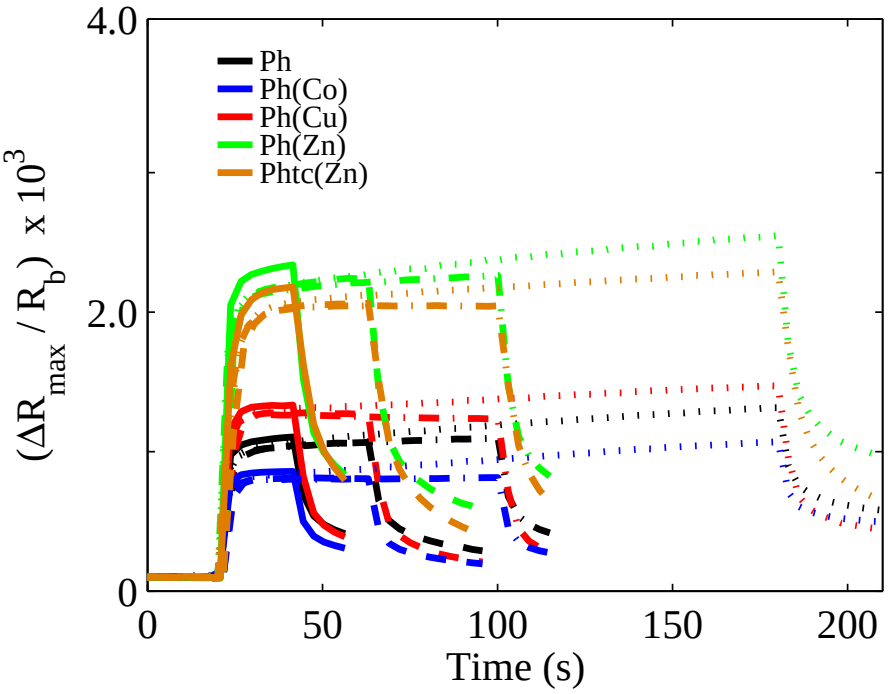

Figure 3.5: Differential resistance response, $\Delta R_{max}/R_b$, values as a function of time for the Ph(M)/CB sensors and Phtc(Zn)/CB upon exposure to 30 ppm of NH_3(g).

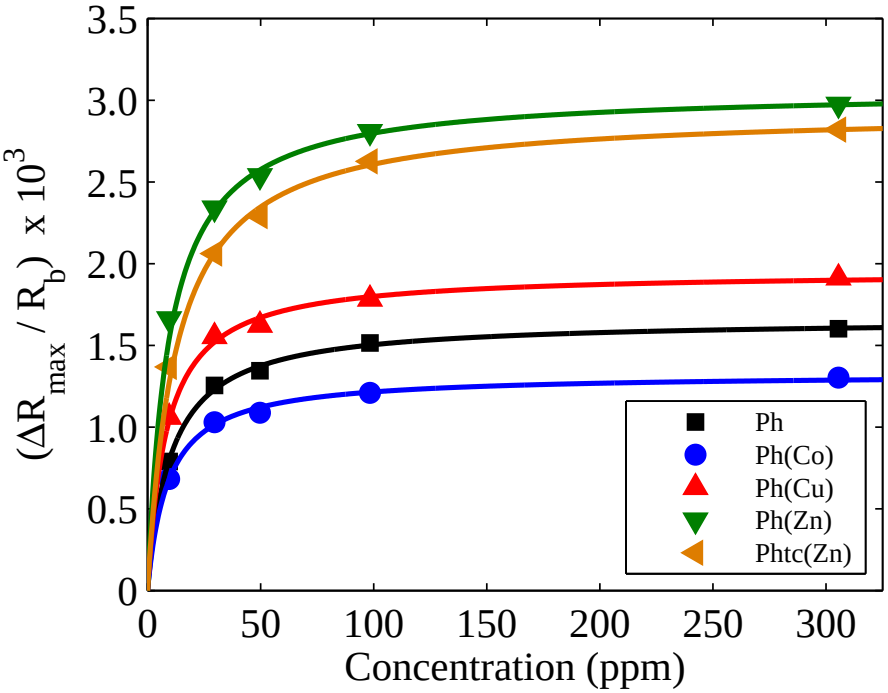

Figure 3.6: $\Delta R_{max}/R_b$, values for the Ph(M)/CB sensors and Phtc(Zn)/CB upon exposure to six different concentrations (10, 30, 50, 98 and 305 ppm) of NH_3(g).

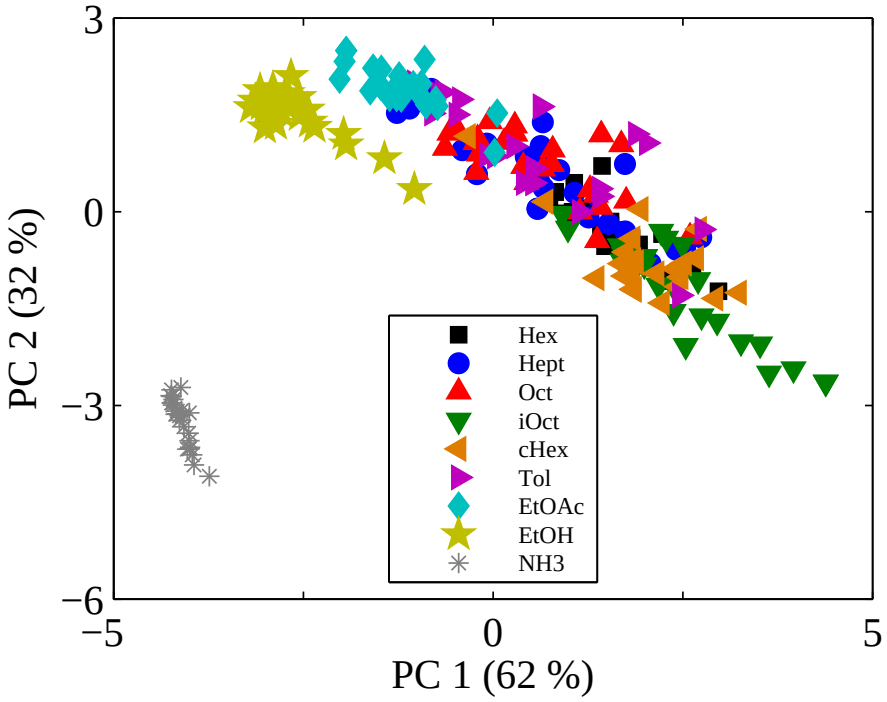

Figure 3.7: Principal components analysis of the response of an array composed of the Ph(M)/CB sensors. The 1st and the 2nd principal components were used for the projection, with their respective captured variance from the $\Delta R_{max}/R_b$ data.

3.4.3 Discrimination Performance

Figure 3.7 displays the PCA projection of an array of Ph(M)/CB sensors upon exposure to eight organic vapors (25 exposures per analyte) as well as upon exposure to NH_3(g). As observed for Phtc(M)/CB sensors,[3] the array of Ph(M)/CB sensors was able to discriminate between the polarity of the vapors, i.e. non-polar vs. polar aprotic vs. polar protic vapors. Conversely, misclassification, or cluster overlapping, was observed for vapors that fell in the non-polar clusters of the Ph(M)/CB sensor array response. The EtOAc and EtOH clusters were well separated from the non-polar vapor cluster group, and the NH_3(g) cluster was well-separated from all of the organic vapors.

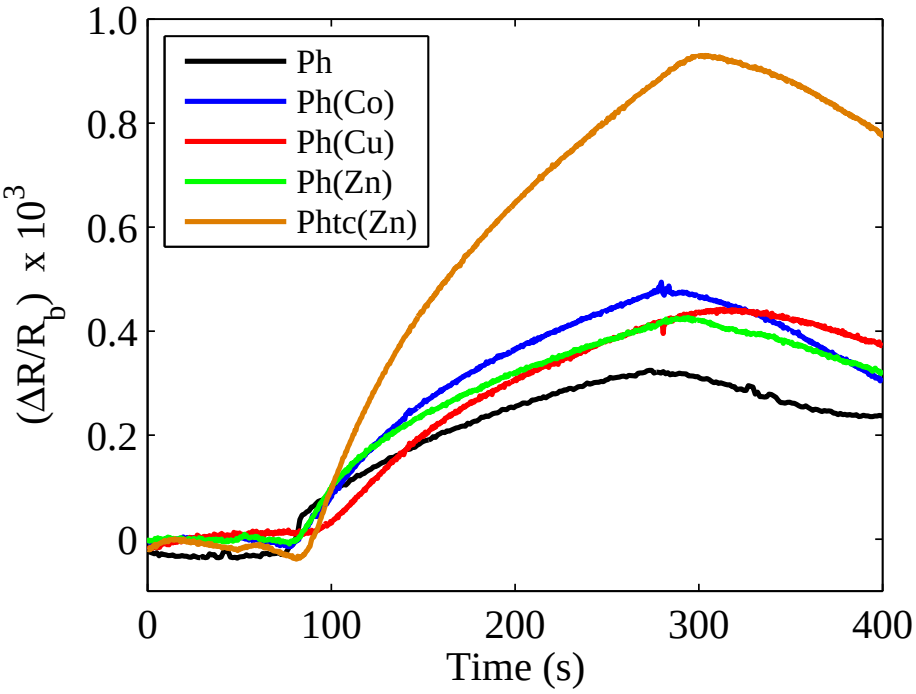

Figure 3.8: Relative differential resistance response, $\Delta R_{max}/R_b$, for the Ph(M)/CB sensors and Phtc(Zn)/CB upon exposure to saturated pulses of 2,4,6-trinitrotoluene (TNT) vapor.

3.4.4 TNT Detection

Figure 3.8 shows the response of the Ph(M)/CB sensor and of a Phtc(Zn)/CB sensor to a 200 s pulse of TNT vapor. The time-response of $\Delta R_{max}/R_b$ was limited by the vapor delivery flow rate (i.e. 150 mL min^{-1}). The Phtc(Zn)/CB sensor produced the highest $\Delta R_{max}/R_b$ response, and the Ph(M)/CB sensors produced mutually similar $\Delta R_{max}/R_b$ values. Figure 3.9 shows a single response of a Ph(Zn)/CB sensor to a variety of saturated vapors (P/P° = 1), such as acetone, toluene, water and TNT. The $\Delta R_{max}/R_b$ response obtained upon exposure to TNT was different from the $\Delta R_{max}/R_b$ responses obtained upon exposure to water, acetone and toluene. Such difference could allow for excellent TNT identification.

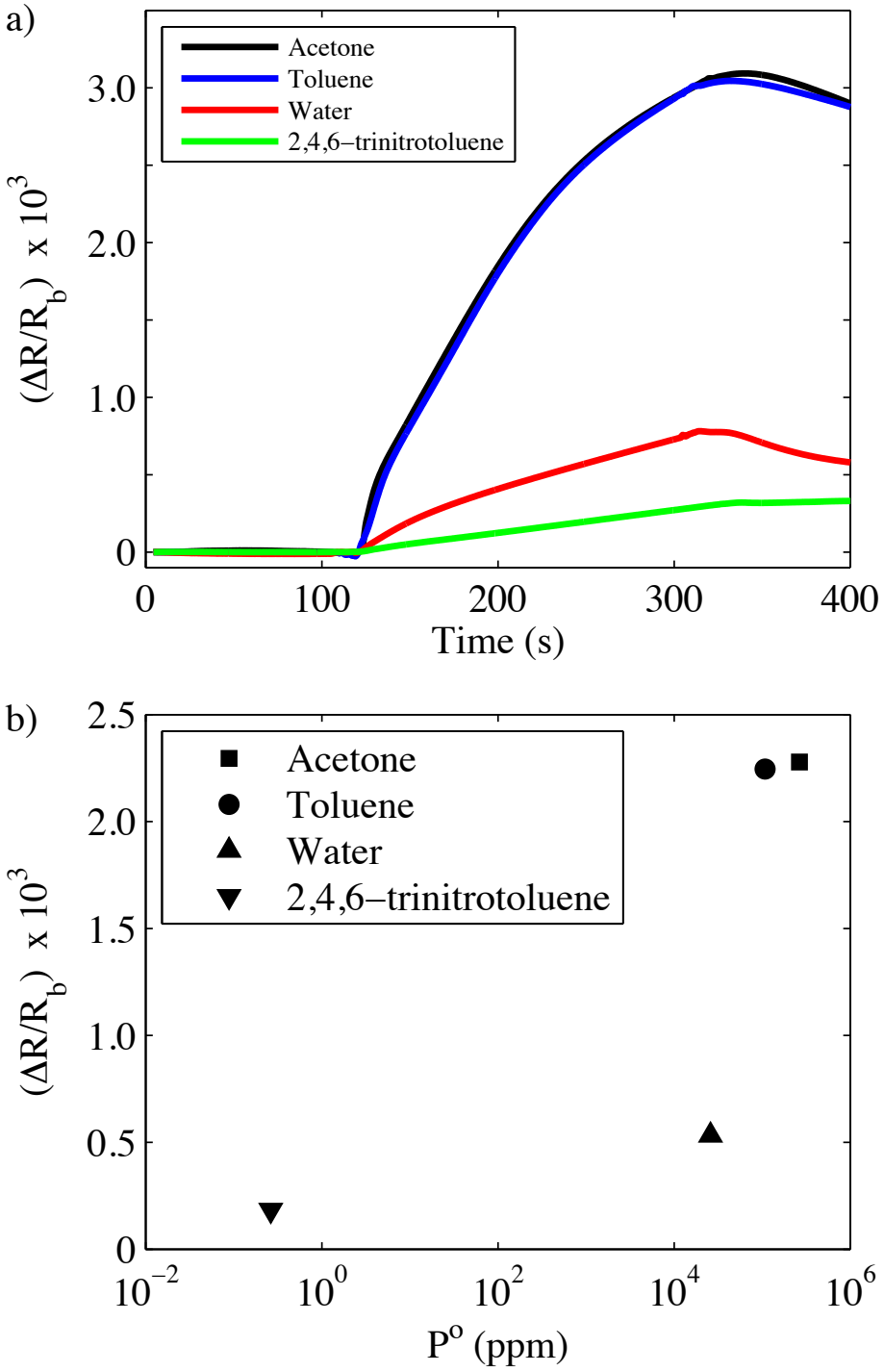

Figure 3.9: (a) Single relative differential resistance response for a Ph(Zn)/CB sensor upon exposure to saturated acetone, toluene, water and 2,4,6-trinitrotoluene, respectively, and (b) maximum differential resistance response, $\Delta R_{max}/R_b$, as a function of P° (ppm) for a Ph(Zn)/CB upon exposure to acetone, toluene, water or 2,4,6-trinitrotoluene.

3.5 Discussion

3.5.1 Response to Organic Vapors

For organic test vapors, only small differences in the value of s_R were observed between the various Phtc(M)/CB and Ph(M)/CB sensors. This is expected because the only significant molecular difference among the molecules was the transition-metal center of the polycyclic compound. The solubility was also different between the porphyrin-based molecules, with Ph(Zn) being the most soluble complex in tetrahydrofuran (THF). The presence of aggregates or insoluble particles in the Ph, Ph(Co) and Ph(Cu) solutions in THF was observed. Such aggregates produced different film morphologies as observed in Figure 3.1, and different amounts of accessible binding sites in the chemiresistive films. The Ph/CB, Ph(Co) and Ph(Cu) films exhibited the presence or π-stacked aggregates, contrary to Ph(Zn)/CB that exhibited a more uniform film with less π-stacked aggregates. Similar results were obtained for the Phtc(M)/CB films. Such differences did not however, produce significant changes in the value of s_R for each sensor measured upon exposure to a given test organic vapor. The high proportion of organic material in each Ph(M)/CB composite, compared to the inorganic transition-metal center, dominated the sorption response behavior and thus produced similar values of s_R for all the sensors studied. Conversely, differences in the peripheral substituents of the polycyclic aromatic compound could increase the chemical diversity and thereby to produce different values of s_R, even if the transition-metal center is maintained constant.[3]

3.5.2 Response to NH_3(g)

The Ph(M)/CB sensors produced higher responses to NH_3(g) than did the Phtc(M)/CB sensors. This behavior is consistent with expectations in which the Ph(M)/CB films exhibit less π-stacking than the Phtc(M)/CB sensors, and thus have a larger number of accessible binding sites available to adsorb analyte. The Ph(Zn) and Phtc(Zn) were the most soluble complexes from each group, hence these films contained fewer π-stacked aggregates. Consistently, for either Ph(M)/CB and Phtc(M)/CB films, the Ph(Zn)/CB or Phtc(Zn)/CB sensor produced the highest observed signals in response to a given analyte.

The $\Delta R_{max}/R_b$ value of all of the sensors increased as the concentration of NH_3(g) increased, until a plateau was reached in the response magnitude. The sensor films have a limited number of adsorption sites, hence at $\sim$ 100 ppm of NH_3(g), the available adsorption sites were saturated with NH_3(g). After the saturation pressure, P_s, was reached, the response value became independent of the NH_3(g) concentration.

3.5.3 Discrimination Performance

The Ph(M)/CB sensor array readily discriminated between non-polar, aprotic polar, protic polar, and NH_3(g) vapors. Furthermore, the response adsorption mechanism of Ph(M)/CB films produced a unique fingerprint for NH_3(g) relative to organic vapors. However, such sensors were not able to differentiate between chemically similar non-polar vapors. The volumetric swelling of such films resulted in mutually similar sorption of the non-polar analytes, producing non-unique s_R values, non-unique response fingerprints, and therefore overlapping PCA clusters.

3.5.4 Response to TNT

Sensitive responses were obtained for TNT exposures, producing SNR values of 910, 980, 760, 860 and 890 for Ph/CB, Ph(Co)/CB, Ph(Cu)/CB, Ph(Zn)/CB and Phtc(Zn)/CB sensors, respectively. The estimated value of LOD (SNR = 3) for the Ph(M)/CB or Phtc(M)/CB composite sensors was $\sim$ 30 ppt, which is comparable to that reported for a hybrid nanosensor,[18] or fluorescence based detectors.[19] The observed difference in the vapor-induced resistance response rate (Figure 3.9) can be attributed to the different sublimation rates of the test analytes.[20,21] The vapor delivery/detection system could be employed for the detection of other analytes, as observed in Figure 3.9. The vapor concentration profile of the containers in Figure 3.2 can be described by:

$$\frac{dC_1(t)}{dt} = -\frac{f_r}{V}C_1(t) + \frac{f_r}{V}C_2(t) + A_{law} - k_{subl}C_1(t) \tag{3.3a}$$

$$\frac{dC_2(t)}{dt} = \frac{f_r}{V}C_1(t) - \frac{f_r}{V}C_2(t) \tag{3.3b}$$

where $C1(t)$ and $C2(t)$ are the concentrations of analyte in container 1 (TNT) and container 2 (sensor array), f_r is the flow rate (150 mL min^{-1}), V is the volume of each container (450 mL min^{-1}), A_{law} is a term associated with the rate law, and k_{subl} is a constant associated with the sublimation rate. The analyte concentration profile in each container is depicted in Figure 3.10. Initially, the analyte in container 1 was at P°. The time needed to reach the inflection point observed can be varied by varying the value of f_r and the value of k_{subl} dominates the rate at which the concentration of vapor reached P° in both containers.

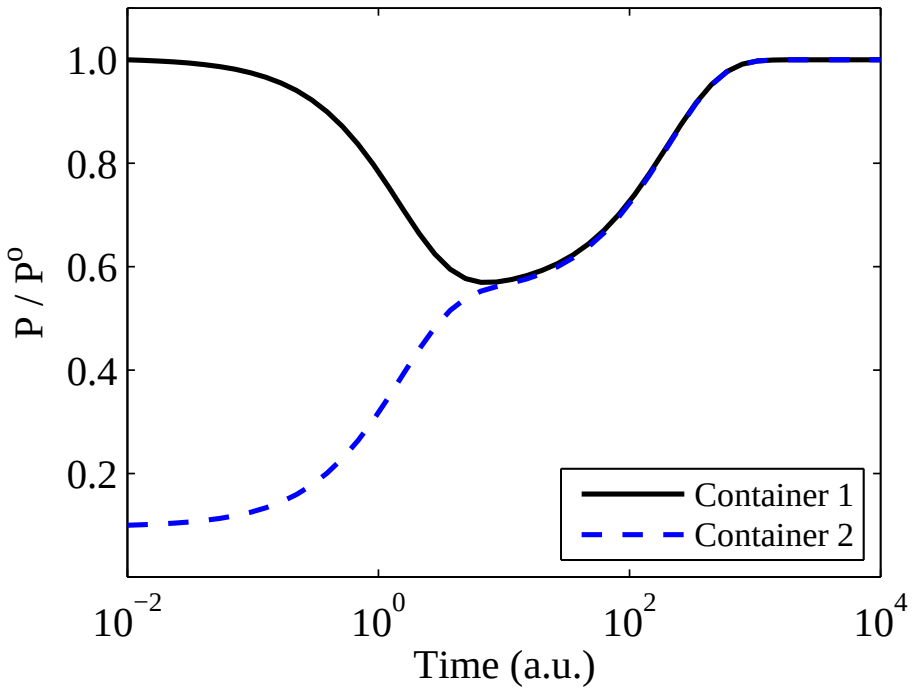

Figure 3.10: Concentration profile for the vapor delivery system used for the TNT saturated vapor.

3.6 Conclusions

Composite chemiresistive sensor films of Ph(M)/CB did not produce distinctive individual sensitivity differences in response to a series of test organic vapors. Nevertheless, an array of sensors comprised of Ph(M)/CB composites exhibited discrimination between different analytes based on their polarity, that is non-polar vapors were separated from aprotic polar vapors, which in turn were separated from protic polar vapors. The resistance response sensitivity of Ph(M)/CB films did not show a dependence on the identity of the transition-metal center in response to assorted organic vapors, because of the high volume or organic material in each Ph(M)/CB composite, compared to the value of the inorganic transition-metal center. The organic phase dominated the sorption response behavior and thus produced

similar values of s_R for organic test vapors.

For NH_3(g) detection, Ph(M)/CB sensors showed reversible responses at concentrations below the 8 h permissible exposure level (50 ppm), and the NH_3(g) array response was easily differentiated from that produced by organic vapors. The NH_3(g) saturation pressure for a Ph(M)/CB or Phtc(M)/CB sensor film was determined to be $\sim$ 100 ppm. An increase in response to NH_3(g) was obtained when Ph(M)/CB sensors were used relative to the Phtc(M)/CB sensors, due to fewer π-stacked molecular aggregates that produced a higher number of binding sites.

For saturated TNT vapor pulses, a signal-to-noise ratio of $\sim$ 900 was obtained using Ph(M)/CB and Phtc(M)/CB sensor films enclosed in a low-power, simple, vapor delivery system. The limit of detection obtained for Ph(M)/CB or Phtc(M)/CB sensors in response to TNT vapor pulses was determined to be $\sim$ 30 ppt, which is comparable to state-of-the art sensors that involves the measurement of the electrochemical reduction of TNT and the interaction of the reduction products with conducting polymer nanojunctions in an ionic liquid.

Bibliography

[1] Gao, T.; Woodka, M. D.; Brunschwig, B. S.; Lewis, N. S. *Chem. Mater.* **2006**, *18*(22), 5193–5202.

[2] Garcia-Berrios, E.; Gao, T.; Maldonado, S.; Woodka, M. D.; Ellsworth, M. W.; Brunschwig, B. S.; Lewis, N. S. *J. Phys. Chem. C* **2010**, *114*, 21914–21920.

[3] Maldonado, S.; Garcia-Berrios, E.; Woodka, M. D.; Brunschwig, B. S.; Lewis, N. S. *Sens. Actuators B* **2008**, *134*(2), 521–531.

[4] Woodka, M. D.; Brunschwig, B. S.; Lewis, N. S. *Langmuir* **2007**, *23*(26), 13232–13241.

[5] Reddy, P. Y.; Giribabu, L.; Lyness, C.; Snaith, H. J.; Vijaykumar, C.; Chandrasekharam, M.; Lakshmikantam, M.; Yum, J. H.; Kalyanasundaram, K.; Graetzel, M.; Nazeeruddin, M. K. *Angew. Chem.* **2007**, *46*(3), 373–376.

[6] Burl, M. C.; Briglin, S.; Doleman, B. J.; Hopkins, A.; Matzger, A.; Ortiz, D. N.; Schaffer, A. C.; Upchurch, S.; Vaid, T. P.; Lewis, N. S. *Soc. Ind. Appl. Math.* **2001**, pages 1–15.

[7] Huang, J.; Dawidczyk, T. J.; Jung, B. J.; Sun, J.; Mason, A. F.; Katz, H. E. *J. Mater. Chem.* **2010**, *20*(13), 2644–2650.

[8] Brittle, S.; Richardson, T. H.; Dunbar, A. D. F.; Turega, S.; Hunter, C. A. *J. Phys. Chem. B* **2008**, *112*(36), 11278–11283.

[9] Dunbar, A. D. F.; Brittle, S.; Richardson, T. H.; Hutchinson, J.; Hunter, C. A. *J. Phys. Chem. B* **2010**, *114*(36), 11697–11702.

[10] Narayanan, A.; Varnavski, O. P.; Swager, T. M.; Goodson, T. *J. Phys. Chem. C* **2008**, *112*(4), 881–884.

[11] Pushkarsky, M. B.; Webber, M. E.; Macdonald, T.; Patel, C. K. N. *Appl. Phys. Lett.* **2006**, *88*(4), –.

[12] Rose, A.; Lugmair, C. G.; Miao, Y. J.; Kim, J.; Levitsky, V. E.; Williams, T. M.; Swager, T. M. *Proc. Int. Soc. Opt. Eng.* **2000**, *4038*, 512–518.

[13] Swager, T. M. *Acc. Chem. Res.* **2008**, *41*(9), 1181–1189.

[14] Tao, S. Y.; Li, G. T.; Zhu, H. S. *J. Mater. Chem.* **2006**, *16*(46), 4521–4528.

[15] Woodka, M. D.; Schnee, V. P.; Polcha, M. P. *Anal. Chem.* **2010**, *82*(23), 9917–9924.

[16] Zhu, D. F.; He, Q. G.; Cao, H. M.; Cheng, J. G.; Feng, S. L.; Xu, Y. S.; Lin, T. *Appl. Phys. Lett.* **2008**, *93*(26), –.

[17] Otto, M. *Statistics and Computer Application in Analytical Chemistry;* Wiley-VCH: New York, 1999.

[18] Aguilar, A. D.; Forzani, E. S.; Leright, M.; Tsow, F.; Cagan, A.; Iglesias, R. A.; Nagahara, L. A.; Amlani, I.; Tsui, R.; Tao, N. J. *Nano Lett.* **2010**, *10*(2), 380–384.

[19] Cumming, C. J.; Aker, C.; Fisher, M.; Fox, M.; la Grone, M. J.; Reust, D.; Rockley, M. G.; Swager, T. M.; Towers, E.; Williams, V. *IEEE Trans. Geosci. Remote Sens.* **2001**, *39*(6), 1119–1128.

[20] Mu, R.; Ueda, A.; Wu, M. H.; Tung, Y. S.; Henderson, D. O.; Chamberlain, R. T.; Curby, W.; Mercado, A. *J. Phys. Chem. B* **2000**, *104*(1), 105–109.

[21] Mu, R.; Ueda, A.; Liu, Y. C.; Wu, M.; Henderson, D. O.; Lareau, R. T.; Chamberlain, R. T. *Surf. Sci.* **2003**, *530*(1-2), L293–L296.

Chapter 4

Response versus Chain Length of Alkanethiol-Capped Au Nanoparticle Chemiresistive Chemical Vapor Sensors

4.1 Abstract

Au nanoparticles capped with a homologous series of straight chain alkanethiols (containing 4-11 carbons in length) have been investigated as chemiresistive organic vapor sensors. The series of alkanethiols was used to elucidate the mechanisms of vapor detection by such capped nanoparticle chemiresistive films and to highlight the molecular design principles that govern enhanced detection. The thiolated Au nanoparticle chemiresistors demonstrated rapid and reversible responses to a set of test vapors (n-hexane, n-heptane, n-octane, iso-octane, cyclohexane, toluene, ethyl acetate, methanol, ethanol, isopropanol, and 1-butanol) that possessed a variety of analyte physicochemical properties. The resistance sensitivity to nonpolar and aprotic polar vapors systematically increased as the chain length of the capping reagent increased. Decreases in the nanoparticle film resistances, which produced negative values of the differential resistance response, were observed upon exposure of the

Reproduced in part with permission from *J. Phys. Chem. C*, **2010**, *114*, 21914-21920

sensor films to alcohol vapors. The response signals became more negative with higher alcohol vapor concentrations, producing negative values of the sensor sensitivity. Sorption data measured on Au nanoparticle chemiresistor films using a quartz crystal microbalance allowed for the measurement of the partition coefficients of test vapors in the Au nanoparticle films. This measurement assumed that analyte sorption only occurred at the organic interface and not the surface of the Au core. Such an assumption produced partition coefficient values that were independent of the length of the ligand. Furthermore, the value of the partition coefficient was used to obtain the particle-to-particle interfacial effective dielectric constant of films upon exposure to analyte vapors. The values of the dielectric constant upon exposure to alcohol vapors suggested that the observed resistance response changes observed were not significantly influenced by this dielectric change, but rather were primarily influenced by morphological changes and by changes in the interparticle spacing.

4.2 Introduction

Sensor arrays have attracted significant interest due to their ability to classify and quantitate analytes in liquid and gaseous environments.[1] Chemiresistive thin films comprised of an insulating organic polymer or small molecule material combined with electronically conductive carbon black particles are attractive because such sensors are low power and are broadly responsive to a variety of analytes.[2–4] Chemiresistive composite sensors generally operate via a volumetric sensing modality wherein a vapor-induced volumetric expansion of the film produces a reversible change in the DC resistance of the film.[2] Sensor films of

Au nanoparticles (Au-NPs) capped with organothiol ligands have also been investigated.[5–7] Organically capped metal nanoparticles consist of a small metal core (typically less than 10 nm in diameter) surrounded by a dense organic layer of insulating material that is used to chemically protect the metal particles. These materials, with an approximate stoichiometry of 3:1 (Au/S-R), are easily synthesized using wet chemical techniques and can remain soluble for extended periods in common organic solvents.[8–10] Sensors can be prepared by the deposition of a thin film of the Au-NPs between two metal electrodes. Measurement of the resistance of the film provides a facile method for transduction of the sorption of organic vapor into a detectable electrical signal. As opposed to conventional polymer/carbon black composites, in which the insulating matrix and conducting species are in physical contact, capped Au-NPs have both constituents chemically bound together. Generally, in such sensors, the amount of analyte sorbed by the film is negligible compared with the amount of material in the organic phase. Upon exposure to organic vapors, analyte partitions into the film, effecting changes in the electrical conductivity of the film through changes in the films morphology (e.g., in the film swelling through changes in the interparticle spacing) or in the physical properties of the film, such as its dielectric constant. In the majority of cases, swelling predominates and the resistance of the film increases upon exposure to an analyte; however, in some cases, decreases in resistance have been Au-NP sensors have been studied (e.g., electric resistance, resonator frequency change) using Au-NPs capped with alkanethiols,[7] dithiols,[11–13] π-conjugated thiols,[14–16] hydroxy and carboxylic-terminated alkanethiols,[11] carboxylic-metal-carboxylic ligands,[17] dendrimers,[12,18–20] and mixture of ligands,[21] as well as other ligands.[22–24] Wohjtlen et al. introduced these materials as chemical sen-

sors using octanethiol-capped Au-NPs.[7] Increases in the electrical resistance were observed when the sensors were exposed to toluene or tetrachloroethylene vapors. Surprisingly, for hydrophilic vapors such as 1-propanol, ethanol, and water, a decrease in the electrical resistance was observed when long chain alkanethiols were used as capping ligands.[7] Guo et al. demonstrated that, when alkanethiol-capped Au- NP films that contained traces of the phase-transfer reagent tetraoctylammonium bromide (TOABr) used in the Au-NP synthesis were used as chemiresistive sensors, the film resistance decreased when the sensors were exposed to water vapor.[25] The ability to control the sign of the sensor response to an analyte by use of different phase-transfer reagents would add unique capabilities to arrays of such sensors and would therefore significantly increase their ability to identify or classify vapors. The electronic conductivity of the organothiol capped Au-NP films is the result of electrons hopping between Au-NP centers in the film. Empirically, the conductivity of a film, σ, can be described by

$$\sigma = \sigma_{\circ} \exp[-A/k_B T] \tag{4.1}$$

where $\sigma_{\circ}$ and A are constants. Initially, the hopping was described by granular metal theory, with A interpreted as an activation energy associated with the creation of a positive and negative pair of NPs from two NPs.[26,27] More recently, Murray and co-workers[21,28–33] have described the hopping as the transfer of an electron from a negative (or neutral) Au-NP site to a neighboring neutral (or positive) Au-NP site. This view treats each hop as equivalent to an electron exchange in a mixed valence system. Thus, for conduction by this method, both oxidized (or reduced) and neutral Au-NP sites must exist in the film. For neutral Au-NP films, the mixed valence sites could be produced by spontaneous disproportionation

$$2[\text{Au-NP}] \rightarrow [\text{Au-NP}]^{+} + [\text{Au-NP}]^{-}$$

Electron-exchange has been theoretically described by Marcus.[34] In this approach, the prefactor $\sigma_\circ$ is related to the coupling between the two centers, and is dependent on distance with a form of

$$\sigma_\circ = \sigma^\circ \exp[-(2a - r)\beta] \tag{4.2}$$

where σ° is the maximum conductance for particles that are separated by a distance $2a$, a is the radius of the NP, and r is the is the NP center-to-center separation distance. In this framework, the value of A in eq. 4.1 is interpreted as arising from the reorganizational barrier that results from the requirement that the electron-transfer pair reorganize to a nuclear configuration that is energetically degenerate for the electron on either center. Thus, A is given by

$$A = \lambda/4 \tag{4.3}$$

where λ is the reorganization energy for the electron exchange process. The reorganization energy is primarily the result of the polarization of the medium by the charged centers, and for particles separated by $2a + \delta$, λ is given by

$$\lambda = \frac{e^2}{4\pi\varepsilon_\circ}\left(\frac{1}{a} - \frac{1}{2a+\sigma}\right)\left(\frac{1}{\epsilon_{op}} - \frac{1}{\epsilon_s}\right) \tag{4.4}$$

where $\varepsilon_\circ$ is the permittivity of free space, and ϵ_{op} and ϵ_s are the optical and static dielectric permittivity of the medium, respectively.[34,35] Murray has advanced a series of arguments in favor of the mixed-valence type of electron hopping dominating the transport in such

films. In this work, we have explored the effect of changing the length of the Au-NP capping alkanethiol (R-SH) on the performance of such films as chemical vapor sensors by investigating the response sensitivity to a variety of vapors. We have also investigated the influence of the physicochemical properties of sorbed analyte on the relative differential resistance response of the Au-NP film by using a dielectric constant model for mixtures of two components (e.g., capping ligand and the sorbed analyte). The relative differential resistance response values were compared to the dielectric constant change produced by analyte sorption, to elucidate whether negative responses arise from a dielectric change or other extrinsic film components. Information about the amount of analyte material sorbed at the Au-NP films was obtained by using the partition coefficient of the sensor/analyte combination as determined by quartz crystal microbalance (QCM) measurements. The determination of the partition coefficients of the Au-NP films assumed that analyte sorption occurred at the organic ligand, and that zero or negligible sorption occurred at the metal core. The response values as a function of temperature have also been investigated.

4.3 Experimental

4.3.1 Materials

Sodium borohydride ($NaBH_4$, 99 %), hydrogen tetrachloroaurate trihydrate ($HAuCl_4 \cdot 3H_2O$, ACS reagent), tetraoctylammonium bromide (TOABr, g 99 %), 1-butanethiol (99 %), 1-pentanethiol (98 %), 1-hexanethiol (97 %), 1-heptanethiol (98 %), 1-octanethiol (98.5 %), 1-nonanethiol (95 %), 1-decanethiol (96 %), 1-undecanethiol (98 %), and the test analytes

(n-hexane, n-heptane, n-octane, iso-octane, cyclohexane, toluene, ethyl acetate, methanol, ethanol, isopropanol, and 1-butanol) were obtained from Aldrich Chemical Corp., except for 1-hexanethiol (97 %), which was obtained from Alfa Aesar. All of the reagents and solvents were used without further purification. The 18 MΩ cm resistivity deionized water was obtained from a Barnstead Nanopure purification system.

Au-NPs capped with R-S functionality were synthesized as described by Brust et al.,[8] with the use of TOABr. Briefly, 4.56 g of TOABr was dissolved in 165 mL of toluene in a 1000 mL round-bottom flask. A solution containing 0.8025 g of $HAuCl_4 \cdot 3H_2O$ dissolved in 60 mL of deionized water was then added. The resulting dark-red biphasic mixture was stirred vigorously while a solution that contained one equivalent of organothiol in 10 mL of toluene was added. Finally, a solution of 0.787 g $NaBH_4$ dissolved in 55 mL of water was added dropwise over 300 s to the vigorously stirred solution. During the addition of $NaBH_4$, the mixture turned dark purple. After stirring for 3 h, the organic phase was separated, transferred to a separatory funnel, and rinsed with water. The soluble product remaining in the organic phase was concentrated by rotary evaporation to a volume of $\sim$ 10 mL and was precipitated in 800 mL of ethanol at 10 °C. After settling overnight, the clear supernatant was decanted and the settled product was collected by centrifugation, followed by a wash with fresh ethanol. The product was redissolved in 10 mL of toluene and then reprecipitated by dropwise addition into 200 mL of rapidly stirred ethanol. After settling overnight at 10 °C, the 200 mL suspension was centrifuged. The precipitate was washed with fresh ethanol, vacuum-dried, and redissolved in toluene (10 mg mL^{-1}). The Au atom to ligand ratio, Au/S-R, was determined by thermogravimetric analysis to be 3($\pm$

0.1):1, and transmission electron microscopy indicated that the metal core had a diameter of approximately 2 ($\pm$ 1) nm. The solution was stored at 10 °C until needed.

The capped Au-NPs are referred to as Au-Cn ($4 \leq n \leq 11$). NP films were prepared on 1×2 cm glass substrates with metal contacts in the form of gold interdigitated electrodes (IDEs; 50 nm of Au over 30 nm of Cr). The electrode pattern produced 20 parallel sets of IDEs, with each IDE having dimensions of 0.240 mm $\times$ 5 mm ($w \times l$), separated by a 10 μm gap. The NP films were cast from a sonicated solution (10 mg mL^{-1} in toluene) by manually depositing a 10 μL suspension directly over the region of the substrate that contained the IDEs. Care was taken to ensure that deposition of the films was performed on substrates that were maintained below the decomposition temperature of the capped colloidal sensor materials. For capping agents longer than eight carbon units, the 10 μm gap between the electrodes was not sufficiently small to yield reproducible measurable film resistances. For shorter units such as propanethiol-capped NPs, dilution was very difficult, producing irreproducible electrical resistances. The stability of these NPs was observed to be low, leaving yellowish gold clusters on the glassware used. For all the sensors discussed herein, well-dispersed solutions were obtained and sensor film resistances were reproducible.

4.3.2 Sensing Measurements

Typically, three nominally identical vapor sensors were prepared at a time. The sensors were loaded into a rectangular, 40-slot chamber, with sensor film replicates positioned randomly. No dependence was observed on the performance of a given sensor on its spatial

position in the array. The 45.5 $\times$ 3.0 $\times$ 1.5 cm ($w \times l \times d$) chamber was connected by Teflon tubing to the gas delivery system. The internal cross-sectional area of the chamber was 1 cm^2. The dc resistance of the sensor array was measured with a digital multimeter (Keithley Model 2002) connected to a multiplexing unit (Keithley Model 7001). The resistance data were collected every 5-7 s from the array. A computer-controlled (LabVIEW) flow system delivered pulses of analyte vapor at a given fraction of the analytes vapor pressure.[36] Oil-free air was obtained from the house compressed air source (1.10 ± 0.15 ppth of water vapor) controlled with a mass flow controller. The test analytes used were six hydrocarbons (n-hexane [Hex], n-heptane [Hept], n-octane [Oct], iso-octane [iOct], cyclohexane [cHex], and toluene [Tol]), four alcohols (methanol [MeOH], ethanol [EtOH], isopropanol [iPOH], and 1-butanol [BuOH]), and ethyl acetate [EtOAc]. The sensor response as a function of vapor concentration was studied over the concentration range that corresponded to $0.0010 \leq P/P^\circ \leq 0.0200$, where P and P° are the partial pressure and vapor pressure of the analyte at room temperature (22 °C), respectively. Table 4.1 shows the saturated vapor pressures (P°, ppm) and the static dielectric constants, ϵ_s, of the analytes used.[37] Each analyte presentation consisted of 70 s of air, followed by 80 s of analyte vapor, followed by 60 s of air to purge the system. The total flow rate for each analyte presentation was 5 L min^{-1}. For the resistance and QCM sensitivity measurements, three exposures at each P/P° (see Table 4.1) were performed.

For resistance measurements as a function of the sensor temperature, the sensor chamber (sealed with plastics and Teflon) was placed in a water bath whose temperature was controlled with a Haake K20/DC5 temperature controller. Only three sensors (Au-C6, Au-C7,

	P°	ϵ_s
Hex	17.41	1.9
Hept	5.11	1.9
Oct	1.54	1.9
*i*Oct	5.58	1.9
*c*Hex	11.27	2.0
Tol	3.17	2.4
EtOAc	1.05	6.0
MeOH	14.06	32.7
EtOH	6.51	24.6
*i*POH	4.93	20.2
BuOH	0.73	17.8

Table 4.1: Saturated vapor pressure, P° (ppm), and dielectric constant, ϵ_s at 22 °C for all analytes.

and Au-C8) were placed in the chamber. During the stabilization of the desired temperature (2 h) an air background flow was continuously exposed to the array. QCM measurements were performed using quartz substrates with a 10 MHz resonant frequency and a diameter of 13.7 mm. The frequency was monitored using a Hewlett-Packard Frequency Counter (Model HP 53181a, 225 MHz), with an aluminum/Teflon chamber of dimensions 8.5 $\times$ 6.0 $\times$ 3.0 cm ($w \times l \times d$). NP films were deposited on the substrates by spraying using an airbrush. Two nominal QCM sensors were used for each Au-Cn system investigated. For optical measurements of the Au-NP plasmon resonance spectra, a Au-NP film was deposited on glass and placed in a sealed Teflon cylindrical chamber that permitted vapor flow through two apertures (inlet and outlet). The volume of the chamber was approximately 100 mL. The spectra were obtained with an Agilent 8453 UV-visible spectrometer. All chemiresistive and QCM sensors were dried under vacuum for 30 min at room temperature. The sensor films were conditioned by analyte exposures for 80 h to reach a steady resistance or frequency baseline, prior to the data collection presented herein.

4.3.3 Data Processing

All data processing was carried out using MATLAB45 with custom written routines.

i. Chemiresistive Sensors. The resistance-based response, r_s, of a vapor sensor to a particular analyte was calculated as $r_s = \Delta R_{max}/R_b$, where R_b is the baseline-corrected resistance of the sensor in the absence of analyte, and ΔR_{max} is the baseline-corrected maximum resistance change upon exposure of the sensor to analyte. R_b values were obtained from fitting a line to the pre-exposure data and extrapolating over the exposure period. ΔR_{max} was the average of the maximum three readings obtained by subtracting R_b from the measured sensor resistance during the exposure time. The sensitivity of a resistance-based vapor sensor film, s_R, was calculated from the slope of r_s versus P/P°, using a linear least-squares fit.

ii. QCM Sensors. The frequency of the QCM crystal was measured before, $f_\circ$, and after deposition of the sensor film, f_f, and after exposure to analyte, f_a. The change in frequency for the QCM crystal upon exposure to analyte was measured using analogous methods to that used for the change in resistance. The change in frequency is directly proportional to the increase in mass of the crystal. Thus, for the film prior to exposure to analyte, $\Delta f_f = f_f - f_0 = Cm_f$, and after exposure, $\Delta f_a = f_a - f_f = C\Delta m_f$, where C is a constant, m_f is the mass of the film, and Δm_f is the increase in mass of the film on exposure to analyte.[38] Assuming that only the thiol ligands and not the metal core sorb analyte, the observed frequency change due to the application of the sensor film to the QCM crystal, Δf_a, was corrected to account for the mass change due to only the proportion of the film that was comprised of the organic ligands. Thus, Δf_a was adjusted by the relative mass

fraction of organic ligand that was obtained from the Au/S-R ratio (3:1):

$$\Delta f_f' = f_{ligand} \Delta f_f \tag{4.5}$$

where f_{ligand} is the mass fraction of thiol ligand in the NP film. The relative mass increase due to analyte sorbed per unit mass of sensor material, r_{QCM}, is then given by

$$r_{QCM} = \frac{\Delta f_a}{\Delta f_f'} = \frac{\Delta m_a}{m_{ligand}} \tag{4.6}$$

where m_{ligand} is the mass of the organic ligands in the film.

Random exposures of the analytes were presented to the Au- NP QCM sensors. The QCM sensitivity, s_{QCM}, was calculated from the slope of r_{QCM} versus P/P° using a linear least-squares fit, with a forced zero intercept. Partition coefficients, K, incorporating responses for $0.0010 \leq P/\ P^\circ \leq 0.0200$, were obtained by using[36]

$$K = \frac{\rho_s RT}{M_{w,A} P^\circ} s_{QCM} \tag{4.7}$$

where ρ_s (g cm^{-3}) is the density of the sorption material (R-SH), R (atm mol^{-1} K^{-1}) is the ideal gas constant, T (K) is the temperature, $M_{w,A}$ (g mol^{-1}) is the molecular weight of the analyte, and P° (atm) is the vapor pressure of the analyte. The density of the sorption material, ρ_s, was taken as that of the R-SH ligands (0.84 g cm^{-3}), assuming that the change in density of the ordered ligands on the surface was negligible.

4.4 Results

4.4.1 Resistance Change Response to Analytes

Typical sensor responses for a Au-C8 sensor to Hex and EtOH at P/P° = 0.0050 are shown in Figure 4.1a and 4.1b, respectively. Positive responses (resistance increases) were observed for all sensors upon exposure to the hydrocarbons or to EtOAc, whereas negative responses (resistance decreases) were observed upon exposure to alcohol vapors. The positive responses of the sensors to EtOAc were significantly smaller than the responses observed upon exposure to the hydrocarbon analytes. Au-NP films showed no change in the amount of organic material before and after the sensing experiments, as determined by thermogravimetric analysis. The sensor response as a function of analyte concentration was generally linear over the P/P° range investigated. Emphasis was placed on measurement of and understanding of the response to relatively dilute analytes, because most situations of interest are likely to involve lower, rather than higher, concentrations of vapor at the position of the sensor itself.

Figure 4.2 shows a linear least-squares fit for a Au-C8 sensor against all of the 11 vapors, with the sensor sensitivity given as the slope, s_R, of the best fit straight line. The fits for the hydrocarbon and EtOAc responses gave nonzero positive intercepts, C, having a value of $\Delta R_{max}/R_b$ between 1.3 and 0.4 ($\times 10^{-2}$). For all of the alcohols except EtOH, a zero intercept was observed, whereas for EtOH vapors, a negative intercept was observed. The responses generally became nonlinear functions of analyte vapor for $P/P^\circ > 0.1$. The sensor sensitivity generally increased as the length of the R-SH capping chain increased

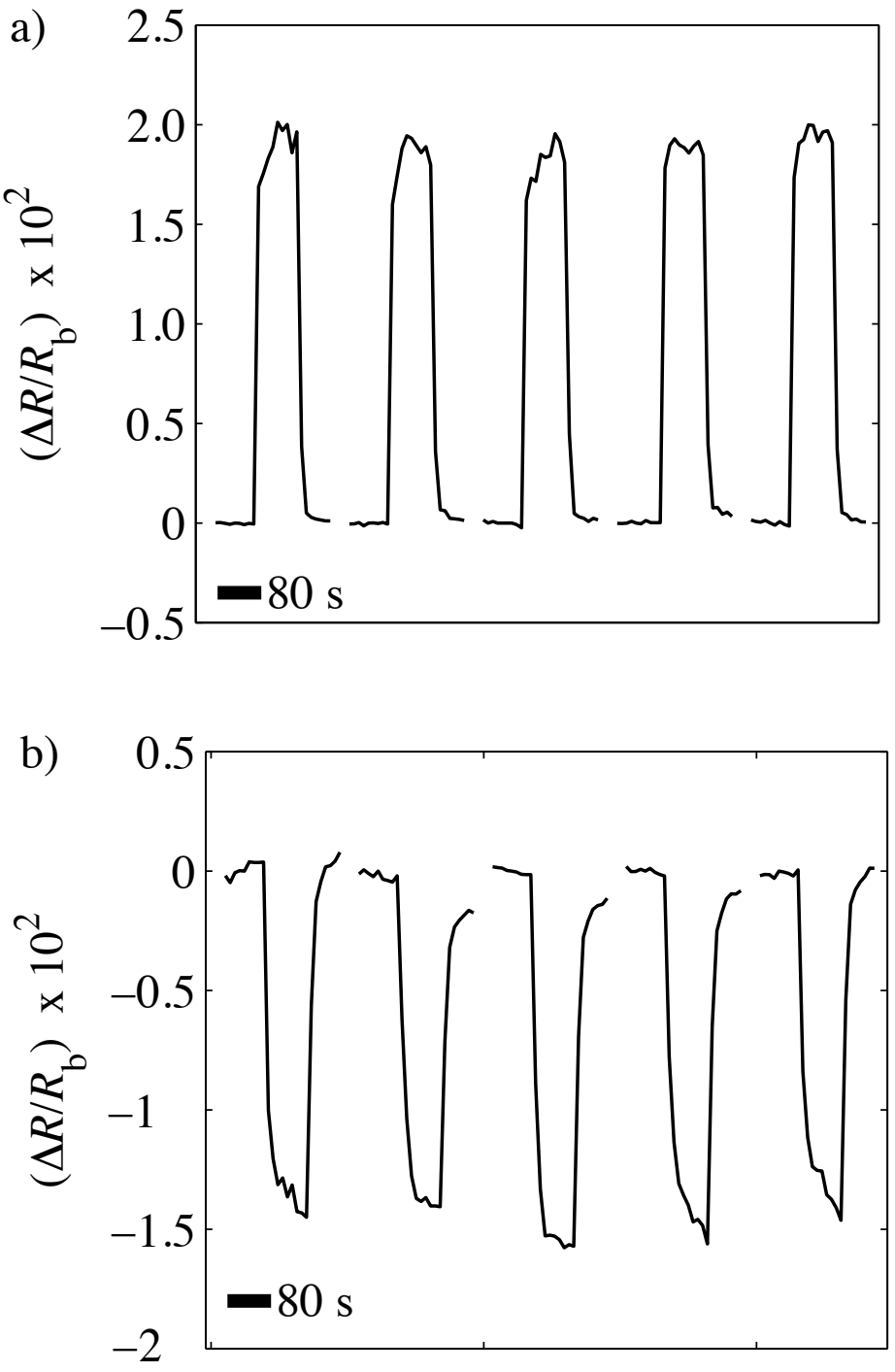

Figure 4.1: Relative differential resistance values, $\Delta R/R_b$, for five different randomly ordered exposures to hexane and ethanol, each at P/P° = 0.0050: (a) hexane exposures to a Au-C8 vapor sensor; (b) ethanol exposures to a Au-C8 vapor sensor.

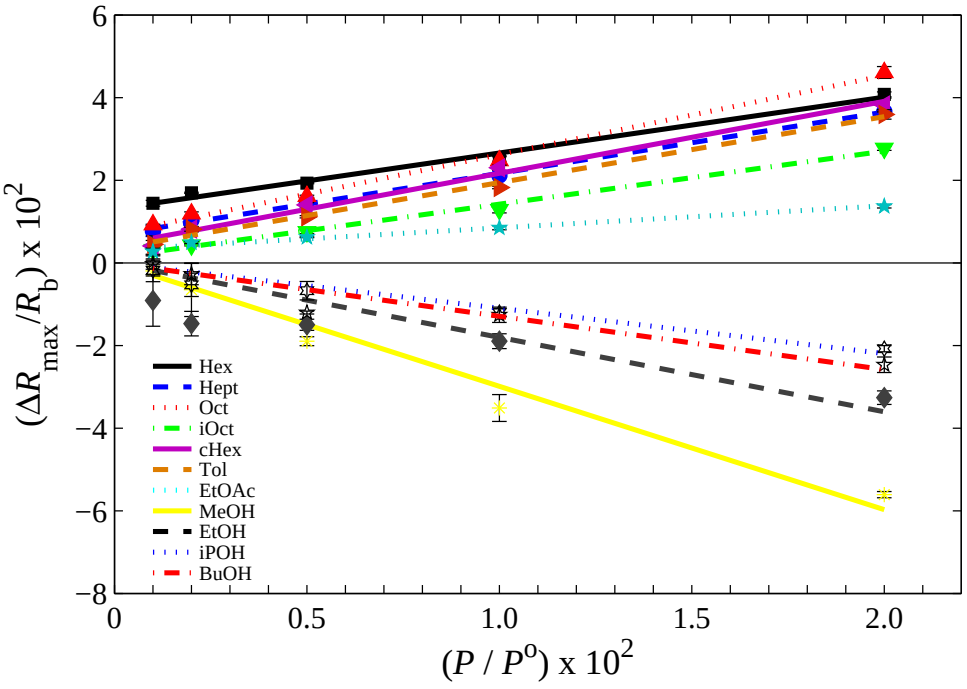

Figure 4.2: Maximum differential resistance responses, $\Delta R_{max}/R_b$, as a function of P/P° for a Au-C8 sensor in response to all analyte vapors.

(Figure 4.3). The sensitivities for iPOH and BuOH were essentially the same for the Au-C7 and Au-C8 NP films.

Figure 4.4 shows the resistance responses to Hex and EtOH as a function of temperature (4 °C $\leq T \leq$ 39 °C) for a Au-C8 sensor. The arrows show the direction of the temperature scan, with the initial scan starting at the lowest temperature. Each r_s value was the average of 50 exposures per analyte. For Hex, r_s decreased as the temperature increased, in accord with changes in the value of P/P° due to an increase in the value of P° as the temperature increased. Upon exposure to Hex, the r_s values were slightly smaller during the reverse temperature scan than those in the increasing temperature scan. Negative responses were observed for a Au-C8 sensor upon exposure to EtOH during the forward temperature scan. However, for the backward temperature scan, positive values of r_s were observed.

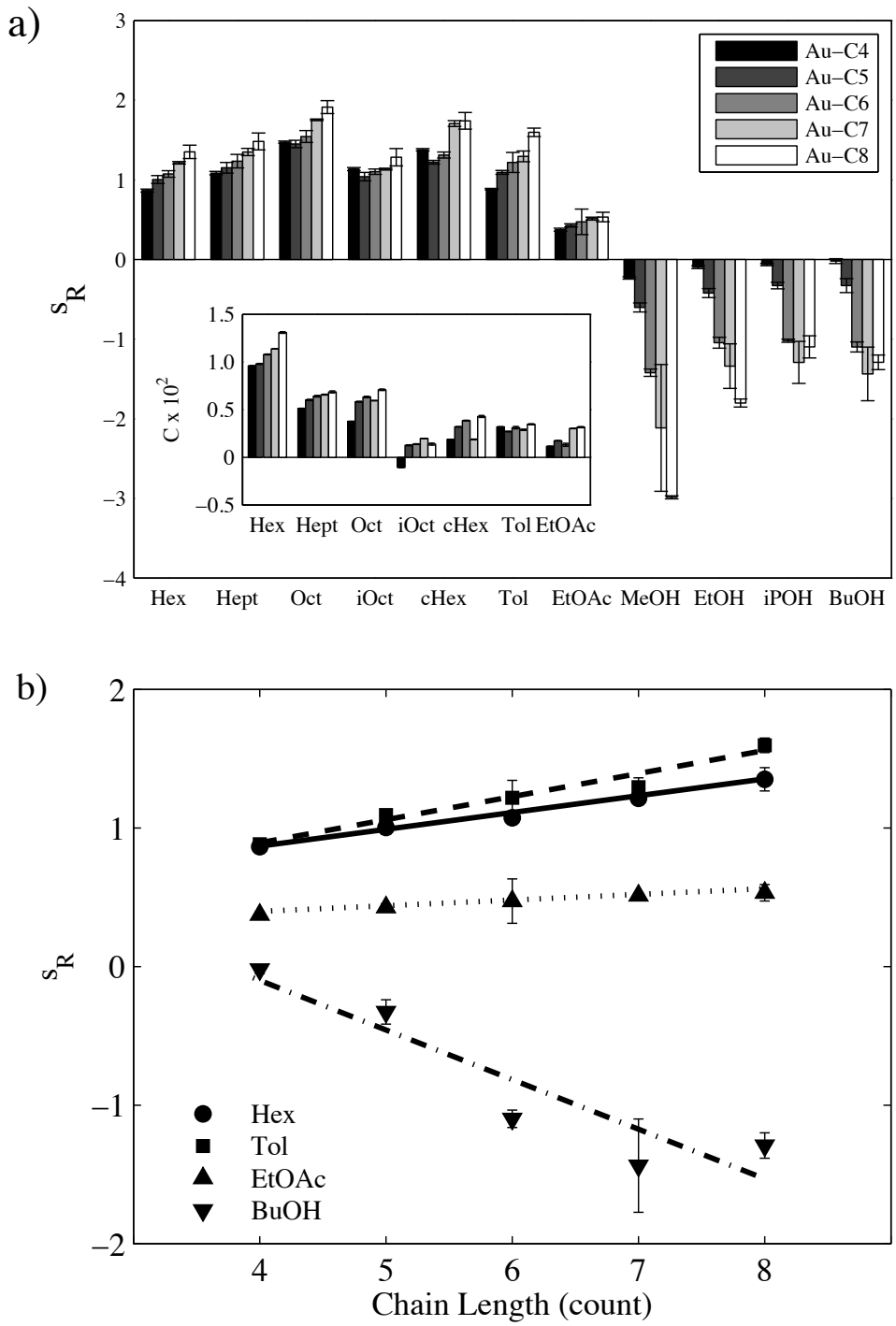

Figure 4.3: (a) Resistance-based sensitivity values, s_R, for all combinations of alkanethiol-capped Au nanoparticles and analytes, for $0.0010 \leq P/P^{\circ} \leq 0.0200$. Each value represents the average of three sensor replicates for every Au-Cn capping ligand. The inset shows the values of the intercept, C, obtained upon exposure to the hydrocarbons. (b) Resistance-based sensitivity, s_R, as a function of chain length (Au-Cn; $4 \leq n \leq 8$) of the Au-capping alkanethiol. The s_R values presented correspond to n-hexane (Hex), toluene (Tol), ethyl acetate (EtOAc), and 1-butanol (BuOH).

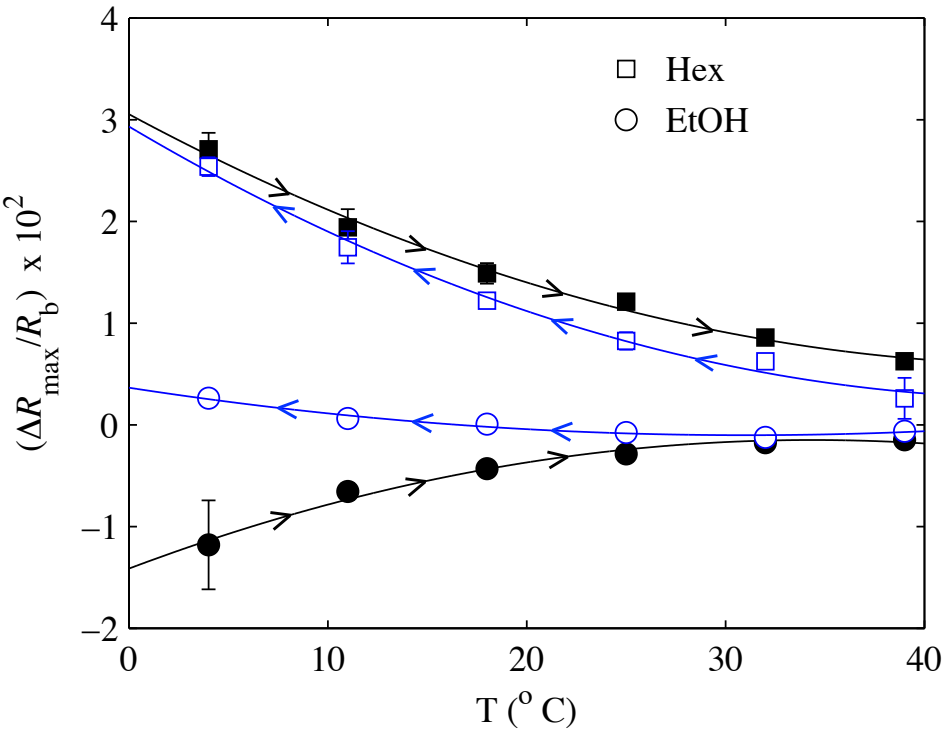

Figure 4.4: Maximum relative differential resistance responses for a Au-C8 sensor upon exposure to Hex (squares) and EtOH (circles) at P/P° = 0.0010, as a function of temperature (4 °C $\leq T \leq$ 39 °C). The arrows in the response pattern represent the direction of the temperature scan. The responses observed as the temperature was increased (black) were generated initially, followed by the blue-line scan for decreases in temperature. Each response value was the average of 50 exposures per analyte.

4.4.2 QCM Response To Analytes

Figure 4.5 shows the QCM frequency changes for a Au-C8 sensor upon exposure to Hex or EtOH at P/P° = 0.0050. The QCM sensitivities, s_{QCM}, were obtained from the linear least-squares slope of a plot of r_{QCM} versus P/P° (Figure 4.6). In all cases, s_{QCM} values were positive and showed no significant dependence on the chain length of the capping ligand. Furthermore, the values of K were generally independent of chain length (Figure 4.7). This behavior is expected because the calculation of r_{QCM}, eq 5, used a film mass that was only the mass of the organic ligands. If the sorption of analyte is only performed by the organic ligands, then the values of r_{QCM} should be independent of the length of the ligands. This behavior would also produce a lack of dependence of s_{QCM} or K on the length of the capping alkane chain.

4.4.3 QCM Response To Analytes

4.5 Discussion

The use of different capping ligands with different lengths allows for control at the molecular level over the interparticle spacing, and the mass of the spacing ligands in the sensor films. This type of control is not possible using materials such as carbon black-polymer composites, which contain a random distribution of conductive particles in an insulating matrix. The values of s_{QCM} and K did not show a dependence on the chain length of the organic capping ligand, due to the normalization of r_{QCM} by the m_{ligand} (eqs 4.5 and 4.6). Thus, the uptake of analyte is approximately linear with the mass of the NP ligands.

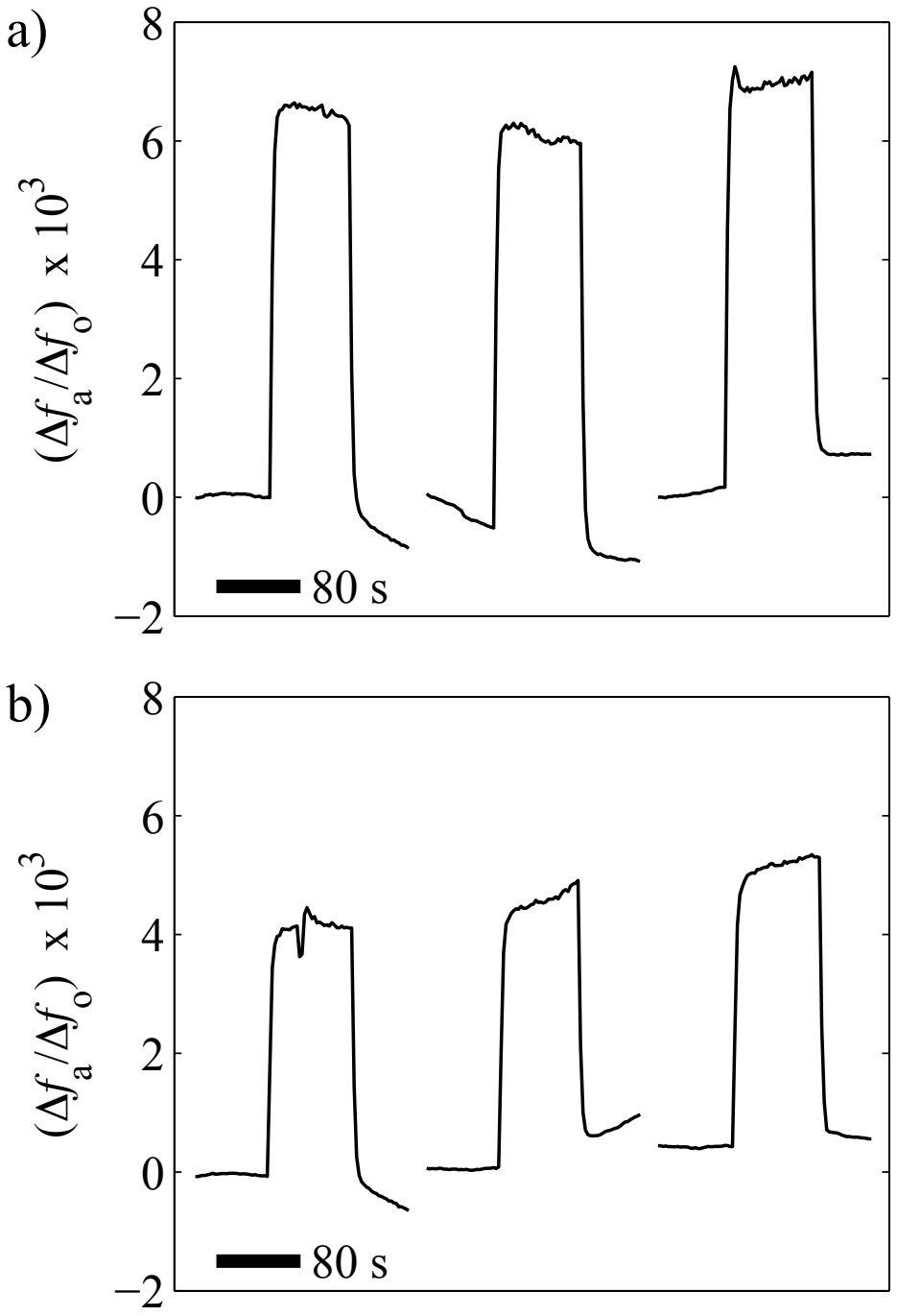

Figure 4.5: QCM sensor responses for a Au-C8 film upon exposure to (a) n-hexane and (b) ethanol, each at P/P° = 0.0050.

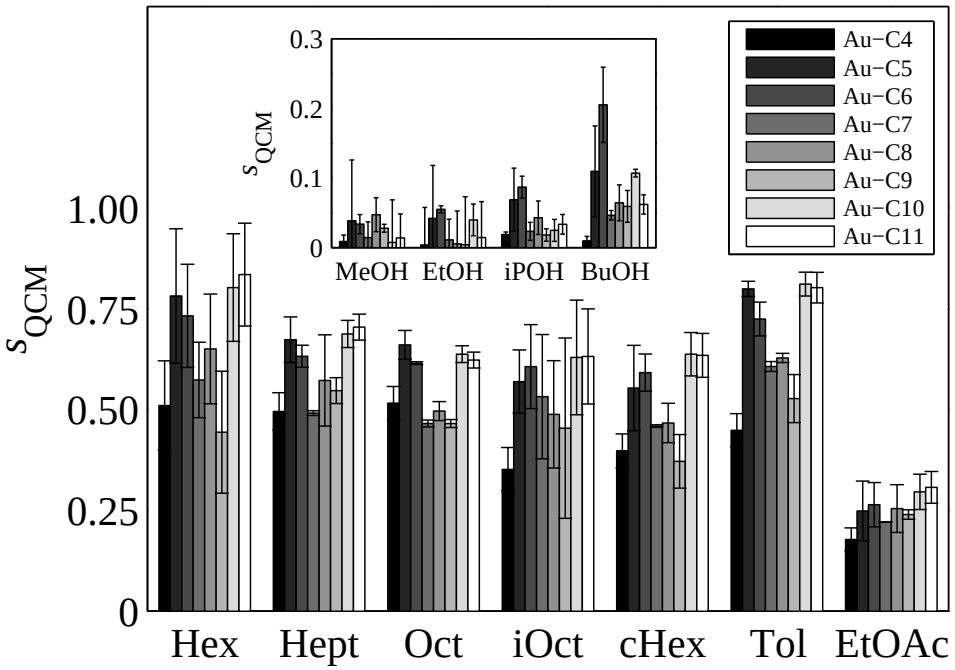

Figure 4.6: Quartz crystal microbalance sensitivity, s_{QCM} (Hz ppm^{-1} $\times$ 10^1) for all combinations of capped Au nanoparticle sensors and analytes, for $0.0010 \leq P/P^{\circ} \leq 0.0200$. Each value corresponds to the average of two sensors per Au-Cn. The inset shows the adjusted s_{QCM} values for alcohol vapors.

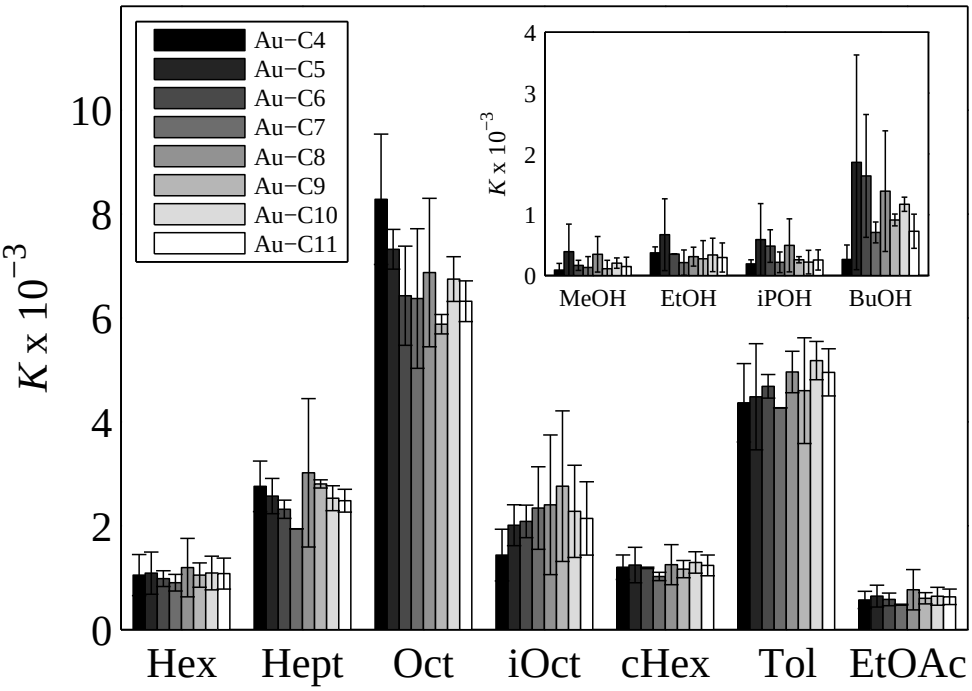

Figure 4.7: Partition coefficients, K, for all combinations of capped Au nanoparticles and analytes, for $0.0010 \leq P/P^{\circ} \leq 0.0200$. Each value corresponds to two sensors per Au-Cn. The inset shows the K values for alcohol vapors.

Although larger ligands sorbed more analyte due to a greater amount of ligand mass, the fractional mass change due to analyte sorption was equal for all of the ligands. This observation suggests that all ligands swelled proportionally the same amount for a given P/P° of the analyte vapor.

For hydrocarbons or EtOAc, the sensor sensitivity values, s_R, generally increased monotonically with chain length. For alcohols, the $\mid s_R \mid$ values increased with chain length for MeOH and EtOH, however for iPOH and BuOH, $\mid s_R \mid$ values were constant for Au-C6 and longer capping ligands. The resistance response sensitivity to hydrocarbons increased as the length of the capping ligand increased. However, if such sensitivities are adjusted by f_{ligand}, the value of s_R is independent of chain length, as observed for s_{QCM} and the K values (Figure 4.7). The purpose of adjusting s_R is to produce a parallel metric to s_{QCM} (i.e., $\mid s_R \mid / f_{ligand}$). The observed $\Delta R_{max}/R_b$ values were thus scaled by f_{ligand}, producing s_R values that were independent of chain length. The values of s_R correlated with the relative chain length changes rather than with the absolute change in distance between NPs. The negative $\Delta R_{max}/R_b$ responses for the alcohol vapors are of note. In general, chemiresistive sorption-based sensors show increases in resistance upon exposure to an analyte. This increase in resistance is normally ascribed to an increase in the separation between the conducting particles (e.g., thiol-capped Au cores) due to swelling of the sensor film upon analyte sorption. Conversely, when negative r_s (i.e., resistance decreases) values are obtained upon exposure to hydrophilic vapors, such behavior is generally associated with a change in the value of ϵ_s for the metal-to-metal interfacial region. The value of ϵ_s can be monitored in conjunction with measurement of the plasmon resonance of Au-NPs ($\lambda_{max} \approx$

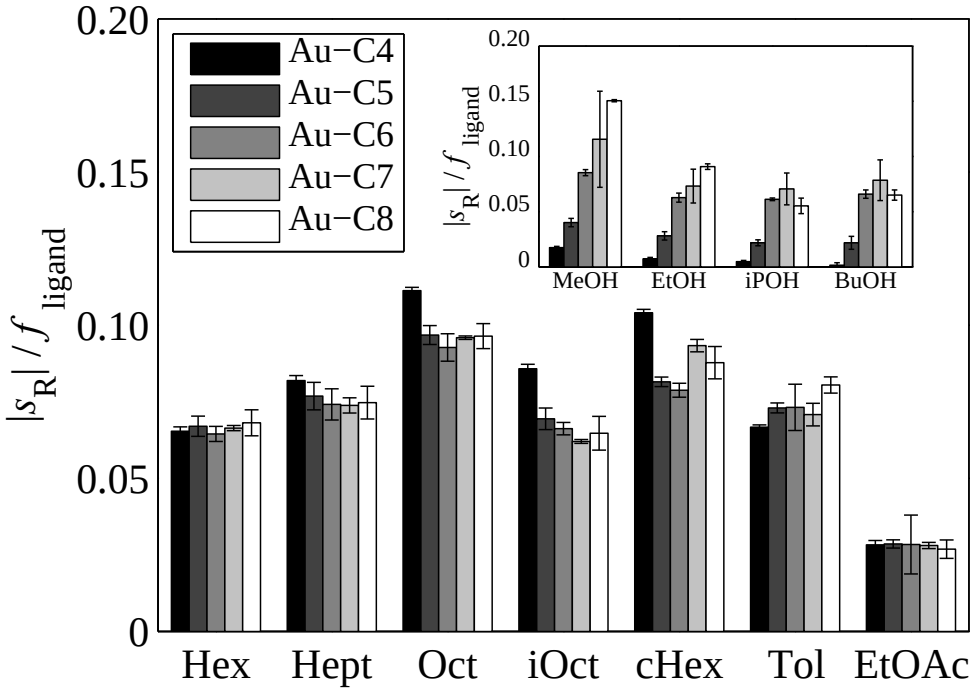

Figure 4.8: Sensitivity values adjusted by the ligand mass percentage, f_{ligand}, for all sensors and analytes. Each value corresponds to the average of two sensors per Au-Cn. The inset shows the adjusted s_R values for alcohol vapors.

522 nm).[39,40] An increase of ϵ_s would cause a red-shift of the plasmon resonance ($\lambda_{max} >$ 522 nm). Figure 4.9 shows the absorption spectra of a Au-C8 film upon exposure to air and to EtOH at $P = P^\circ$, indicating that no significant change in λ_{max} was observed upon exposure to saturated EtOH. The concentration of analyte sorbed by the sensing material at equilibrium can be calculated by use of the value of K of the analyte/material combination in Figure 4.7 by

$$K = \frac{C_{A,film}}{C_V} \tag{4.8}$$

where $C_{A,film}$ (mol L^{-1}) is the concentration of analyte in the film and C_V (mol L^{-1}) is the concentration of analyte in the vapor phase. $C_{A,flim}$ is obtained with the value of K in conjunction with the use of P/P° to calculate C_V through the ideal gas equation

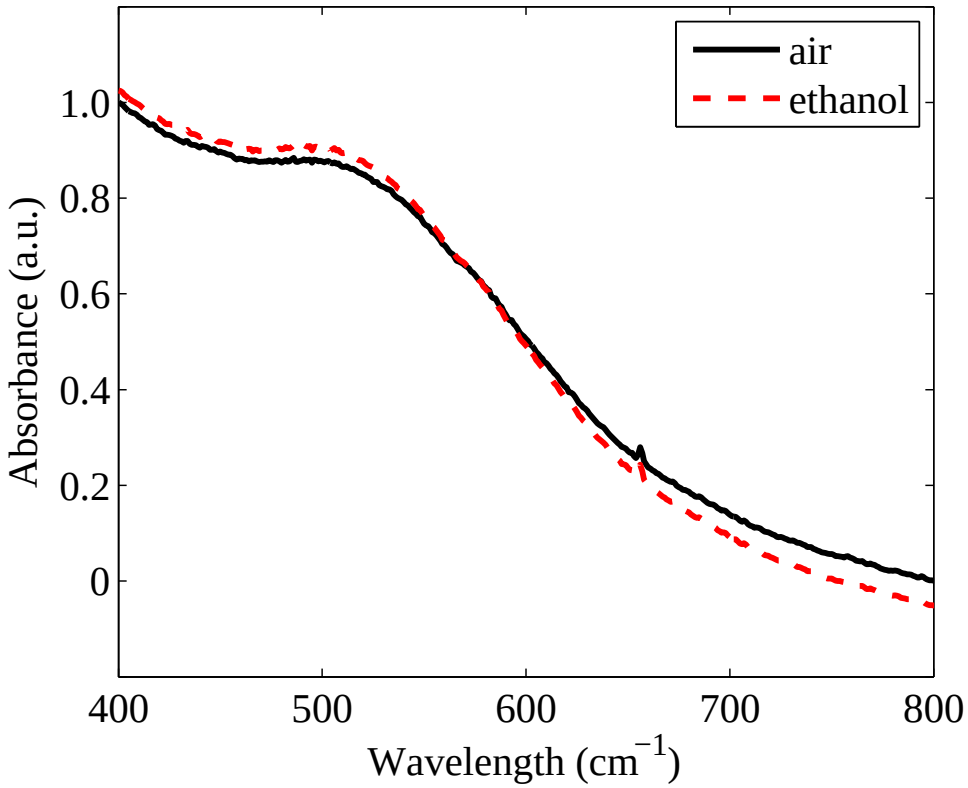

Figure 4.9: Absorption spectra for a Au-C8 film during exposure to air (5 L min^{-1}) and ethanol at P°. No change in the plasmon resonance is observed. A red-shift in the plasmon resonance would have indicated an increase of the dielectric constant of the film.

($C_V = P/(RT)$). The resulting dielectric constant of the analyte/ligand mixture can be calculated by using $C_{A,film}$. Because it is assumed that sorption can only take place at the organic layer, the ligand concentration, C_{ligand}, in the film can be obtained from the density of the condensed ligand ($\sim$ 0.84 g mL^{-1}). The sorbed analyte mole ratio, χ_A, is then $\chi_A = C_{A,film}/(C_{A,film} + C_{ligand})$. The dielectric constant of a mixture of two components depends on the volume fraction of both components, γ_1 and γ_2. For a given mixture of two substances having dielectric constants ϵ_1 and ϵ_2, respectively

$$\gamma_1 + \gamma_2 = 1 \tag{4.9}$$

For independent substances, having D_1 and D_2, the 2-component value of the electric displacement is given by $D = \gamma_1 D_1 + \gamma_2 D_2$. The electric field, E, throughout the mixture is given by $E = \gamma_1 E_1 + \gamma_2 E_2$. Hence, the resulting dielectric constant of the mixture is given by $\epsilon_s = D/E$, where for each component, $D_1 = \epsilon_1 E_1$ and $D_2 = \epsilon_2 E_2$. Reynolds et al. demonstrated that an expression describing ϵ_s for a mixture of two components can be derived: ϵ_s for a mixture of two components can be derived

$$\epsilon_s = \epsilon_2 + (\epsilon_1 - \epsilon_2)\gamma_1 F_1 \tag{4.10}$$

where F_1 is assumed to approach unity and γ_1 is the volume ratio of one of the components of the mixture.[41] This determination of γ_1 and K differs from the work of Steinecker et al. in that γ_1 is the volumetric analyte/ligand ratio and K accounts for both the metal core and the passivating ligand.[42] The ϵ_s value for the ligand is 3.0.[43] At higher values of C_V, higher

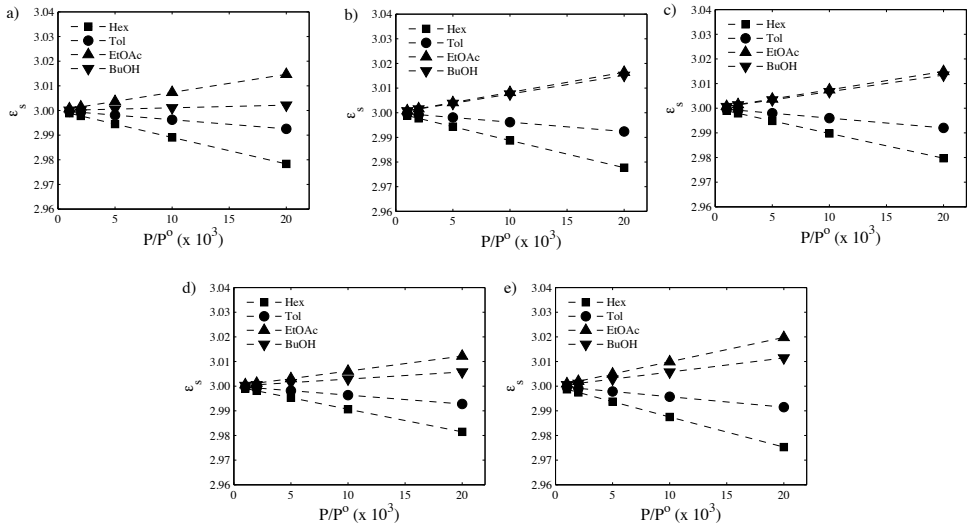

Figure 4.10: Static dielectric constant, ϵ_s, of the ligand/analyte organic interface as a function of P/P° for Hex, Tol, EtOAc and BuOH; a) Au-C4, b) Au-C5, c) Au-C6, d) Au-C7, e) Au-C8

$\gamma_{analyte}$ should be produced, so ϵ_s could be significantly affected by the vapor. Figures 4.10 shows the value of ϵ_s as a function of P/P°. The value of ϵ_s is slightly minimized upon exposure to Hex or Tol, whereas for EtOAc and BuOH, ϵ_s slightly increases. In the case of Hex and Tol, swelling, accompanied by an increase in δ, is expected to dominate the r_s response. For the alcohols, the change in the value of ϵ_s is about 0.5 %, which produces a 0.2 % change in λ for P/P° = 0.0200 and ϵ_{op} = 1.85 (i.e., pentanes refractive index, η^2 = 1.36, $\epsilon_{op} = \eta^2$).[37] In contrast, the observed change in r_s suggests a 2 % change in resistance at P/P° = 0.0200 for a Au-C8 sensor upon exposure to BuOH. Au-NPs that are capped with alkanethiol ligands (e.g., C4-C8) cannot be dissolved in alcoholic solvents, specifically MeOH or EtOH. In fact, EtOH is used to precipitate the particles in solution when using the Brust et al. method.[8] The presence of an alcohol solvent promotes NP aggregation. Exhaustive exposure of a saturated EtOH vapor promotes an irreversible morphology change of a Au-C8 film (Figure 4.11). The morphology change observed in Figure 4.11c

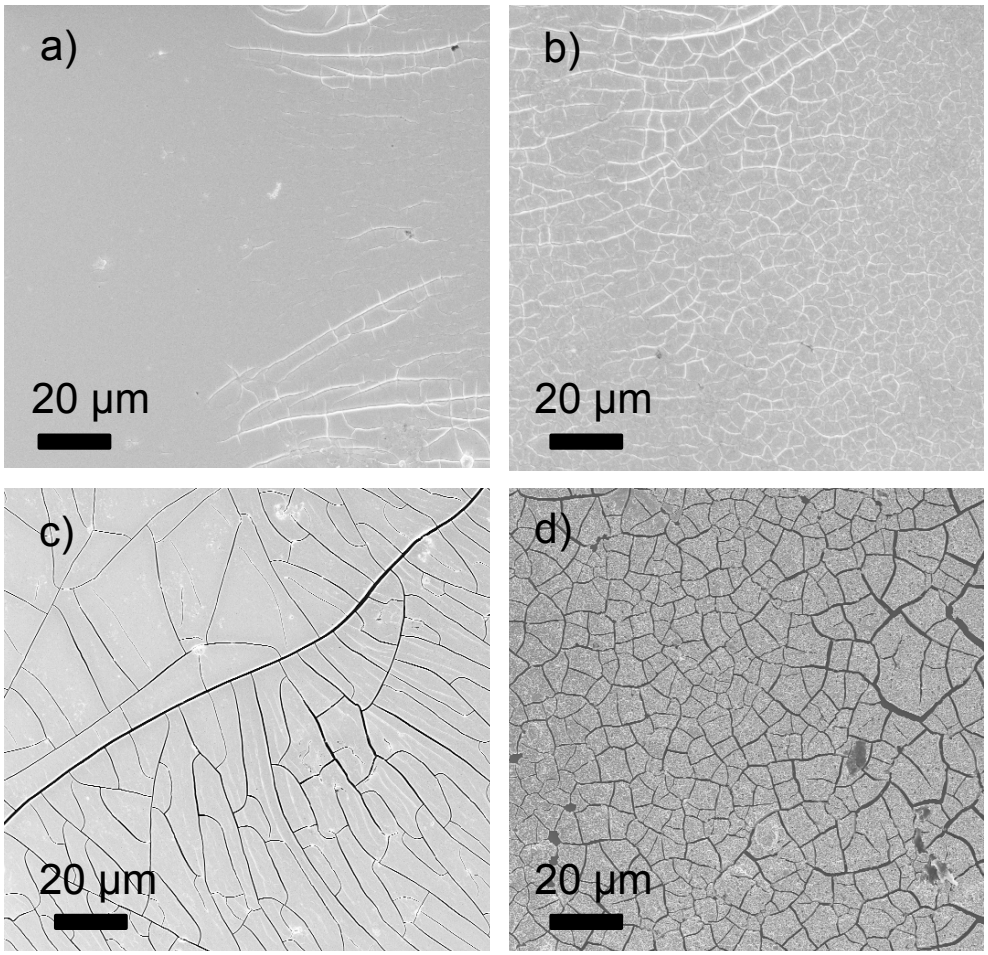

Figure 4.11: Scanning electron micrographs of a Au-C8 film that was treated under different vapors. Micrograph a) shows the as prepared Au-C8 film, micrograph b) shows a film that was presented to a saturated Hex vapor stream for 12 h, micrograph c) shows a film that was presented to a saturated EtOH vapor stream for 12 h, and micrograph d) shows a film that was presented to a saturated H_2O vapor stream for 12 h.

due to EtOH exposure suggests a reduction of the interparticle spacing and an increase in the number of electron hopping pathways. However, for hydrocarbon vapors, NP solvation or swelling occurs. Contrary to significantly changing the value of ϵ_s, the response data suggests that the negative r_s values are associated with a reversible change in film morphology, as opposed to a change in the value of ϵ_s. Conversely, an irreversible morphology change was produced when the sensor was heated to 39 °C, as observed in Figure 4.4.

4.6 Conclusions

Au-NPs capped by five different R-SH ligands having variable chain lengths were synthesized and investigated as chemical vapor sensors. The resistance response sensitivity to hydrocarbons increased as the length of the capping ligand increased, whereas for alcohols, negative sensitivities were observed, with increasingly negative sensitivities measured as the length of the capping chain increased. The Au-Cn sensors with larger ligands sorbed more analyte due to a greater amount of organic mass. The fractional mass change due to analyte sorption was equal for all of the Au-Cn, suggesting that for any given P/P°, all Au-Cn swelled proportionally the same amount. Consistently, the partition coefficient of all Au-Cn was approximately equal for every analyte, under the assumption that vapor sorption only occurred in the ligand matrix. The measurement of partition coefficients of the NP films allowed for estimation of the dielectric constant of the interparticle organic phase upon exposure to the analyte vapor. The dielectric constant change due to sorbed vapor molecules was an order of magnitude lower than what would be needed to account for the observed resistance responses, suggesting that interparticle distance and/or morphology changes dominate the resistance response. Irreversible morphology changes resulted from heating the Au-Cn sensors at 40 °C, and the presence of such changes was supported by the change in the sign of the resistance response value upon exposure to EtOH. This observation suggests that the Au-Cn chemiresistive films can reach a more chemically stable state after such perturbations.

Bibliography

[1] Albert, K. J.; Walt, D. R. *Anal. Chem.* **2000**, *72*(9), 1947–1955.

[2] Severin, E.; Doleman, B.; Lewis, N. *Anal. Chem.* **2000**, *72*(4), 658–668.

[3] Gao, T.; Woodka, M. D.; Brunschwig, B. S.; Lewis, N. S. *Chem. Mater.* **2006**, *18*(22), 5193–5202.

[4] Woodka, M. D.; Brunschwig, B. S.; Lewis, N. S. *Langmuir* **2007**, *23*(26), 13232–13241.

[5] Pearson, R. G. *J. Am. Chem. Soc.* **1963**, *85*(22), 3533–.

[6] Sellers, H.; Ulman, A.; Shnidman, Y.; Eilers, J. E. *J. Am. Chem. Soc* **1993**, *115*(21), 9389–9401.

[7] Wohltjen, H.; Snow, A. W. *Anal. Chem.* **1998**, *70*(14), 2856–2859.

[8] Brust, M.; Fink, J.; Bethell, D.; Schiffrin, D. J.; Kiely, C. J. *J. Chem. Soc., Chem. Commun.* **1995**, pages 1655–1656.

[9] Johnson, S. R.; Evans, S. D.; Brydson, R. *Langmuir* **1998**, *14*(23), 6639–6647.

[10] Woehrle, G. H.; Brown, L. O.; Hutchison, J. E. *J. Am. Chem. Soc.* **2005**, *127*(7), 2172–2183.

[11] Han, L.; Daniel, D. R.; Maye, M. M.; Zhong, C. J. *Anal. Chem.* **2001**, *73*(18), 4441–4449.

[12] Joseph, Y.; Besnard, I.; Rosenberger, M.; Guse, B.; Nothofer, H. G.; Wessels, J. M.; Wild, U.; Knop-Gericke, A.; Su, D. S.; Schlogl, R.; Yasuda, A.; Vossmeyer, T. *J. Phys. Chem. B* **2003**, *107*(30), 7406–7413.

[13] Joseph, Y.; Guse, B.; Yasuda, A.; Vossmeyer, T. *Sens. Actuators B* **2004**, *B98*(2-3), 188–195.

[14] Evans, S. D.; Johnson, S. R.; Cheng, Y. L.; V., S. T. *J. Mater. Chem.* **2000**, *10(1)*, 183–188.

[15] Zhang, H. L.; Evans, S. D.; Henderson, J. R.; Miles, R. E.; Shen, T. H. *Nanotech.* **2002**, *13*(3), 439–444.

[16] Grate, J. W.; Nelson, D. A.; Skaggs, R. *Anal. Chem.* **2003**, *75*(8), 1868–1879.

[17] Leopold, M. C.; Donkers, R. L.; Georganopoulou, D.; Fisher, M.; Zamborini, F. P.; Murray, R. W. *Faraday Discuss.* **2003**, *125*, 63–76.

[18] Krasteva, N.; Guse, B.; Besnard, I.; Yasuda, A.; Vossmeyer, T. *Sens. Actuators B* **2003**, *92*(1-2), 137–143.

[19] Krasteva, N.; Krustev, R.; Yasuda, A.; Vossmeyer, T. *Langmuir* **2003**, *19*(19), 7754–7760.

[20] Joseph, Y.; Krasteva, N.; Besnard, I.; Guse, B.; Rosenberger, M.; Wild, U.; Knop-Gericke, A.; Schlogl, R.; Krustev, R.; Yasuda, A.; Vossmeyer, T. *Faraday Discuss.* **2004**, *125*, 77–97.

[21] Zamborini, F. P.; Leopold, M. C.; Hicks, J. F.; Kulesza, P. J.; Malik, M. A.; Murray, R. W. *J. Am. Chem. Soc.* **2002**, *124*(30), 8958–8964.

[22] Foos, E. E.; Snow, A. W.; Twigg, M. E.; Ancona, M. G. *Chem. Mater.* **2002**, *14*(5), 2401–2408.

[23] Ahn, H.; Chandekar, A.; Kang, B.; Sung, C.; Whitten, J. E. *Chem. Mater.* **2004**, *16*(17), 3274–3278.

[24] Briglin, S. M.; Gao, T.; Lewis, N. S. *Langmuir* **2004**, *20*(2), 299–305.

[25] Guo, J. L.; Pang, P. F.; Cai, Q. Y. *Sens. Actuators B* **2007**, *120*(2), 521–528.

[26] Abeles, B.; Sheng, P.; Coutts, M. D.; Arie, Y. *Adv. Phys.* **1975**, *24*(3), 407–461.

[27] Joseph, Y.; Peic, A.; Chen, X. D.; Michl, J.; Vossmeyer, T.; Yasuda, A. *J. Phys. Chem. C* **2007**, *111*(34), 12855–12859.

[28] Brennan, J. L.; Branham, M. R.; Hicks, J. F.; Osisek, A. J.; Donkers, R. L.; Georganopoulou, D. G.; Murray, R. W. *Anal. Chem.* **2004**, *76*(19), 5611–5619.

[29] Choi, J. P.; Murray, R. W. *J. Am. Chem. Soc.* **2006**, *128*(32), 10496–10502.

[30] Hicks, J. F.; Zamborini, F. P.; Osisek, A.; Murray, R. W. *J. Am. Chem. Soc.* **2001**, *123*(29), 7048–7053.

[31] Menard, L. D.; Gao, S. P.; Xu, H. P.; Twesten, R. D.; Harper, A. S.; Song, Y.; Wang, G. L.; Douglas, A. D.; Yang, J. C.; Frenkel, A. I.; Nuzzo, R. G.; Murray, R. W. *J. Phys. Chem.* **2006**, *110*(26), 12874–12883.

[32] Parker, J. F.; Choi, J. P.; Wang, W.; Murray, R. W. *J. Phys. Chem. C* **2008**, *112*(36), 13976–13981.

[33] Terrill, R. H.; Postlethwaite, T. A.; Chen, C. H.; Poon, C. D.; Terzis, A.; Chen, A. D.; Hutchison, J. E.; Clark, M. R.; Wignall, G.; Londono, J. D.; Superfine, R.; Falvo, M.; Johnson, C. S.; Samulski, E. T.; Murray, R. W. *J. Am. Chem. Soc.* **1995**, *117*(50), 12537–12548.

[34] Marcus, R. A.; Sutin, N. *Biochim. Biophys. Acta* **1985**, *811*(3), 265–322.

[35] Sutin, N. *Nuclear and Electronic Factors in Electron Factors in Electron Transfer, Distance Dependence of Electron-Transfer Rates*, Vol. 228; Eds. Advances in Chemistry Series 228, American Chemical Society: Washington, DC, 1991.

[36] Maldonado, S.; Garcia-Berrios, E.; Woodka, M. D.; Brunschwig, B. S.; Lewis, N. S. *Sens. Actuators B* **2008**, *134*(2), 521–531.

[37] *CRC Handbook of Chemistry and Physics;* CRC Press: New York, 77 ed., 1996-1997.

[38] Sauerbrey, G. *Z. Physik.* **1955**, *155*, 206.

[39] Templeton, A. C.; Pietron, J. J.; Murray, R. W.; Mulvaney, P. *J. Phys. Chem. B* **2000**, *104*(3), 564–570.

[40] Underwood, S.; Mulvaney, P. *Langmuir* **1994**, *10*(10), 3427–3430.

[41] Reynolds, J. A.; Hough, J. M. *Proc. Phys. Soc.* **1957**, *70*(8), 769–775.

[42] Steinecker, W. H.; Rowe, M. P.; Zellers, E. T. *Anal. Chem.* **2007**, *79*(13), 4977–4986.

[43] Hicks, J. F.; Templeton, A. C.; Chen, S. W.; Sheran, K. M.; Jasti, R.; Murray, R. W.; Debord, J.; Schaaf, T. G.; Whetten, R. L. *Anal. Chem.* **1999**, *71*(17), 3703–3711.

Chapter 5

Response and Discrimination Performance of Arrays of Organothiol-Capped Au Nanoparticle Chemiresistive Vapor Sensors

5.1 Abstract

The response and discrimination performance of an array that consisted of 20 different organothiol-capped Au nanoparticle chemiresistive vapor sensors was evaluated during exposure to 13 different organic vapors. The passivating organothiol ligand library consisted of collections of straight-chain alkanethiols, branched alkanethiols, and aromatic thiols. A fourth collection of sensors was formed from composites of 2-phenylethanethiol-capped Au nanoparticles and non-polymeric aromatic materials that were co-embedded in a sensor film. The organic vapors consisted of six hydrocarbons (n-hexane, n-heptane, n-octane, isooctane, cyclohexane, and toluene), three polar aprotic vapors (chloroform, tetrahydrofuran, and ethyl acetate), and four alcohols (methanol, ethanol, isopropanol, and 1-butanol). Trends in the resistance response of the sensors were consistent with expected trends in

Reproduced in part with permission from *J. Phys. Chem. C*, **2011**, *115*, 6208-6217

sorption due to the properties of the test vapor and the molecular structure of the passivating ligands in the sensor films. Classification algorithms including principal components analysis and Fishers linear discriminant were used to evaluate the discrimination performance of an array of such sensors. Each collection of sensors produced accurate classification of most vapors, with misclassification occurring primarily for vapors that had mutually similar polarity. The classification performance for an array that contained all of the sensor collections produced nearly perfect discrimination for all vapors studied. The dependence of the array size (i.e., the number of sensors) and the array chemical diversity on the discrimination performance indicated that, for an array of 20 sensors, an array size of 13 sensors or more produced the maximum discrimination performance.

5.2 Introduction

An array of broadly cross-reactive sensors, in which each individual sensor responds to a variety of odors, is known as an electronic nose. Patterns of responses across the array produce a fingerprint for each odorant. Pattern recognition algorithms can then be employed to obtain information on the polarity and/or physicochemical properties, and concentration, of the vapor(s) exposed to the sensor array.[? ? ? ?]

Sensor arrays in which each individual sensor contains a unique functional group have attracted interest because of the ability of such arrays to classify organic and inorganic vapors.[? ? ?] In one approach, the functional group can be varied in polymers that are combined with a percolative network of carbon black (CB).[? ?] Another approach involves the use of an array of non-polymeric organic materials (NPOM) as the organic sorption phase

in composites with CB.[?] In these systems, sorption of an analyte effects a swelling of the organic phase, producing an increase in the resistance of the CB composite sensor film.

Films of Au nanoparticles (Au-NPs) capped with organothiol ligands have also been investigated as chemical vapor sensors.[???] Organically capped metal nanoparticles consist of a small metal core (typically less than 10 nm in diameter) surrounded by a dense organic layer of insulating material that is used to chemically passivate the metal particles. These materials, with a stoichiometry of $\sim$ 3:1 (Au:S-R), are easily synthesized using wet chemical techniques, and can remain soluble and chemically stable for extended periods in common organic solvents.[???] When exposed to a vapor, each Au-NP sensor film in the array will swell due to sorption of the analyte vapor. Sorption of vapor into Au-NP films produces either an increase or a decrease in film resistance upon exposure to analyte vapors.[????] This sensing mechanism thus allows exploitation of a unique capability of the Au-NP materials relative to other materials such as polymer/CB sensors. The ability to control the direction of the sensor resistance response could significantly increase the ability of such an array to identify or classify vapors. Han et al. and Wang et al. showed that arrays composed of a series of carboxylate-terminated ligands, dithiol ligands, and 1-decanethiol ligands, that had been embedded in the same matrix, could discriminate between n-hexane, benzene, toluene, and other nitro-aromatic compounds, at a variety of concentrations, by use of principal components analysis (PCA) or by use of artificial neural networks.[???]

In this work, the response and the discrimination performance of four groups of organothiol-capped Au-NPs sensor arrays has been evaluated in response to a variety of test vapors. The sensitivity values have been correlated to the molecular structure of the passivating

ligand, to elucidate the response mechanism of the sensor films. The first group of film compositions consisted of Au-NPs capped with straight-chain alkanethiols (R-SH), the second group consisted of Au-NPs capped with branched alkanethiols (R′-SH), and the third group consisted of Au-NPs capped with aromatic ligands (Ar-SH). The fourth group consisted of NPOM/Au-NP composite sensors formed by mixing with the NPOM passivated Au-NPs that contained a ligand with a terminated functional group that would have a homogeneous molecular interaction, with the NPOM. Such Au-NPs were capped with 2-phenylethanethiol mixed with aromatic molecules, to produce a film that was composed of 25 % organic matrix and 75 % Au by mass (C2Ph(Ar)). The library of analytes studied herein expands the number of analyte vapors that can be classified by Au-NPs sensor arrays. The analytes were chosen to have similar physicochemical properties, because vapor classification becomes more difficult as the vapor properties become increasingly mutually similar. The library of tested analyte vapors included six hydrocarbons (n-hexane, n-heptane, n-octane, isooctane, cyclohexane, and toluene), three polar aprotic vapors (chloroform, tetrahydrofuran, and ethyl acetate), and four alcohols (methanol, ethanol, isopropanol, and 1-butanol). The discrimination performance analysis involved the evaluation of the ability of each sensor array group to classify the test chemical vapors. The discrimination performance of an array that included all of the sensors investigated herein was also studied. Vapor discrimination was also evaluated as a function of the array size (i.e., number of sensors) and the average sensitivity of the array. The discrimination analysis was explored using PCA to visualize the array response clustering, and using Fishers linear discriminant (FLD) to determine the resolution factor of binary combination of analyte responses. FLD

was also used to quantify the cluster separation and the overlapping of responses between different analytes when PCA projections were used.

5.3 Experimental

5.3.1 Materials

Lithium aluminum hydride (95 %), sodium borohydride (98 %), hydrogen tetrachloroaurate trihydrate ($HAuCl_4 \cdot 3H_2O$, 99.9 %), tetraoctylammonium bromide (99 %), 1-butanethiol (99 %), 1-pentanethiol (98 %), 1-heptanethiol (98 %), 1-octanethiol (98.5 %), 2-methyl-1-propanethiol (92 %), 2-methyl-1-butanethiol (97 %), 3-methyl-1-butanethiol (95 %), cyclohexanethiol (97 %), 2-ethylhexanethiol (97 %), benzenethiol (98 %), 2-naphthalenethiol (99 %), 4-biphenylsulfonyl chloride, 2-anthracenesulfonyl chloride (90 %), 1,1',4',1"-terphenyl-4-thiol (97 %), naphthalene (99 %), biphenyl (99 %), anthracene(99 %), and p-terphenyl (99 %), and the test analytes n-hexane(Hex), n-heptane (Hept), n-octane (Oct), isooctane (iOct), and cyclohexane (cHex) were obtained from Sigma-Aldrich. Toluene (Tol), chloroform (Chl), tetrahydrofuran (THF), ethyl acetate (EtOAc), methanol (MeOH), ethanol (EtOH), isopropanol (iPOH) and 1-butanol (BuOH) were obtained from EM Science and 1-hexanethiol (97 %) was obtained from Alfa Aesar. All of the reagents and solvents were used without further purification. Deionized water with 18 MΩ cm resistivity was obtained from a Barnstead Nanopure purification system.

The synthesis of 4-biphenylthiol and 2-anthracenethiol was performed by the reduction of the sulfonyl chloride with lithium aluminum hydride, followed by the addition of

diluted hydrochloric acid.[?,?,?] Characterization of these ligands was performed by nuclear magnetic resonance and by mass spectrometry.

The organothiol-capped Au-NPs were synthesized as described by Brust et al., to produce Au-NPs with a diameter of $\sim$ 2 nm.[?] The mole ratio between $HAuCl_4 \cdot 3H_2O$ and the passivating ligands was 1:1. The Au-NPs were rinsed with water in a separatory funnel, concentrated by rotary evaporation, and precipitated in MeOH. The Au-NPs were then stored at 10 °C for 12 h. The Au-NPs were collected by centrifugation, redispersed in toluene, and reprecipitated in MeOH. After 12 h (10 °C), the Au-NPs were recollected by centrifugation and were subsequently vacuum-dried. Table 5.1 shows the abbreviations of the sensor/ligands studied herein. The NP films were prepared on 1 cm $\times$ 2 cm glass substrates that contained metal contacts in the form of a patterned set of interdigitated electrodes (IDEs) consisting of 50 nm of Au deposited over 30 nm of Cr. The electrode pattern produced 20 parallel sets of IDEs, with each IDE having dimensions of 0.240 $\times$ 5 mm (width $\times$ length), separated by a 10 μm gap. The NP films were cast from a sonicated solution (10 mg mL^{-1} in Tol) by manually depositing a 10 μL drop directly over the region of the substrate that contained the IDEs. The R-SH- and R′-SH-capped Au-NPs were soluble in Tol, whereas poor solubility in Tol was observed for Au-NPs that had the Ar-SH group. Sonication was necessary to increase the Au-NP dispersion. The films were dried under vacuum for 30 min. Thermogravimetric analysis was used to determine the ratio of Au atoms to ligands. For the R-SH-capped Au-NPs, the Au:S-R average mole ratio was 3:1. For the R′-SH-capped Au-NPs, the Au:S-R′ average mole ratio was 3.1:1, whereas for the Ar-SH-capped Au-NPs, the Au:S-Ar average mole ratio was 3.4:1. For the films that

R-SH	
1-butanethiol	Au-C4
1-pentanethiol	Au-C5
1-hexanethiol	Au-C6
1-heptanethiol	Au-C7
1-octanethiol	Au-C8
R′-SH	
2-methyl-1-propanethiol	Au-C3(2C)
2-methyl-1-butanethiol	Au-C4(2C)
3-methyl-1-butanethiol	Au-C4(3C)
1-cylohexanethiol	Au-cC6
2-ethyl-1-hexanethiol	Au-C6(2C2)
Ar-SH	
1-phenylthiol	Au-Ph
1-naphthalenethiol	Au-Naph
4-biphenylthiol	Au-Biph
2-anthracenethiol	Au-Ant
1,1',4',1"-terphenyl-4-thiol	Au-Terph
C2Ph(Ar)	
2-phenylethanethiol	Au-C2Ph
C2Ph, naphthalene	Au-C2Ph(Naph)
C2Ph, biphenyl	Au-C2Ph(Biph)
C2Ph, anthracene	Au-C2Ph(Ant)
C2Ph, terphenyl	Au-C2Ph(Terph)

Table 5.1: Abbreviations for the organothiol-capped Au nanoparticle chemical sensors. The C2Ph sensor was composed of functionalized C2Ph Au-NPs, and the C2Ph(Ar) sensors were composed of 25 % Ar/C2Ph and 75 % Au by mass

contained the C2Ph(Ar) group, the Au:C2Ph mass ratio was 80 % Au and 20 % C2Ph. Aromatic molecules were added to the solution to produce a sensor film that was composed by mass of 75 % Au and 25 % organic matrix. Table 5.2 shows the library of organic vapors, which consisted of six hydrocarbons (A), three polar aprotic vapors (B), and four alcohols (C).

5.3.2 Sensing Measurements

An array that contained 20 different types of sensors (two replicates per sensor type) was exposed simultaneously to the test analytes. The sensors were loaded into a rectangular, 40-slot chamber with sensor film replicates positioned randomly. The 45.5 $\times$ 3.0 $\times$ 1.5 cm ($w \times l \times d$) chamber was connected by Teflon tubing to the gas delivery system. The

	$P^{\circ}(\times 10^{-4})$
A	
Hex	17.41
Hept	5.11
Oct	1.54
*i*Oct	5.58
*c*Hex	11.27
Tol	3.17
B	
Chl	22.50
THF	21.30
EtOAc	10.49
C	
MeOH	14.06
EtOH	6.51
*i*POH	4.93
BuOH	0.73

Table 5.2: Saturated vapor pressure, P° (ppm), at 22 °C for all vapor analytes

internal cross-sectional area of the chamber was 1 cm^2 The dc resistance of the sensor array was measured with a digital multimeter (Keithley Model 2002) connected to a multiplexing unit (Keithley Model 7001). The resistance data were collected every 5-7 s from the array. A computer-controlled (LabVIEW) flow system delivered pulses of analyte vapor at a given fraction of the analytes vapor pressure. Oil-free air was obtained from the house compressed air source (1.10 ± 0.15 ppth of water vapor) controlled with a mass flow controller. The total flow rate was 5 L min^{-1} for the duration of the experiment.

The resistance sensitivity of the organothiol-caped Au-NPs sensor films was measured by determining the sensor response as a function of vapor concentration over the concentration range that corresponded to $0.0010 \leq P/P^{\circ} \leq 0.0200$, where P and P° are the partial pressure and vapor pressure, respectively, of the analyte at room temperature (22 °C), respectively. For the discrimination performance analysis of the sensor arrays, the analyte concentration was maintained at P/P° = 0.0100 (22 °C). Each analyte exposure consisted of 70 s of clean laboratory air, 80 s of analyte vapor in air, and 60 s of clean air (to purge the system). A total of 50 exposures per analyte were delivered to the sensor array. The

individual exposures were presented in random order. The time required for the 650 total exposures spanned approximately 38 h.

5.3.3 Data Processing

All data processing was carried out using MATLAB with custom-written routines. The resistance-based response, r_s, of a vapor sensor to a particular analyte was calculated as $r_s = \Delta R_{max}/R_b$, where R_b is the baseline-corrected resistance of the sensor in the absence of analyte, and ΔR_{max} is the baseline-corrected maximum resistance change upon exposure of the sensor to analyte. A spline was fitted to the baseline data obtained during the pre-exposure period, and values of $\Delta R_{max}/R_b$ were calculated by subtracting the values of the spline, extrapolated over the time of the exposure, from the observed sensor resistance during the exposure period.[?] Prior studies have shown that $\Delta R_{max}/R_b$ is a more reproducible metric than ΔR_{max}.[?] The sensitivity of a resistance-based vapor sensor film, s_R, was calculated from the slope of r_s vs P/P°, using a linear least-squares fit.

5.3.4 Discrimination Performance

To remove any systematic variation in the data that might be produced by changes in the concentration of analyte produced by the vapor delivery system, prior to analysis, the $\Delta R_{max}/R_b$ responses were sum-normalized:[?]

$$S'_{ij} = S_{ij} \left(\sum_{j=1}^{n} S_{ij}^2) \right)^{-1/2} \tag{5.1}$$

where S_{ij} is the $\Delta R_{max}/R_b$ sensor response signal of the j^{th} sensor (out of n total sensors) to the i^{th} analyte exposure, and S'_{ij} represents the sum-normalized analog of S_{ij}.

i. Principal Components Analysis. Differences in the sensor response data were visualized using PCA. The normalized data were mean-centered, and diagonalization of the covariance matrix of the data set provided a transformed set of dimensions that best described the data in terms of principal components (PCs). The first PC captured the largest amount of variance in the data; the second PC captured the second most variance in the data (subject to being orthogonal to the first PC), etc. The mean-centered data were then projected onto the first, second, and third PCs, and the data were plotted with respect to these coordinate vectors to observe the natural clustering of the data points. The eigenvalues of the mean-centered covariance matrix provided the relative amounts of variance in each of the corresponding eigenvectors, allowing quantification of the amount of the variance that was captured in the 3-dimensional PC space.

ii. Fishers Linear Discriminant. FLD was used on the normalized data to evaluate the pairwise discrimination performance of the array response between the various test analytes. FLD rotates the n-dimensional data space from the exposures to two analytes, and projects an orthogonal vector that maximizes the distance between the average sensor response values. This approach reduces the classification complexity from n-dimensions to one dimension. The optimal separation direction is found by maximization of the resolution factor, rf:[?]

$$rf = \frac{d}{(\sigma_1^2 + \sigma_2^2)^{1/2}} \tag{5.2}$$

where d is the distance between the population means, and σ_1 and σ_2 are the standard deviations of the projected populations that correspond to the two analytes of the classification. The rf value is similar to a sigma metric; i.e., rf = 1 indicates that statistically $\sim$ 72 % of the data points would be assigned to the correct class of the two possible analytes in the pair; with rf = 2, the correct assignment would occur for $\sim$ 92 % of the data points; whereas with rf = 3, the correct assignment would occur statistically for $\sim$ 98 % of the data points.

Training data were used to determine the projection vector that maximized rf and to create a decision boundary for each binary separation task. The decision boundary was a hyperplane normal to the projection vector that assumed a Gaussian clustering of the data. Statistically, points lying on the decision boundary have an equal likelihood of belonging to either of the two clusters. This decision boundary was then used to classify unknown exposures.

The FLD method was applied to all possible pairwise combinations of the 13 analytes tested. The first 25 exposures to each analyte were used to establish the decision boundary. A set of subsequent 25 exposures was then used as unknowns and the test data were classified based on their positions relative to the decision boundary.

5.4 Results

5.4.1 Response Sensitivity

Figure 5.1 shows the R_b (kΩ) values for the R-SH-, R′-SH-, and Ar-SH-capped Au-NPs chemiresistive films as a function of chain length (i.e., number of carbons). For all of the organothiol-capped Au-NPs, the value of R_b increased as the chain length of the organic ligand increased. The length of each organothiol was chosen by finding the longest carbon chain within the molecule. Figure 5.2 shows the s_R values for the organothiol-capped Au-NP sensors upon exposure to the analytes tested. For the R-SH-capped Au-NPs, positive s_R values were observed upon exposure to group A and B vapors, whereas negative s_R values were observed upon exposure to group C vapors. Upon exposure to group A and B vapors, for the R-SH and R′-SH sensors, as the number of carbon atoms in the ligand increased, the value of s_R also increased. Positive values of s_R were observed for the R′-SH sensors upon exposure to group C vapors. The Au-C4(3C) sensor produced very small s_R values upon exposure to group C vapors. In the case of the Ar-SH group, the s_R values obtained upon exposure to the group B and C vapors were higher than those observed upon exposure to the group A vapors. For the A vapors, the Ar-SH-based sensors produced very small values. The C2Ph(Ar) group produced higher s_R values for the group A and B vapors than for the group C vapors. For all of the vapors, considerably lower s_R values were exhibited by the Au-C2Ph(Naph) and Au-C2Ph(Ant) sensors. Generally, the Au-C2Ph sensor produced the highest s_R values among the Au-C2Ph(Ar) sensor group.

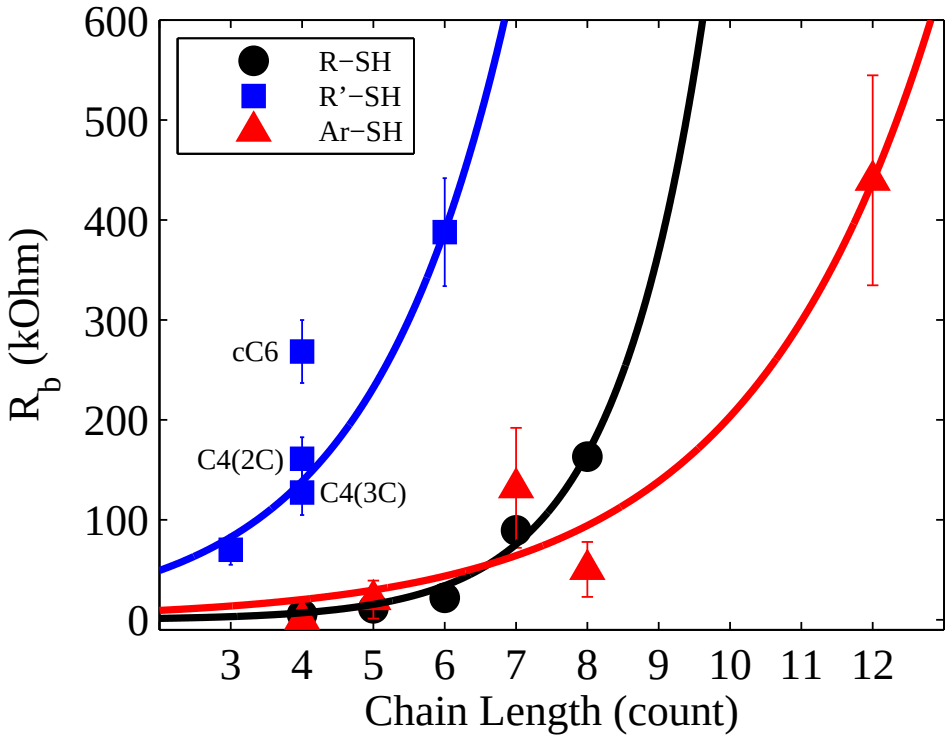

Figure 5.1: Baseline resistance, R_b (kΩ), obtained from two replicates of each chemiresistive sensor for the R-SH-, R′-SH-, and Ar-SH-capped AuNP films, as a function of chain length.

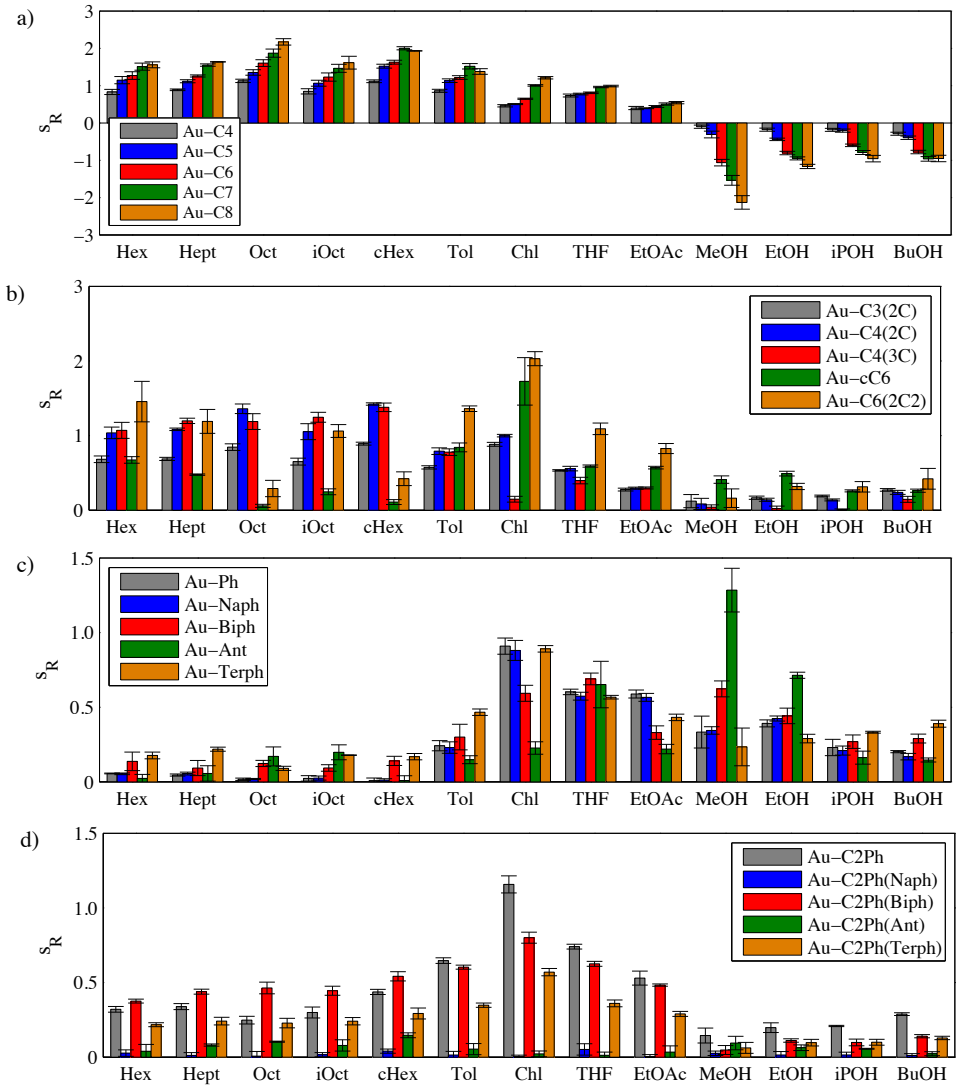

Figure 5.2: Average resistance-based sensitivities, s_R, for the organothiol-capped Au-NPs exposed to 13 analytes at $0.001 \leq P/P^{\circ} \leq 0.0200$. Each value is the average of two vapor sensors per sensor type. (a) s_R values for the R-SH-capped Au-NPs sensors, (b) s_R values for the R′-SH-capped Au-NPs sensors, (c) s_R values for the Ar-SH-capped Au-NPs sensors, and (d) s_R values for the C2Ph(Ar) functionalized Au-NPs sensors.

5.4.2 Discrimination Performance

i. Principal Components Analysis. Figure 5.3 shows the PCA projection of the first, second, and third principal components of the sum-normalized data. The axes show the fraction of the variance captured by each PC. Figure 5.3a shows the PC projection of the R-SH-capped Au-NP sensors, showing that the group C vapor clusters were clearly separated from the other vapors, but significant overlap was observed between iPOH and EtOH. The Chl cluster was well separated from the rest of the vapors. Cluster overlapping was observed between Hex, Hept, Oct, and iOct, as well as overlap between cHex and Tol.

Figure 5.3b shows the PC projection of the R′-SH-capped AuNP sensors. All of the group A vapors overlapped, whereas Chl was well separated from the rest of the vapors. The MeOH and EtOH clusters were scattered but fairly well separated from the other vapors, whereas the EtOAc cluster was slightly separated. Figure 5.3c shows the PC projection observed for the Ar-SH group of sensors. The only well-separated clusters were MeOH and EtOH. Figure 5.3d shows the PC projection for the C2Ph(Ar) group of sensors. Overlap between all the vapors was observed, and the only minor cluster separation observed was between the THF and Chl vapors.

Figure 5.3e shows the PC projection for the entire organothiol-capped Au-NP array. The group C vapors were well separated from the group A and B vapors. Overlaps between BuOH and iPOH, iPOH and EtOH, and EtOH and MeOH were observed. The group B vapors were separated from the group A and C vapors. For the group A clusters, cHex, iOct, and Tol were separated from Hex, Hept, and Oct, with slight overlaps between Hex and Hept. The Chl, THF, and EtOAc vapor clusters were well separated.

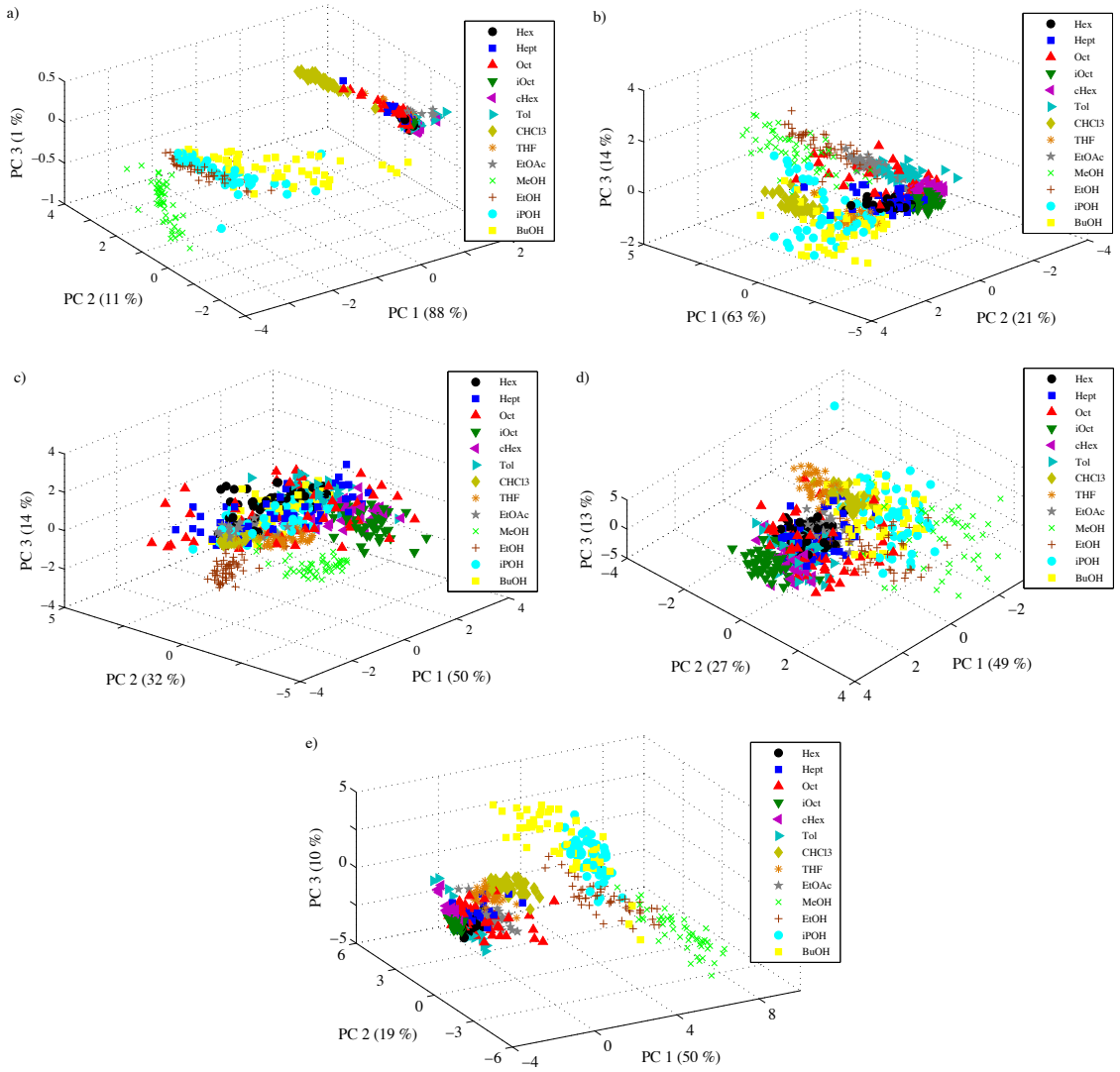

Figure 5.3: PCA projection of 13 analytes presented to the organothiol-capped Au-NPs at $P/P^{\circ} = 0.0100$: (a) projection for a sensor array of R-SH-capped Au-NP sensors (5 sensors total), (b) projection for a sensor array of R′-SH-capped Au-NP sensors (5 sensors total), (c) projection for a sensor array of Ar-SH-capped Au-NP sensors (5 sensors total), (d) projection for a sensor array of CPh2(Ar) functionalized Au-NP sensors (5 sensors total), and (e) projection for a sensor array of all sensor types (20 sensors total).

Figure 5.4 displays the variance that was captured in the first five PCs for the five different types of sensor arrays. For the first PC, the R-SH array captured the highest variance, followed by the R′-SH array. The first PC captured approximately the same variance for the Ar-SH and C2Ph(Ar) sensor arrays. For the second, third, and fourth PCs, the captured variance for the R-SH array was the lowest relative to those obtained for the other sensor arrays. The variance captured by the second, third, and fourth PCs, for the R′-SH, Ar-SH and C2Ph(Ar) sensor arrays, was approximately the same. The values of the variances captured in the first five PCs for an array that contained all of the sensor types were similar to those obtained from the Ar-SH and C2Ph(Ar) arrays.

ii. Fishers Linear Discriminant. Table 5.3 shows the rf values for the test analytes with three different Au-NP sensor arrays. The respective discrimination performance values are shown in parentheses. A performance value of 1.0 signifies 100 % discrimination. Table 5.3a shows the rf values obtained for an array of R-SH-capped Au-NP sensors. The most difficult discrimination tasks (i.e., lower rf values) were the binary combinations that included vapors with the same polarity (i.e., nonpolar, polar aprotic, polar protic). Analytes of different polarity were well discriminated. Table 5.3b shows the rf values obtained for an array of R′-SH-capped Au-NP sensors. The binary combinations that included the group B analytes showed the highest rf values. Contrary to the R-SH array, the R′-SH array did not produce high rf values for binary combinations that included the group C vapors. Table 5.3c shows the rf values obtained for an array of Ar-SH-capped Au-NP sensors. Binary combinations that included iOct and MeOH produced the highest rf values. Table 5.3d shows the rf values for an array of C2Ph(Ar) sensors. The highest rf values were

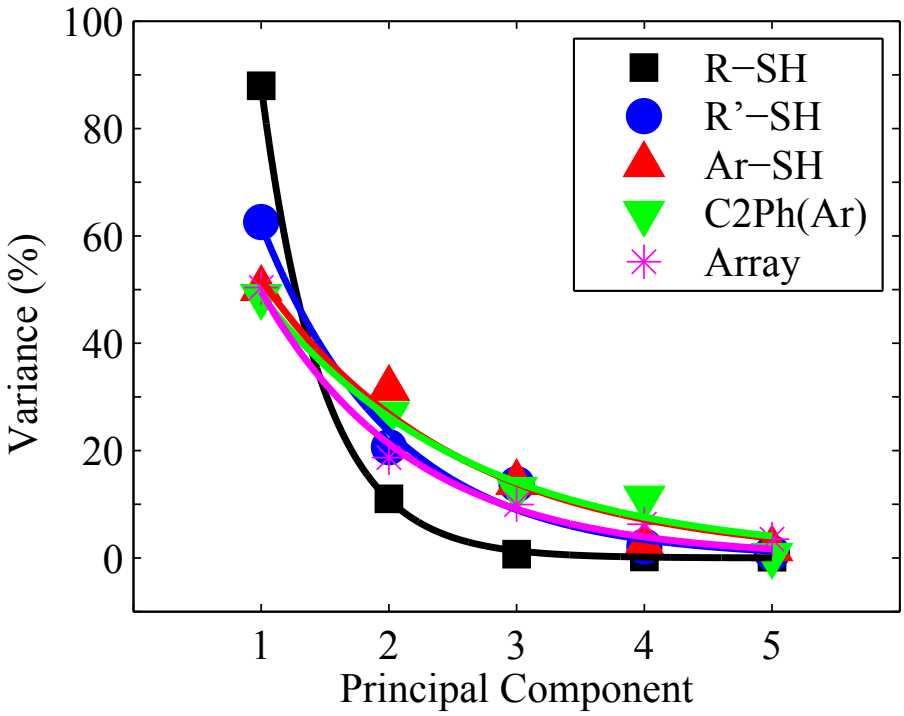

Figure 5.4: Variance captured as a function of the principal components vector number for five different sensor arrays.

obtained between vapors that had very different polarities, whereas binary combinations that included vapors within the same polarity group showed the lowest rf values. Table 5.3e shows the rf values obtained for an array that contained all of the sensor materials studied. The only binary combination that showed low discrimination was Hept and Oct (rf = 1.1).

a)	Hept	Oct	*i*Oct	*c*Hex	Tol	Chl	THF	EtOAc	MeOH	EtOH	*i*POH	BuOH
Hex	0.55 (0.74)	1.1 (0.76)	0.31 (0.64)	2.1 (0.90)	0.52 (0.66)	7.6 (1.0)	3.0 (0.96)	1.4 (0.86)	29 (1.0)	29 (1.0)	32 (1.0)	16 (1.0)
Hept		0.32 (0.56)	0.51 (0.64)	1.9 (0.92)	0.74 (0.74)	4.3 (1.0)	2.1 (0.96)	0.94 (0.78)	31 (1.0)	27 (1.0)	30 (1.0)	15 (1.0)
Oct			0.99 (0.68)	1.9 (0.78)	0.98 (0.62)	3.3 (1.0)	2.3 (0.82)	1.1 (0.80)	27 (1.0)	27 (1.0)	26 (1.0)	14 (1.0)
*i*Oct				3.2 (1.0)	0.75 (0.74)	9.2 (1.0)	3.5 (0.98)	2.7 (0.98)	25 (1.0)	28 (1.0)	33 (1.0)	16 (0.90)
*c*Hex					1.5 (0.88)	9.7 (1.0)	2.4 (1.0)	3.1 (1.0)	31 (1.0)	28 (1.0)	31 (1.0)	16 (1.0)
Tol						4.7 (1.0)	0.81 (0.80)	1.3 (0.84)	27 (1.0)	22 (1.0)	22 (0.98)	13 (0.90)
Chl							6.2 (1.0)	5.7 (1.0)	34 (1.0)	24 (1.0)	34 (1.0)	19 (1.0)
THF								1.3 (0.76)	33 (1.0)	28 (1.0)	32 (1.0)	16 (1.0)
EtOAc									31 (1.0)	26 (1.0)	27 (1.0)	15 (1.0)
MeOH										2.8 (1.0)	3.5 (0.98)	4.1 (1.0)
EtOH											5.4×10^{-4} (0.52)	1.7 (0.90)
*i*POH												1.3 (0.90)

b)	Hept	Oct	*i*Oct	*c*Hex	Tol	Chl	THF	EtOAc	MeOH	EtOH	*i*POH	BuOH
Hex	0.66 (0.64)	1.4 (0.92)	2.8 (1.0)	3.7 (1.0)	5.1 (1.0)	6.5 (0.98)	2.6 (0.96)	5.7 (1.0)	3.8 (0.90)	4.5 (0.98)	2.3 (0.80)	2.3 (0.80)
Hept		0.85 (0.74)	1.1 (0.82)	1.4 (0.80)	2.9 (0.94)	7.5 (1.0)	3.0 (0.90)	3.7 (0.98)	3.1 (0.96)	3.4 (0.92)	2.4 (0.96)	2.7 (0.98)
Oct			1.3 (0.88)	0.95 (0.74)	1.9 (0.82)	4.6 (0.98)	2.3 (0.90)	2.4 (0.86)	1.9 (0.92)	2.0 (0.74)	1.7 (0.88)	2.4 (0.82)
*i*Oct				1.5 (0.86)	3.5 (0.94)	9.8 (1.0)	4.1 (1.0)	4.0 (0.94)	5.0 (1.0)	5.3 (0.96)	3.1 (0.88)	2.8 (0.88))
*c*Hex					2.5 (0.92)	12 (1.0)	4.6 (1.0)	3.2 (0.96)	5.3 (1.0)	4.0 (0.98)	3.4 (0.86)	3.0 (0.82)
Tol						9.6 (1.0)	6.0 (1.0)	1.2 (0.80)	4.4 (1.0)	2.2 (0.96)	4.0 (1.0)	3.9 (0.82)
Chl							4.9 (1.0)	12 (1.0)	4.2 (1.0)	6.6 (0.98)	3.0 (0.96)	4.6 (0.98)
THF								6.4 (1.0)	3.8 (0.98)	3.9 (0.98)	1.0 (0.80)	0.90 (0.72)
EtOAc									4.2 (0.96)	2.3 (0.96)	3.8 (0.86)	3.8 (0.80)
MeOH										1.6 (0.78)	2.3 (0.96)	3.7 (0.98)
EtOH											2.5 (0.82)	3.3 (0.76)
*i*POH												0.65 (0.74)

c)	Hept	Oct	*i*Oct	*c*Hex	Tol	Chl	THF	EtOAc	MeOH	EtOH	*i*POH	BuOH
Hex	0.41 (0.6)	0.47 (0.52)	3.4 (1.0)	2.6 (0.98)	1.2 (0.84)	1.8 (0.74)	1.8 (0.74)	1.2 (0.7)	3.8 (0.96)	2.5 (0.84)	0.89 (0.72)	0.26 (0.6)
Hept		0.10 (0.54)	2.7 (1.0)	2.3 (0.92)	1.3 (0.82)	1.6 (0.66)	1.9 (0.68)	1.1 (0.66)	2.8 (0.96)	2.7 (0.76)	0.78 (0.74)	0.37 (0.56)
Oct			2.0 (0.96)	1.7 (0.88)	1.0 (0.72)	1.1 (0.66)	1.2 (0.56)	0.71 (0.56)	1.8 (0.88)	1.6 (0.76)	0.68 (0.6)	0.49 (0.58)
*i*Oct				0.65 (0.66)	1.7 (0.92)	7.1 (1.0)	6.2 (0.98)	5.1 (1.0)	6.8 (0.98)	6.0 (0.94)	3.3 (1.0)	2.7 (0.98)
*c*Hex					1.2 (0.82)	4.9 (0.96)	4.0 (0.9)	3.7 (0.94)	5.9 (1.0)	5.2 (0.92)	2.7 (0.98)	2.0 (0.92)
Tol						4.6 (1.0)	4.5 (0.92)	3.7 (0.96)	6.4 (1.0)	5.2 (0.96)	2.8 (0.96)	1.2 (0.82)
Chl							2.6 (0.96)	2.1 (0.94)	5.5 (1.0)	3.6 (0.98)	1.4 (0.64)	2.9 (0.8)
THF								3.1 (0.96)	4.2 (1.0)	2.9 (0.96)	1.6 (0.78)	2.3 (0.78)
EtOAc									7.1 (1.0)	4.4 (1.0)	0.52 (0.6)	1.8 (0.76)
MeOH										2.8 (0.8)	4.2 (0.98)	3.6 (0.98)
EtOH											3.2 (0.96)	3.9 (0.92)
*i*POH												1.2 (0.82)

d)	Hept	Oct	*i*Oct	*c*Hex	Tol	Chl	THF	EtOAc	MeOH	EtOH	*i*POH	BuOH
Hex	1.2 (0.82)	0.86 (0.82)	4.2 (1.0)	2.4 (1.0)	2.4 (1.0)	7.2 (1.0)	4.5 (1.0)	3.5 (0.96)	2.9 (0.84)	1.6 (0.82)	3.3 (0.96)	2.8 (0.96)
Hept		0.24 (0.64)	2.9 (0.92)	1.2 (0.78)	1.4 (0.86)	6.6 (1.0)	3.9 (0.86)	2.8 (0.94)	2.3 (0.94)	1.3 (0.82)	2.8 (1.0)	2.5 (1.0)
Oct			1.6 (0.86)	0.65 (0.70)	0.65 (0.70)	4.0 (0.98)	2.3 (0.96)	1.8 (0.82)	2.5 (0.88)	1.2 (0.82)	2.7 (0.96)	2.4 (0.94)
*i*Oct				2.3 (0.94)	1.6 (0.78)	13 (1.0)	8.4 (1.0)	4.2 (1.0)	4.9 (0.96)	3.0 (0.96)	6.1 (1.0)	5.1 (1.0)
*c*Hex					1.5 (0.78)	15 (1.0)	9.0 (1.0)	4.4 (0.98)	4.5 (0.92)	2.9 (0.96)	6.0 (1.0)	4.8 (1.0)
Tol						8.3 (1.0)	5.5 (1.0)	2.1 (0.88)	3.5 (0.94)	1.7 (0.88)	4.0 (1.0)	3.4 (0.96)
Chl							3.7 (0.96)	5.5 (1.0)	2.2 (0.84)	4.8 (1.0)	2.2 (0.84)	3.2 (0.88)
THF								3.1 (0.98)	2.3 (0.94)	3.2 (1.0)	2.4 (0.98)	2.7 (0.98)
EtOAc									2.1 (0.8)	1.8 (0.92)	2.9 (0.96)	2.6 (0.88)
MeOH										1.4 (0.86)	0.53 (0.64)	0.66 (0.62)
EtOH											1.9 (0.90)	2.1 (0.98)
*i*POH												0.14 (0.54)

e)	Hept	Oct	*i*Oct	*c*Hex	Tol	Chl	THF	EtOAc	MeOH	EtOH	*i*POH	BuOH
Hex	3.5 (0.98)	3.1 (1.0)	4.8 (1.0)	5.5 (1.0)	5.5 (1.0)	7.9 (1.0)	5.1 (1.0)	8.3 (1.0)	17 (1.0)	16 (1.0)	38 (1.0)	12 (1.0)
Hept		1.1 (0.74)	2.5 (0.98)	3.6 (1.0)	2.7 (0.94)	4.8 (1.0)	4.4 (1.0)	5.2 (1.0)	11 (1.0)	11 (1.0)	22 (1.0)	12 (1.0)
Oct			2.2 (0.98)	3.0 (1.0)	3.2 (0.98)	5.5 (1.0)	3.4 (0.96)	4.1 (0.98)	12 (1.0)	10 (1.0)	19 (1.0)	9.9 (1.0)
*i*Oct				4.0 (1.0)	4.0 (0.98)	15 (1.0)	8.0 (1.0)	6.5 (1.0)	27 (1.0)	12 (1.0)	28 (1.0)	14 (1.0)
*c*Hex					3.1 (0.90)	14 (1.0)	7.8 (1.0)	6.6 (1.0)	22 (1.0)	18 (1.0)	27 (1.0)	15 (1.0)
Tol						10 (1.0)	6.3 (1.0)	4.2 (1.0)	13 (1.0)	9.6 (1.0)	12 (1.0)	8.9 (1.0)
Chl							8.3 (1.0)	16 (1.0)	11 (1.0)	14 (1.0)	24 (1.0)	16 (1.0)
THF								5.4 (1.0)	15 (1.0)	13 (1.0)	27 (1.0)	16 (1.0)
EtOAc									15 (1.0)	13 (1.0)	16 (1.0)	14 (1.0)
MeOH										3.7 (1.0)	3.1 (0.98)	3.8 (1.0)
EtOH											3.1 (0.94)	3.8 (0.98)
*i*POH												2.2 (0.98)

Table 5.3: Resolution factors, rf, and performance values (parentheses) for all possible binary combinations of analytes tested at P/P° = 0.0100 by using the $\Delta R_{max}/R_b$ values; (a) discrimination values obtained for the R-SH Au-NP array; (b) discrimination values obtained for the R′-SH Au-NP array; (c) discrimination values obtained for the Ar SH Au-NP array; d) discrimination values obtained for the C2Ph(Ar) Au-NP array; e) discrimination values obtained for the combination of all sensor types studied.

5.5 Discussion

5.5.1 Sensor Response Mechanism

The tunneling constant, β_n (carbon^{-1}), for the R-SH-, R′-SH-, and Ar-SH-capped AuNPs films was determined by

$$R_b = R_\circ \exp\left[n\beta_n\right] \tag{5.3}$$

where n is the chain length. The values of β_n were 0.8, 0.5, and 0.4 carbon^{-1}, for the R-SH-, R′-SH-, and Ar-SH-capped Au-NPs, respectively. The response of Au-cC6 was excluded in the determination of β_n, due to the deviation of its R_b from the trend exhibited by other ligands, which may reflect the molecular unsaturation of the ligand resulting in a different Au-NP surface passivation as compared to the other R′-SH ligands. The value of β_n obtained for R-SH-capped Au-NPs was similar to that determined in previous studies[?] as well as to that determined for aromatic organothiols.[?] The value of β_n for R′-SH-capped AuNPs was lower than the value of β_n obtained for R-SH-capped Au-NPs. This behavior may reflect the strong hydrophobic interactions of the R′-SH ligands,[?] which could lead to surface voids and thus result in smaller distances between neighboring Au-NPs, thereby increasing the rate of electron hopping between particles in the film.

The R-SH-capped Au-NP sensors showed a characteristic response behavior of exhibiting both positive and negative values of s_R. Conversely, R′-SH did not exhibit such dual response behavior, which could be due to the presence of surface voids that allowed for alcohol vapors to partition into the film. Positive values of s_R were obtained for the reminder of the organothiol-capped Au-NP sensor library. The ligand and/or NPOM organization of

the R′-SH, Ar-SH, and C2Ph(Ar) sensors produced a film morphology that allowed alcohol vapors to partition into the sensing film and increase the distance between the Au-NPs (e.g., swelling), unlike the straight-chain alkanethiol-capped Au-NP sensors, where decreases in the distance between Au-NPs upon exposure to alcohol vapors have been observed.[?]

The high selectivity of the Ar-SH group toward group B and C vapors is of note. Polycyclic aromatic compounds pack rigidly on Au surfaces, due to the conjugation of the phenyl rings.[?] The presence of packed molecular islands with different orientations leads to voids on the surface of the Au-NP, which could facilitate the sorption of analyte at the Au-NP surface, as has been observed for at Au electrodes.[?] Such surface defects could also contribute to low value of β_n. The sorption of polar analytes increases the polarity of the film, facilitating the sorption of more molecules of the same vapor. The low s_R value observed upon exposure to the group A vapors can be attributed to impermeability of the π-stacked system toward nonpolar vapors. In the case of Tol, a high s_R value was obtained due to the permeating aromatic phenyl moiety. The addition of chemical substituents on the terminal Ph ring of the Ar-SH ligands could allow for control over the selectivity of such films. For example, Zhang et al. investigated CH_3-Ph-SH and OH-Ph-SH-capped AuNPs in response to dichloromethane and MeOH. For CH_2Cl_2 vapors, Ph-CH_3 produced a higher response than did Ph-OH, whereas for MeOH vapors, OH-Ph produced higher responses than Ph-CH_3.[?] For R-COOH and R-NH_2 groups, Johnson et al. observed that HOOC-Ph-SH and NH_2-Ph-SH-capped Au-NPs were prone to significant aggregation through hydrogen bond formation.[?] Rowe et al. described the synthesis and electrical properties of 4-mercaptodiphenylacetylene (DPA)- capped Au-NPs.[?] Such

DPA-capped Au-NPs demonstrated lower resistances, and thus a higher hopping rate, than R-SH-capped Au-NPs of similar mass.[?] Such ligands could also be chemically modified with different functional groups to control the sensitivity of Au-NPs films.

The difference in the chemical structures of the nonbonding aromatic NPOMs, which were embedded into the C2Ph-capped Au-NP films, produced different s_R values for the various sensors. Low s_R values were observed for Au-C2Ph(Naph) and AuC2Ph(Ant), whereas high s_R values were observed for AuC2Ph(Biph) and Au-C2Ph(Terph). The rigid π-stacked formation of Naph and Ant could decrease the availability of vapor sorption sites in the sensor film. Conversely, the rotational single bonds of Biph and Terph allowed for less molecular π-stacking, and allows for more vapor to be sorbed. The influence of the NPOM phase on the s_R values opens a new approach to the development of Au-NP sensor films that can produce a variety of vapor-sensing selectivities, especially for NPOM phases that do not have a coordinating functional group for the Au-NP.

5.5.2 Discrimination Performance

i. Clustering and Overlap Quantification. FLD can be used to obtain a quantitative measure of the array clustering and overlap, by using the variance captured by the first five PCs. Table 5.4 shows the rf values and their respective discrimination performance values (parentheses), for each of the sensor arrays, used to produce the PC projections of Figure 5.3. The rf values obtained from the PC projections were generally somewhat higher than the rf values displayed in Table 5.3. This small increase can be attributed to the filtering of response noise using a limited number of PC vectors.

a)	Hept	Oct	*i*Oct	*c*Hex	Tol	Chl	THF	EtOAc	MeOH	EtOH	*i*POH	BuOH
Hex	0.58 (0.74)	1.0 (0.78)	0.67 (0.70)	2.2 (0.92)	0.51 (0.66)	11 (1.0)	2.9 (0.96)	1.9 (0.92)	150 (1.0)	120 (1.0)	44 (1.0)	18 (1.0)
Hept		0.24 (0.68)	0.71 (0.76)	2.3 (0.94)	0.86 (0.70)	4.8 (1.0)	2.1 (0.96)	1.0 (0.78)	34 (1.0)	47 (1.0)	40 (1.0)	18 (1.0)
Oct			0.79 (0.66)	2.1 (0.94)	1.1 (0.76)	3.6 (0.96)	1.6 (0.86)	1.1 (0.76)	26 (1.0)	24 (1.0)	26 (1.0)	17 (1.0)
*i*Oct				3.6 (1.0)	0.58 (0.86)	21 (1.0)	3.4 (0.98)	2.8 (0.98)	240 (1.0)	150 (1.0)	52 (1.0)	19 (1.0)
*c*Hex					0.94 (0.76)	19 (1.0)	3.0 (0.98)	2.7 (1.0)	333 (1.0)	94 (1.0)	39 (1.0)	15 (1.0)
Tol						7.0 (1.0)	2.0 (0.94)	1.5 (0.82)	59 (1.0)	37 (1.0)	16 (1.0)	11 (0.98)
Chl							6.8 (1.0)	8.9 (1.0)	20 (1.0)	17 (1.0)	15 (1.0)	15 (1.0)
THF								1.3 (0.74)	47 (1.0)	74 (1.0)	49 (1.0)	17 (1.0)
EtOAc									200 (1.0)	73 (1.0)	30 (1.0)	14 (1.0)
MeOH										2.9 (0.98)	3.5 (0.98)	4.3 (0.98)
EtOH											0.71 (0.68)	2.0 (0.86)
*i*POH												1.5 (0.92)

b)	Hept	Oct	*i*Oct	*c*Hex	Tol	Chl	THF	EtOAc	MeOH	EtOH	*i*POH	BuOH
Hex	1.4 0.76)	2.2 (0.94)	2.8 (0.98)	4.0 (1.0)	5.3 (1.0)	6.0 (1.0)	2.9 (0.94)	4.6 (0.96)	6.3 (1.0)	5.6 (0.98)	3.5 (0.96)	3.1 (0.92)
Hept		1.0 (0.76)	0.57 (0.64)	1.4 (0.86)	2.5 (0.90)	3.2 (1.0)	3.1 (0.94)	3.9 (0.86)	2.8 (0.94)	3.7 (0.90)	2.8 (0.92)	3.5 (0.98)
Oct			1.0 (0.78)	0.68 (0.70)	2.0 (0.82)	3.1 (0.98)	3.2 (0.98)	2.2 (0.74)	1.7 (0.90)	1.7 (0.72)	2.1 (0.94)	3.0 (0.96)
*i*Oct				1.4 (0.78)	3.1 (0.94)	23 (1.0)	6.0 (1.0)	4.4 (0.98)	7.5 (1.0)	8.9 (1.0)	3.9 (1.0)	4.5 (0.92)
*c*Hex					2.5 (0.92)	35 (1.0)	6.9 (1.0)	4.4 (0.94)	7.6 (1.0)	9.1 (1.0)	4.3 (0.98)	5.2 (1.0)
Tol						6.0 (1.0)	5.1 (1.0)	0.43 (0.70)	5.2 (1.0)	2.9 (0.98)	4.3 (1.0)	5.3 (0.98)
Chl							2.8 (0.96)	6.4 (1.0)	4.7 (1.0)	4.3 (0.98)	2.6 (1.0)	5.0 (0.96)
THF								4.8 (1.0)	4.4 (1.0)	4.0 (1.0)	1.1 (0.84)	1.0 (0.82)
EtOAc									4.0 (1.0)	1.6 (0.94)	3.9 (1.0)	5.7 (1.0)
MeOH										1.4 (0.90)	2.3 (0.88)	4.3 (0.98)
EtOH											2.6 (0.96)	4.7 (0.98)
*i*POH												0.56 (0.70)

c)	Hept	Oct	*i*Oct	*c*Hex	Tol	Chl	THF	EtOAc	MeOH	EtOH	*i*POH	BuOH
Hex	1.6 (0.80)	1.1 (0.74)	3.7 (1.0)	3.1 (0.96)	1.2 (0.82)	2.7 (0.96)	4.3 (1.0)	1.4 (0.74)	7.3 (1.0)	5.5 (1.0)	1.4 (0.76)	0.65 (0.72)
Hept		0.20 (0.60)	2.4 (0.86)	2.1 (0.86)	1.9 (0.80)	2.0 (0.76)	3.0 (0.90)	1.0 (0.56)	4.1 (0.98)	3.6 (0.92)	0.37 (0.58)	0.95 (0.80)
Oct			2.2 (0.76)	1.9 (0.74)	1.4 (0.70)	1.8 (0.76)	2.0 (0.74)	1.1 (0.74)	2.2 (0.98)	2.1 (0.72)	0.42 (0.70)	0.85 (0.78)
*i*Oct				0.62 (0.66)	1.9 (0.92)	18 (1.0)	5.4 (1.0)	6.4 (0.96)	8.3 (1.0)	12 (1.0)	2.0 (0.88)	1.9 (0.88)
*c*Hex					1.4 (0.88)	14 (1.0)	5.9 (1.0)	4.7 (0.96)	11 (1.0)	14 (1.0)	1.8 (0.82)	1.7 (0.92)
Tol						8.6 (1.0)	6.4 (0.98)	4.1 (0.96)	11 (1.0)	14 (1.0)	2.2 (0.80)	0.82 (0.70)
Chl							2.8 (0.96)	1.2 (0.90)	7.1 (1.0)	4.8 (1.0)	1.3 (0.72)	3.1 (0.80)
THF								2.7 (0.94)	2.6 (0.96)	2.5 (0.94)	1.8 (0.84)	3.6 (0.96)
EtOAc									5.9 (1.0)	3.7 (1.0)	0.64 (0.66)	1.3 (0.68)
MeOH										2.6 (0.94)	3.4 (0.98)	3.4 (0.98)
EtOH											2.3 (0.96)	2.9 (0.86)
*i*POH												0.85 (0.76)

d)	Hept	Oct	*i*Oct	*c*Hex	Tol	Chl	THF	EtOAc	MeOH	EtOH	*i*POH	BuOH
Hex	1.2 (0.78)	1.7 (0.86)	3.9 (0.94)	3.1 (0.92)	2.8 (0.98)	4.0 (0.98)	2.8 (0.98)	2.5 (0.96)	5.6 (0.98)	4.1 (1.0)	3.5 (0.98)	3.0 (0.94)
Hept		0.24 (0.60)	1.5 (0.82)	1.4 (0.84)	1.1 (0.76)	4.0 (1.0)	3.2 (0.92)	1.3 (0.78)	3.1 (0.98)	2.0 (0.76)	3.4 (0.94)	3.0 (0.94)
Oct			1.4 (0.84)	1.7 (0.84)	1.0 (0.80)	4.4 (1.0)	3.0 (0.96)	1.1 (0.80)	2.4 (0.94)	1.3 (0.76)	2.5 (0.94)	3.1 (0.96)
*i*Oct				1.6 (0.84)	0.72 (0.66)	23 (1.0)	13 (1.0)	1.3 (0.78)	9.7 (1.0)	4.0 (1.0)	6.5 (0.94)	9.4 (0.98)
*c*Hex					0.84 (0.72)	13 (1.0)	10 (1.0)	1.4 (0.82)	7.9 (0.98)	3.7 (0.98)	5.1 (0.94)	8.3 (1.0)
Tol						11 (1.0)	8.5 (1.0)	0.88 (0.74)	6.4 (0.98)	3.0 (0.98)	5.2 (1.0)	6.2 (1.0)
Chl							3.6 (1.0)	5.9 (1.0)	4.8 (1.0)	5.0 (1.0)	2.3 (0.98)	1.1 (0.76)
THF								3.7 (0.98)	5.1 (0.98)	4.5 (0.98)	2.7 (0.92)	1.8 (0.90)
EtOAc									3.3 (0.96)	2.3 (0.80)	3.1 (0.98)	4.2 (1.0)
MeOH										0.77 (0.76)	1.2 (0.90)	2.6 (0.98)
EtOH											2.0 (0.84)	3.0 (0.92)
*i*POH												1.1 (0.70)

e)	Hept	Oct	*i*Oct	*c*Hex	Tol	Chl	THF	EtOAc	MeOH	EtOH	*i*POH	BuOH
Hex	3.4 (1.0)	3.1 (1.0)	4.7 (1.0)	4.7 (1.0)	4.1 (0.96)	9.3 (1.0)	5.0 (0.98)	7.1 (1.0)	20 (1.0)	16 (1.0)	12 (1.0)	11 (1.0)
Hept		1.2 (0.80)	3.3 (1.0)	2.4 (1.0)	2.6 (0.84)	3.8 (1.0)	3.3 (0.98)	4.5 (0.96)	11 (1.0)	11 (1.0)	9.9 (1.0)	8.8 (1.0)
Oct			1.7 (0.90)	1.9 (0.92)	2.2 (0.88)	5.8 (1.0)	3.3 (1.0)	3.2 (0.96)	7.8 (1.0)	8.9 (1.0)	9.1 (1.0)	8.9 (1.0)
*i*Oct				3.3 (1.0)	3.1 (0.92)	29 (1.0)	15 (1.0)	7.8 (1.0)	14 (1.0)	19 (1.0)	12 (1.0)	10 (1.0)
*c*Hex					2.4 (0.82)	26 (1.0)	16 (1.0)	7.0 (1.0)	15 (1.0)	25 (1.0)	10 (1.0)	9.1 (1.0)
Tol						8.8 (1.0)	8.9 (1.0)	3.1 (0.98)	13 (1.0)	9.6 (1.0)	8.2 (1.0)	10 (1.0)
Chl							8.0 (1.0)	10 (1.0)	16 (1.0)	8.3 (1.0)	14 (1.0)	7.7 (1.0)
THF								6.2 (1.0)	13 (1.0)	14 (1.0)	9.9 (1.0)	11 (1.0)
EtOAc									14 (1.0)	9.3 (1.0)	9.4 (1.0)	8.0 (1.0)
MeOH										3.7 (0.98)	5.2 (1.0)	4.6 (1.0)
EtOH											4.0 (1.0)	2.9 (0.96)
*i*POH												1.4 (0.86)

Table 5.4: Resolution factors, rf, and performance values (parentheses) for all possible binary combinations of analytes tested at P/P° = 0.0100 by using the $\Delta R_{max}/R_b$ values; (a) discrimination values obtained for the R-SH Au-NP array; (b) discrimination values obtained for the R′-SH Au-NP array; (c) discrimination values obtained for the Ar SH Au-NP array; d) discrimination values obtained for the C2Ph(Ar) Au-NP array; e) discrimination values obtained for the combination of all sensor types studied.

ii. Vapor and Polarity Discrimination Performance. The results obtained in Tables 5.3 can be summarized by averaging the rf values obtained for each analyte vs each polar group studied. Table 5.5 shows the average rf values, rf, for all the binary combinations obtained from the $\Delta R_{max}/R_b$ responses (first column), and the rf values obtained vs each vapor group (second to fourth column). For the R-SH group, the highest rf values were obtained for the group C vapors, due to the negative sign of the $\Delta R_{max}/R_b$ response values. Vapor misclassification was obtained when the binary combination contained analytes within the same vapor group. For group C vapors, as the carbon chain became longer, the rf became lower due to an increase of the proportion of nonpolar moiety. The R′-SH group produced discrimination rf values for most of the binary combinations, except for the combinations that contained vapors within the same polarity group, such as the A and C groups. The rf values obtained for the binary combinations within the A group were higher than those produced by the R-SH array. The higher rf values were obtained for the group B vapors. The R-SH produced higher overall rf values than the R′-SH group. Conversely, for binary combinations of analytes within the same polarity group, the R′-SH group performed better. The Ar-SH group, in comparison with the other sensor groups, produced the highest rf values for vapors within the C group. In the case of the C2Ph(Ar) group, the highest discrimination rf values were obtained for the group B vapors. Table 5.5e shows the rf values produced for an array that contained of all the sensor types. Vapor discrimination rf values were obtained for all combinations except for the combinations of Oct vs group A vapors and iPOH vs group C vapors.

iii. Discrimination Performance Dependence on Sensor Array Size and Sensitivity. The

	$\overline{rf}$	$\overline{rf}$ vs A	$\overline{rf}$ vs B	$\overline{rf}$ vs C		$\overline{rf}$	$\overline{rf}$ vs A	$\overline{rf}$ vs B	$\overline{rf}$ vs C
a) R-SH					**b) R′-SH**				
Hex	10	0.92	4.0	26		3.4	2.7	4.9	3.2
Hept	9.6	0.81	2.4	26		2.7	1.4	4.7	2.9
Oct	8.8	1.1	2.2	24		2.0	1.3	3.1	2.0
*i*Oct	10	1.2	5.1	26		3.7	2.1	5.9	4.1
*c*Hex	11	2.1	5.1	26		3.8	2.0	6.6	3.9
Tol	7.9	0.90	2.3	21		3.9	3.2	5.6	3.6
Chl	13	6.5	6.0	28		7.1	8.3	8.3	4.6
THF	11	2.4	3.8	27		3.6	3.8	3.8	2.4
EtOAc	9.8	1.8	3.5	25		4.4	3.4	3.4	3.5
MeOH	23	28	32	3.5		3.6	3.9	4.1	2.5
EtOH	20	27	26	1.5		3.4	3.5	4.2	2.4
*i*POH	23	29	31	1.6		2.5	2.8	2.6	1.8
BuOH	12	15	17	2.4		2.8	2.8	3.1	2.5
c) Ar-SH					**d) C2Ph(Ar)**				
Hex	1.7	1.6	1.6	1.9		3.1	2.2	5.1	2.6
Hept	1.5	1.3	1.6	1.7		2.4	1.4	4.4	2.2
Oct	1.1	1.1	1.0	1.1		1.7	0.80	2.7	2.2
*i*Oct	4.0	2.1	6.1	4.7		4.8	2.5	8.5	4.8
*c*Hex	3.1	1.7	4.2	3.9		4.6	1.6	9.6	4.5
Tol	2.9	1.3	4.3	3.9		3.0	1.5	5.3	3.2
Chl	3.3	3.5	2.3	3.3		6.3	9.0	4.6	3.1
THF	3.0	3.3	2.8	2.7		4.3	5.6	3.4	2.6
EtOAc	2.9	2.6	2.6	3.4		3.1	3.1	4.3	2.4
MeOH	4.6	4.6	5.6	3.5		2.5	3.5	2.2	0.97
EtOH	3.7	3.9	3.6	3.3		2.2	1.9	3.2	1.8
*i*POH	1.9	1.9	1.2	2.9		2.9	4.2	2.5	0.85
BuOH	1.9	1.2	2.3	2.9		2.7	3.5	2.8	1.0
e) All 20 Sensors									
Hex	11	4.5	7.1	21					
Hept	7.0	2.7	4.8	14					
Oct	6.4	2.5	4.3	13					
*i*Oct	11	3.5	9.7	20					
*c*Hex	11	3.9	9.5	20					
Tol	6.9	3.7	6.8	11					
Chl	12	9.5	12	16					
THF	9.9	5.8	6.9	18					
EtOAc	9.5	5.8	11	14					
MeOH	13	17	14	3.5					
EtOH	11	13	13	3.6					
*i*POH	18	24	22	2.8					
BuOH	11	12	15	3.3					

Table 5.5: Average resolution factors, $\overline{rf}$, obtained from $\Delta R_{max}/R_b$ values for each of the analyte vapors versus each polar group for five different sensor arrays: (a) R-SH, (b) R′-SH, (c) Ar-SH, (d) C2Ph(Ar), and (e) All 20 Sensors. The groups were divided into nonpolar vapors (A: Hex, Hept, Oct, *i*Oct, *c*Hex, Tol), polar aprotic vapors (B: Chl, THF, EtOAc), and polar protic vapors (C: MeOH, EtOH, *i*POH, BuOH).

magnitude of the rf values obtained in Table 5.3e was also influenced by the array size. The total number of combinations, C, per array size, N, is given by

$$C = \frac{N_{Total}!}{N!(N_{Total} - N)!} \tag{5.4}$$

where N_{Total} is the total number of sensors (N_{Total} = 20), and N is the array size (i.e., number of sensors in array). Figure 5.5 shows the average rf values, rf, for all possible combinations of sensors for each possible array size. As the value of N increased, the $\overline{rf}$ value also increased. Arrays of two sensors are not displayed due to high standard deviations and low values of recognition, as observed by Park et al.? The maximum $\overline{rf}$ value was obtained for N = 13 sensors. The larger number of sensors is beneficial for resolving, on average, a generalized set of test vapors. A larger number of sensors and descriptors increases the probability that the dimensionality of vapor space is fully spanned by the array.

The value of s_R for each sensor in the array, and the average sensitivity, $\overline{s_R}$, of the array could influence the discrimination performance. Figure 5.6 shows the $\overline{rf}$ values obtained for all possible arrays for N = 4, 10, and 19 sensors, as a function of $\overline{s_R}$, for each possible array of a given N. A linear least-squares fit has also been depicted. For N = 4 and 10 sensors, as the $\overline{s_R}$ increased, the value of $\overline{rf}$ also increased. Conversely, for N = 19 sensors, as the value of $\overline{s_R}$ increased, the value of $\overline{rf}$ decreased. Figure 5.7 shows the slope, ζ, obtained from linear least-squares fit (i.e., red line) depicted in Figure 5.6 as function of N. The magnitude of ζ increased from N = 3 to 4; however, the value decreased until reaching an inflection point at $\sim$ 10 sensors. For N = 13 sensors, the value of the slope was

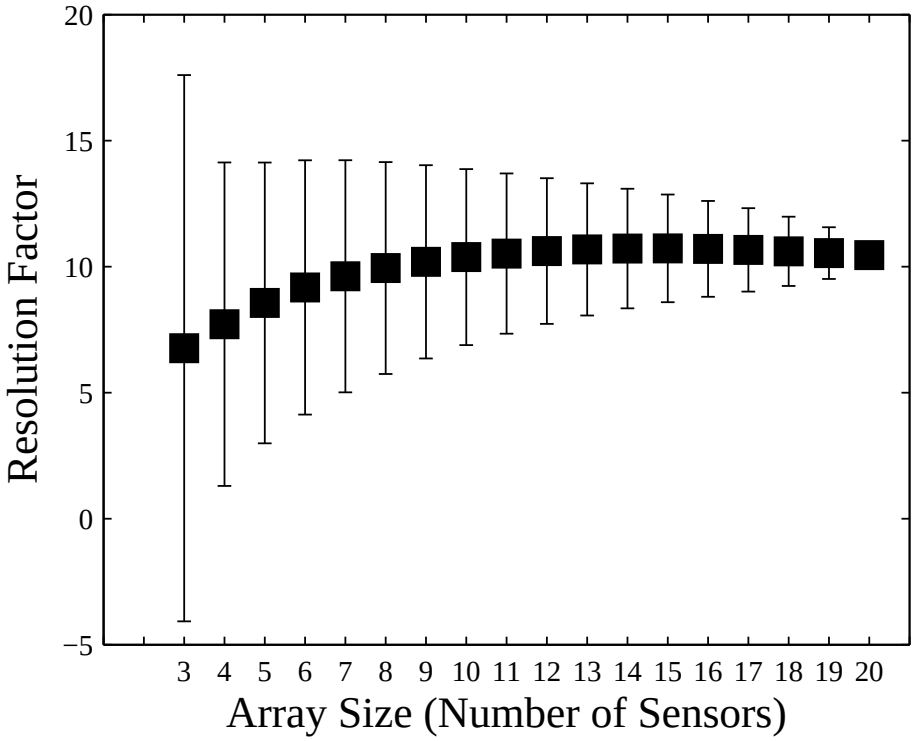

Figure 5.5: Average resolution factor values, $\overline{rf}$, as a function of array size (i.e., number of sensors), N. Each $\overline{rf}$ value represents the average of all binary combinations of analytes, for all possible array sizes in each system.

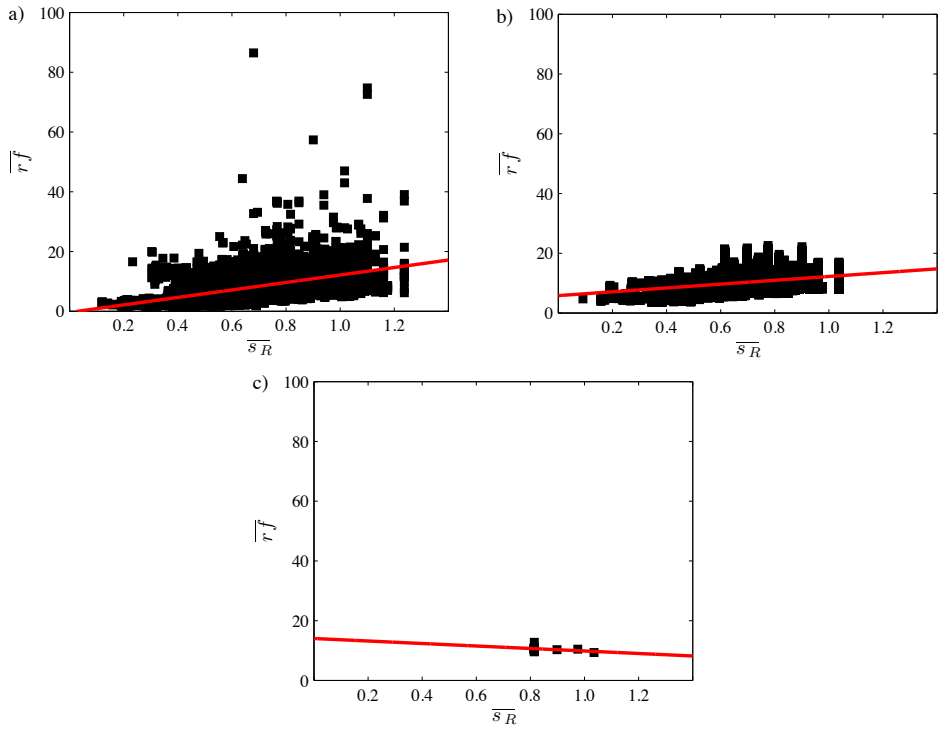

Figure 5.6: Average resolution factor, $\overline{rf}$, as a function of the average resistance sensitivity, $\overline{s_R}$, for all possible arrays for three different values of N, (a) N = 4 sensors, (b) N = 10 sensors, and (c) N = 19 sensors. Each square represents the average rf value for an array with an average s_R. The red line represents the linear least-squares fit.

$\sim$ 0, becoming negative for $N > 13$ sensors. The 0 value of ζ for N = 13 confirmed that approximately the maximum discrimination performance of an array of organothiol-capped Au-NPs was reached at such N, as observed in Figure 5.5.

5.6 Conclusions

The vapor selectivity, as determined by the resistance response sensitivity, of an array of organothiol-capped Au-NPs is well described by considering the polarity of the vapor and the passivating ligand, as well as the chemical structure of the passivating ligand. For straight-chain alkanethiol-capped Au-NPs, a dual response mechanism was observed, in

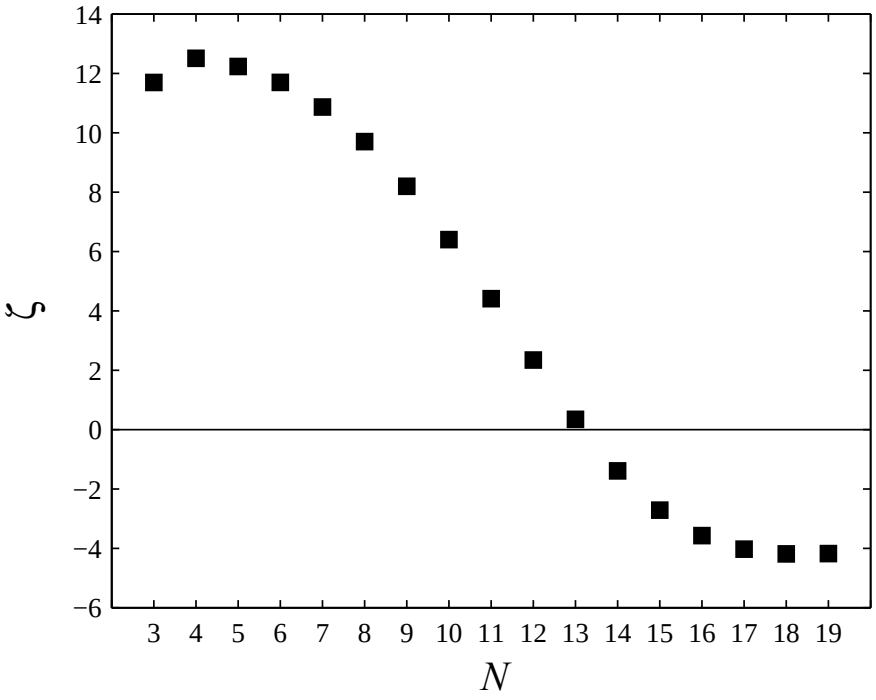

Figure 5.7: Slope, ζ, as a function of the array size (i.e., number of sensors), N.

which positive $\Delta R_{max}/R_b$ values were obtained upon exposure to hydrocarbons and polar analytes, whereas negative $\Delta R_{max}/R_b$ values were obtained upon exposure to alcohols. The value of $\mid s_R \mid$ increased as the length of the alkanethiol increased. Branched alkanethiol-capped Au-NPs did not shown a dual response mechanism, perhaps due to surface defects, but their responses followed a monotonic chain length trend (except of Au-cC6), in which a higher number of carbons in the ligand produced higher values of $\mid s_R \mid$. Functionalized Au-NPs with aromatic thiols showed high selectivity toward polar vapors, due to the presence of molecular π-stacked islands on the surface of the NP, which allowed for voids to sorb polar analytes. The incorporation of NPOMs in the organothiol-capped Au-NP films allowed for control at the molecular level over the selectivity of the sensor film. The dual response mechanism for the alkanethiol-capped Au-NPs detectors produced better discrim-

ination performance for group C vapor responses, but misclassified vapors that contained a mutually similar functionality. In contrast, a R′-SH-containing sensor array was able to discriminate vapors that had a mutually similar chemical functionality. The Ar-SH group classified alcohol vapors better than did the other arrays, whereas the C2Ph(Ar) sensor array classified aprotic polar vapors better than did the other arrays. A sensor array that consisted of 20 different organothiol-capped Au-NPs exhibited a 100 % discrimination between 13 test organic vapors at a partial pressure of P/P° = 0.0100. Maximum classification for an array of organothiol-capped Au-NPs was achieved for an array size of 13 or more sensors.

Chapter 6

Composites of Carboxylate-Capped TiO_2 Nanoparticles and Carbon Black as Chemiresistive Vapor Sensors

6.1 Abstract

Titanium (IV) dioxide (TiO_2) nanoparticles (NPs) with a 1-5 nm diameter were synthesized by a sol-gel method, functionalized with carboxylate ligands, and combined with carbon black (CB) to produce chemiresistive chemical vapor sensor films. The TiO_2 acted as an inorganic support phase for the swellable, organic capping groups of the NPs, and the CB imparted electrical conductivity to the film. Such sensor composite films exhibited a reproducible, reversible change in relative differential resistance upon exposure to a series of organic test vapors. The response of such chemiresistive composites was comparable to, but generally somewhat smaller than, that of organothiol-capped Au-NPs. For a given analyte, the resistance response and signal-to-noise ratio of the capped TiO_2-NP/CB composites varied with the identity of the capping ligand. Hence, an array of TiO_2-NP/CB composites, with each film having a compositionally different carboxylate capping ligand,

Reproduced in part with permission from the *Sens. Actuators B*, In press.

provided good vapor discrimination and quantification when exposed to a series of organic vapors. Principal components analysis of the relative differential resistance response of the sensor array revealed a clear clustering of the response for each analyte tested. This approach expands the options for composite-based chemiresistive vapor sensing, from use of organic monomeric or polymeric sorbent phases, to use of electrically insulating capped inorganic NPs as the nonconductive phase of chemiresistive composite vapor sensors.

6.2 Introduction

Chemiresistive vapor sensors arrays have been prepared from composites of monomeric,[1,2] or polymeric organic phases,[3,4] as well as from metal nanoparticles (NPs) capped with organic ligands.[5–9] Specifically, arrays of metal NPs functionalized with different ligands have attracted significant interest for their ability to detect and discriminate between different analyte vapors.[6,10–12] The ability to synthesize NPs with different functionalities allows the detection of various analytes and produces unique sensor array responses for a large range of different analytes. Pattern recognition algorithms can then be employed to obtain information on the physicochemical properties, and concentration, of the vapor(s) exposed to the sensor array.[13–16]

Sensors composed of organothiol-capped Au-NPs are interesting because they have shown high sensitivity towards certain test vapors,[5] and because such sensors allow for good discrimination between organic vapors.[6,10–12] Given that the Au core of such capped NPs serves as a supporting and conducting phase for the organic ligands that effect the vapor sorption and resulting swelling of the sensor film, it ought to be possible to replace

Carboxylate Ligand	Abbreviation
1-octanoic acid	C8
1-dodecanoic acid	C12
tetracosanoic acid	C24
12-hydroxydodecanoic acid	C12-OH
1-adamantaneacetic acid	C2(2*c*C10)
2-hexyldecanoic acid	C10(C6)
3-methyl-2-phenylvaleric acid	C5(2Ph)(3C)

Table 6.1: TiO_2-NP capping ligands and their respective abbreviations.

the Au core by other chemically-inert inorganic nanoparticle phases, such as titanium (IV) dioxide (TiO_2). TiO_2-NPs must however contain an additional component to provide electrical conductivity through the chemiresistive sensor film, such as a percolative network of carbon black (CB) particles.

Capped TiO_2-NPs have been synthesized previously,[17] with the surface ligation produced by binding carboxylate groups[18–23] to the oxide/hydroxide functionality on the TiO_2-NPs. A wide variety of carboxylated organic ligands groups are readily prepared, thereby facilitating the straightforward preparation of a diverse array of capped groups for TiO_2-NP, or other inorganic oxides (e.g. ZnO), for use in chemiresistive composite vapor detectors.

In this work, we describe the vapor response of an exemplary set of such functionalized, metal oxide based, NP composites, using capped TiO_2-NPs with CB as the electrically conductive phase of the vapor sensors. TiO_2-NPs with a 1-5 nm size range were synthesized by a sol-gel method, and were capped with seven different carboxylate-functionalized ligands (Table 6.1). Composites of these insulating, capped inorganic NP phases, with a percolative CB conductive network phase, were prepared and their performance was measured in a representative series of vapor detection, classification, and quantification tasks.

6.3 Experimental

6.3.1 Materials

The chemicals 2-propanol (anhydrous, 99.5 %), titanium (IV) isopropoxide (99.999 %), nitric acid (99.999 %), 1-octanoic acid (99.5 %), 1-dodecanoic acid (99.5 %), tetracosanoic acid (99 %), 12-hydroxydodecanoic acid (97 %), 1-adamantaneacetic acid (98 %), 2-hexyldecanoic acid (96 %) and 3-methyl-2-phenylvaleric acid (97 %), and the solvents used to generate the test organic vapors (n-hexane, n-heptane, n-octane, iso-octane, cyclohexane, ethanol and ethyl acetate) were obtained from Sigma-Aldrich. All chemicals were used as received. 18 MΩ cm resistivity deionized water was obtained from a Barnstead Nanopure purification system.

6.3.2 TiO_2 Nanoparticle Synthesis and Carboxylation

The TiO_2-NPs were prepared by a procedure reported by Khoudiakov et al.[17] To obtain the TiO_2-NPs, a solution of 0.9 mL of titanium(IV) isopropoxide in 9 mL of anhydrous 2-propanol was added dropwise at a rate of 1 drop min^{-1} to a vigorously stirred solution that contained 100 mL of H_2O and HNO_3 at a pH of 1.3 under N_2(g). The solution was maintained at 1 °C for 24 h after the addition of the titanium(IV) isopropoxide solution. A slightly cloudy solution was obtained when the desired particle sizes (1-5 nm in diameter) had been produced. The TiO_2-NP solution was then centrifuged with a Sorvall RC-5B Refrigerated Superspeed Centrifuge (DuPont) and was washed by subsequent additions of 2-propanol, ethanol and n-hexane.

The TiO_2-NPs were then combined with stoichiometric amounts (mol ratio 1:1) of the desired carboxylate capping ligand in acetone. The resulting solutions were sonicated for 24 h. The different carboxylate-capped TiO_2-NPs were then filtered and redispersed in acetone. Thermogravimmetric analysis of the particles showed that the amount of ligands present on the TiO_2-NPs comprised 4-7 % of the total capped-nanoparticle by mass.

6.3.3 Characterization by TEM and FTIR

i. Transmission Electron Microscopy. Transmission electron microscopy (TEM) was performed using a Philips EM430 (300 KV) with a point-to-point resolution of 2.3 Å. Samples for TEM analysis were prepared by placing a drop of the non-capped TiO_2-NPs suspended and sonicated (1 hr) in 2-propanol (0.5 mg mL^{-1}) onto a Cu TEM grid that had been coated with amorphous carbon. TEM images were obtained two days after the NPs had been initially synthesized.

ii. Fourier Transform Infrared Spectroscopy. KBr-pressed pellets were used to characterize the carboxylate-capped TiO_2-NPs by Fourier transform infrared spectroscopy (FTIR). Spectra were recorded on a Vertex 70 FTIR spectrometer (Bruker Optics Inc., Billerica, MA) that was equipped with a liquid N_2-cooled HgCdTe detector (InfraRed Associates Inc.). The spectral resolution was 4 cm^{-1} and 64 scans were collected per spectrum. A KBr background spectrum was subtracted from the measured spectrum of the NPs to provide the desired FTIR characterization data.

6.3.4 Sensor Fabrication

The capped NP solutions were cast with 50 % CB by mass in acetone, followed by sonication for 2 h. These solutions were sprayed on substrates using an airbrush. The substrates were 0.5 cm $\times$ 2.5 cm glass slides that had a 2 mm gap between the electrical contact regions. The metalized contact regions were formed by evaporation, through a contact mask, of 35 nm of Cr followed by 65 nm of Au. All chemiresistive sensors were dried under vacuum for 30 min. The sensor films were then conditioned by exposure to analytes for 24 h to reach a steady resistance or frequency baseline, and a reproducible steady sensor response, prior to the data collection reported herein.

6.3.5 Sensing Measurements

Typically, 4 nominally identical vapor sensors were prepared at a time. The sensors were loaded into a rectangular, 40-slot chamber, with sensor film replicates positioned randomly. No dependence was observed on the performance of a given sensor on the spatial position of the sensors in the array. The 45.5 $\times$ 3.0 $\times$ 1.5 cm ($w \times l \times d$) chamber was connected by Teflon tubing to the gas delivery system. The internal cross-sectional area of the chamber was 1 cm^2. The dc resistance of the sensor array was measured with a digital multimeter (Keithley Model 2002) that was connected to a multiplexing unit (Keithley M4odel 7001). The resistance data were collected every 5-7 s from the array. A computer-controlled (LabVIEW) flow system delivered pulses of analyte vapor at a given fraction of the analytes vapor pressure. Oil-free air was obtained from the house compressed air source (1.10 ± 0.15 ppth of water vapor) and was controlled with a mass flow controller. The test

analytes used were n-hexane (Hex), n-heptane (Hept), n-octane (Oct), iso-octane (iOct), cyclohexane (cHex), ethyl acetate (EtOAc), and ethanol (EtOH). The sensor response as a function of vapor concentration was studied over the concentration range that corresponded to $0.0010 \leq P/P^{\circ} \leq 0.0500$, where P and P° are the partial pressure and vapor pressure of the analyte at room temperature (22 °C), respectively. Each analyte presentation consisted of 70 s of air, followed by 80 s of analyte vapor, followed by 60 s of air to purge the system. The total flow rate for each analyte presentation was 5 L min^{-1}.

The sensor response was expressed as the maximum relative differential resistance change ($\Delta R_{max}/R_b$), where R_b is the baseline resistance of the sensor in the absence of analyte, and ΔR_{max} is the average of five maximum resistance data points measured at the end of each analyte exposure response. During the pre-exposure period, a correcting spline was used to fit the baseline drift.[5] The values of $\Delta R_{max}/R_b$ were calculated by subtracting the values of the spline extrapolated over the time of the exposure from the observed resistance.

6.3.6 Principal Components Analysis

Differences in the sensor response data were visualized using Principal Components Analysis (PCA).The normalized data were mean-centered, and diagonalization of the covariance matrix of the data set provided a transformed set of dimensions that best described the data in terms of principal components (PCs). The 1st PC captured the largest amount of variance in the data; the 2nd PC captured the second most variance in the data (subject to being orthogonal to the 1st PC), etc. The mean-centered data were then projected onto the

first and second PCs, and the data were plotted with respect to these coordinate vectors to observe the natural clustering of the data points. The eigenvalues of the mean-centered covariance matrix provided the relative amounts of variance in each of the corresponding eigenvectors, allowing quantification of the amount of the variance that was captured in the 2-dimensional PC space.

6.4 Results

6.4.1 Characterization

i. Transmission Electron Microscopy. Figure 6.1 shows a TEM micrograph of the TiO_2-NPs, revealing particles having diameters between 1-5 nm. A consistent slow addition of the Ti complex was required to produce particles that had such small diameters. Particles with a larger diameter ($>$ 10 nm) were obtained if large aggregates formed in the acidic solution after the addition of the metal precursor. Such particles were not used for the fabrication of chemiresistive vapor sensors that were evaluated in this work.

ii. Fourier Transform Infrared Spectroscopy. Figure 6.2 shows the FTIR absorption spectra of three different carboxylate-capped TiO_2-NPs. When a carbonyl stretch was observed at $\sim$ 1710 cm^{-1}, due to the presence of physisorbed carboxylic acid, the capped NPs were re-filtered. The asymmetric and symmetric bound carboxylate group vibrations at $\sim$ 1530 cm^{-1} and $\sim$ 1420 cm^{-1} were observed for C12, C12-OH and C5(2Ph)(3C)-capped NPs. The vibration of the C5(2Ph)(3C) ligand overlapped the scissoring frequency of-CH2- at $\sim$ 1460 cm-1, and consequently the band was broadened. The observed C=O stretching

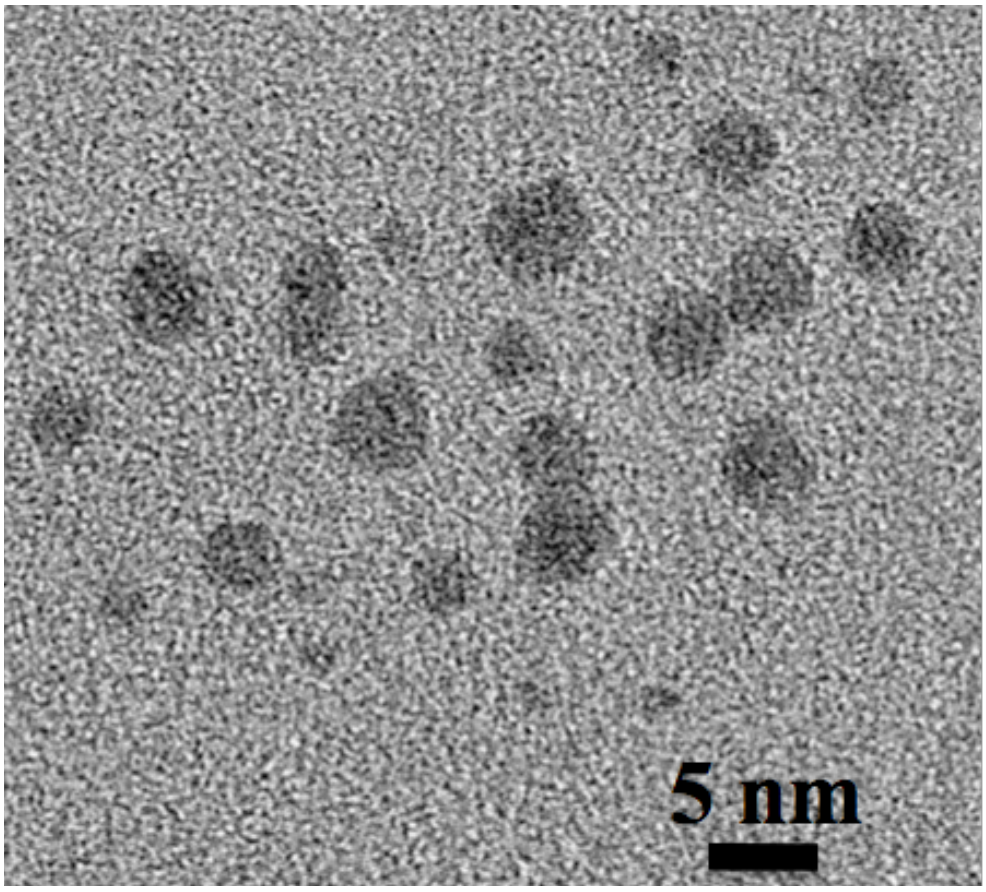

Figure 6.1: Transmission electron micrograph of TiO_2-NPs on a Cu grid. The NPs were dispersed in 2-propanol (0.5 mg mL^{-1}).

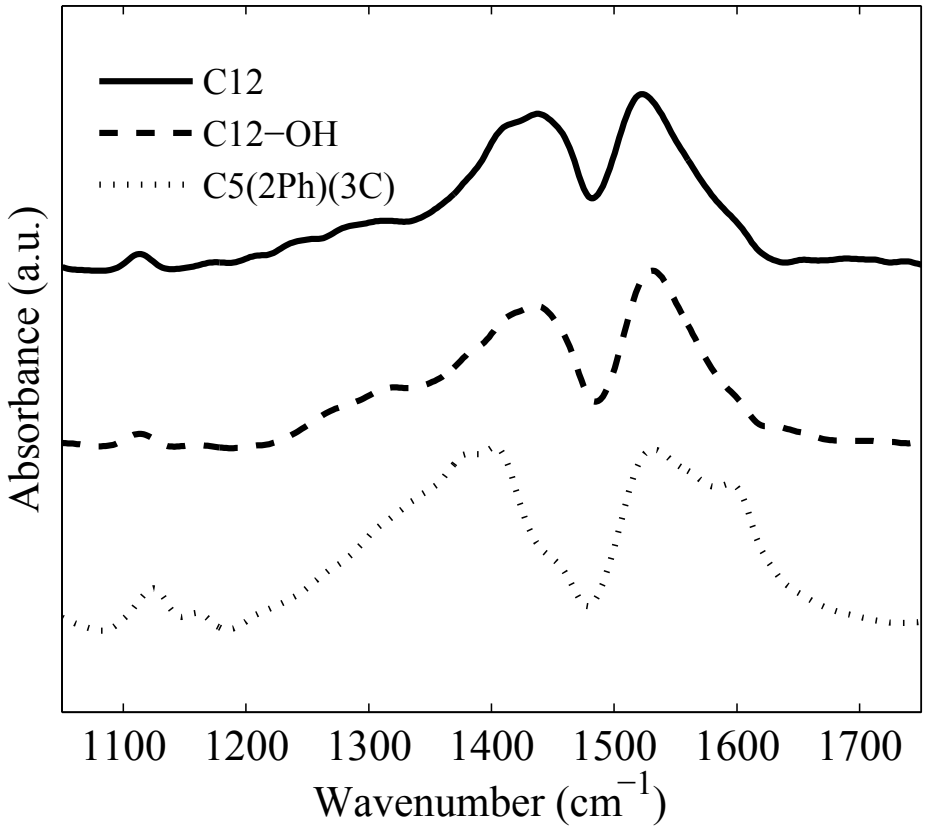

Figure 6.2: FTIR spectra of carboxylate-capped TiO_2-NP on a KBr pellet at a resolution of 4 cm^{-1}, with KBr as the background.

frequency suggests a bidendate (chelate) structure.[24] The C5(2Ph)(3C) spectrum also displayed an aromatic C=C stretch at $\sim$ 1600 cm^{-1}.

6.4.2 Sensor Response

Different CB loadings were tested (25, 50, and 75 % CB by mass), and composites having 50 % CB yielded the highest signal-to-noise ratio (SNR). Figure 6.3 shows the response of several sensors upon exposure to Hex and EtOAc at P/P° = 0.0050. All of the sensors showed rapid, reversible responses to each analyte vapor tested. Figure 6.4 displays the average values of $\Delta R_{max}/R_b$ obtained from 200 exposures to each analyte. The responses of

two well studied CB-based polymer composites, poly(ethylene-co-vinyl acetate) (PEVA) and poly(ethylene oxide) (PEO), are presented for comparison.[25,26] Each sensor responded differently to each of the test vapors. For the hydrocarbons, among the TiO_2-NP/CB composites, the highest $\Delta R_{max}/R_b$ values were obtained for the C5(2Ph)(3C) sensor. For all of the vapors, C24 showed the lowest $\Delta R_{max}/R_b$ values. For the TiO_2-NP/CB composites, the $\Delta R_{max}/R_b$ values obtained upon exposure to EtOH were very similar to each other. The reference PEVA/CB sensor produced $\Delta R_{max}/R_b$ values that were higher than those of the TiO_2-NP/CB sensors, however the $\Delta R_{max}/R_b$ values obtained from a PEO/CB sensors were generally comparable to those obtained from the TiO_2-NP/CB composites.

Figure 6.5 shows the $\Delta R_{max}/R_b$ response as a function of analyte concentration over the range $0.0010 \leq P/P^\circ \leq 0.0500$ for Hex and for EtOH. For Hex, the highest $\Delta R_{max}/R_b$ values were obtained for the C2(2cC10) sensor, whereas C12-OH produced the lowest $\Delta R_{max}/R_b$ values. However, the slope for the four sensors displayed was approximately the same, specifically for $0.0100 \leq P/P^\circ \leq 0.0500$. For EtOH, C12-OH produced the highest $\Delta R_{max}/R_b$ values, whereas C12 produced the lowest $\Delta R_{max}/R_b$ values. The slopes at $0.0010 \leq P/P^\circ \leq 0.0500$ were different among the different sensors.

6.4.3 Principal Component Analysis

Figure 6.6 shows the PCA projection of the 1st and 2nd PCs of the sum-normalized data. The PCA projection showed clear separation between cHex, EtOAc, EtOH and the saturated alkane vapors. The left inset depicts the alkane region of Figure 6.6, and displays the overlap of the alkane vapors. The iOct cluster interfered with the other three solvents, and

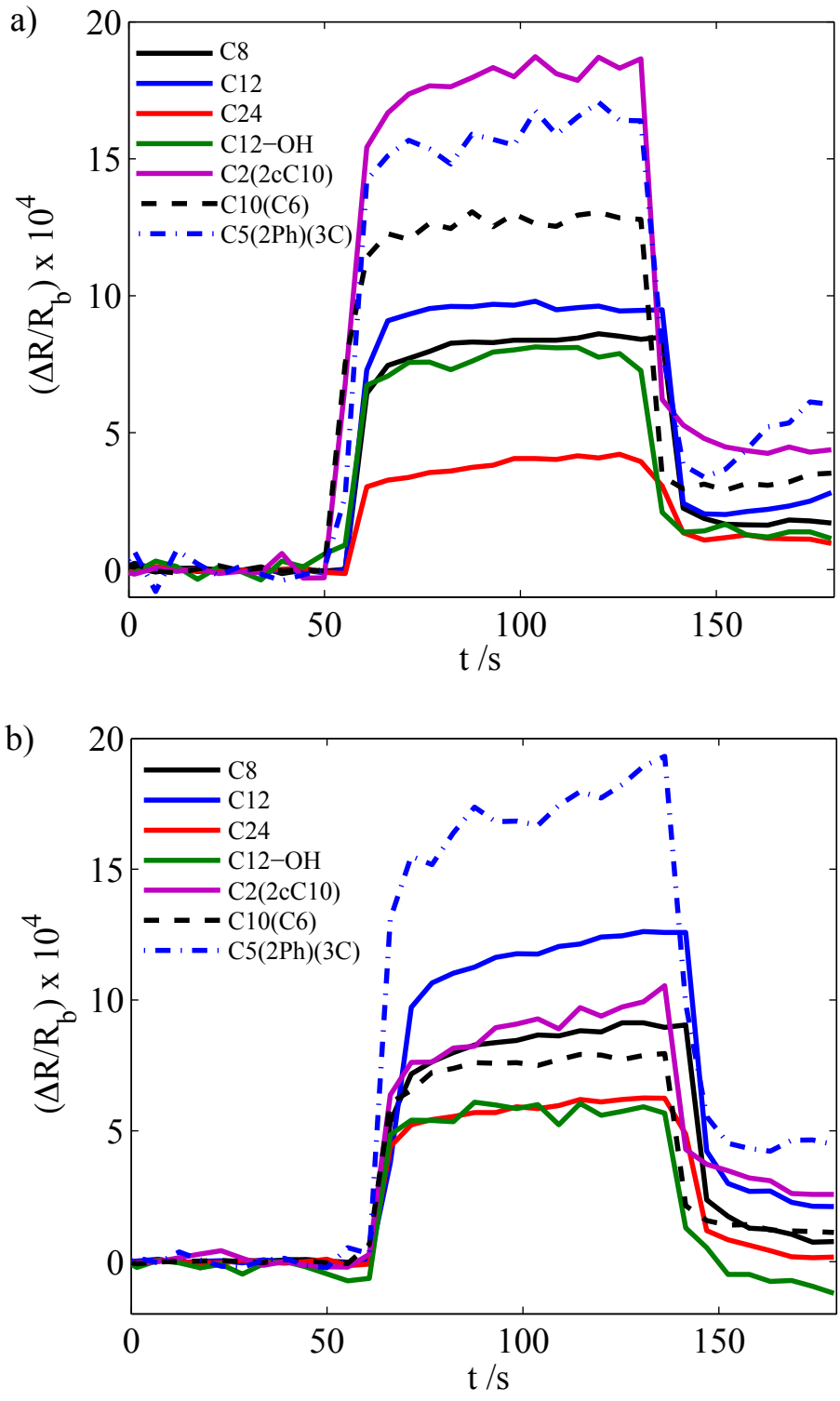

Figure 6.3: Relative differential resistance response, $\Delta R/R_b$, for the seven carboxylate-capped TiO_2-NP/CB composites; (a) response to n-hexane at P/P° = 0.0050; (b) response to ethyl acetate at P/P° = 0.0050.

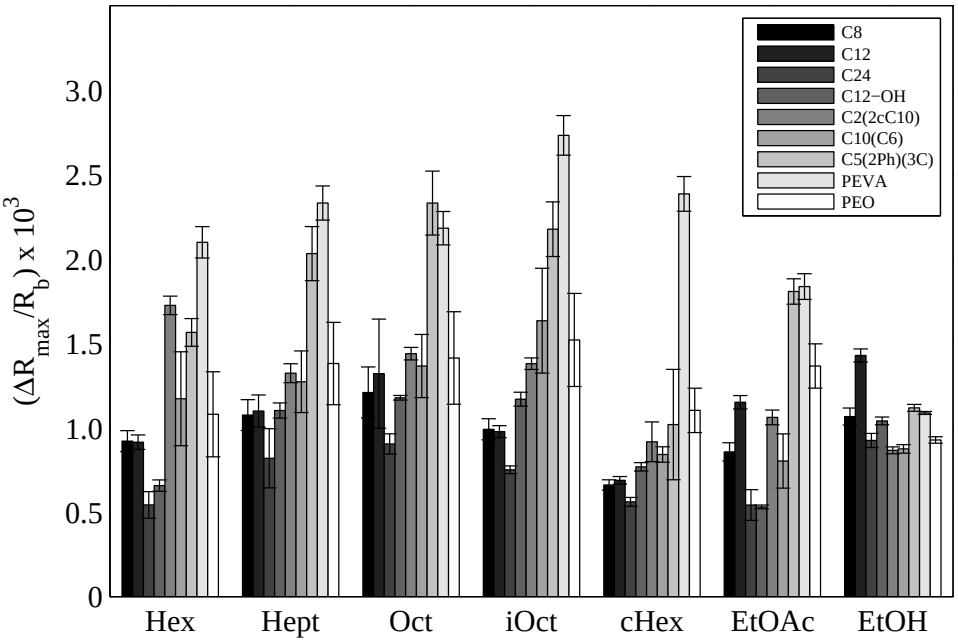

Figure 6.4: Maximum relative differential resistance, $\Delta R_{max}/R_b$, for all carboxylate-capped TiO_2-NP/CB sensors at P/P° = 0.0050. The values for PEVA/CB and PEO/CB are presented for comparison.

prevented good separation. The right inset of Figure 6.6 shows a fairly good separation between the tested analytes Hex, Hept and Oct, after removing the projection of the iOct cluster.

6.5 Discussion

6.5.1 Sensor Response

The interparticle spacing, and thus the sensitivity, of the sensor films can be controlled at the molecular level using capping ligands with different lengths, structure and functionalities. The magnitude of the $\Delta R_{max}/R_b$ values for the carboxylate-capped TiO_2-NP/CB composites was somewhat smaller than the $\Delta R_{max}/R_b$ values of other chemiresistive CB

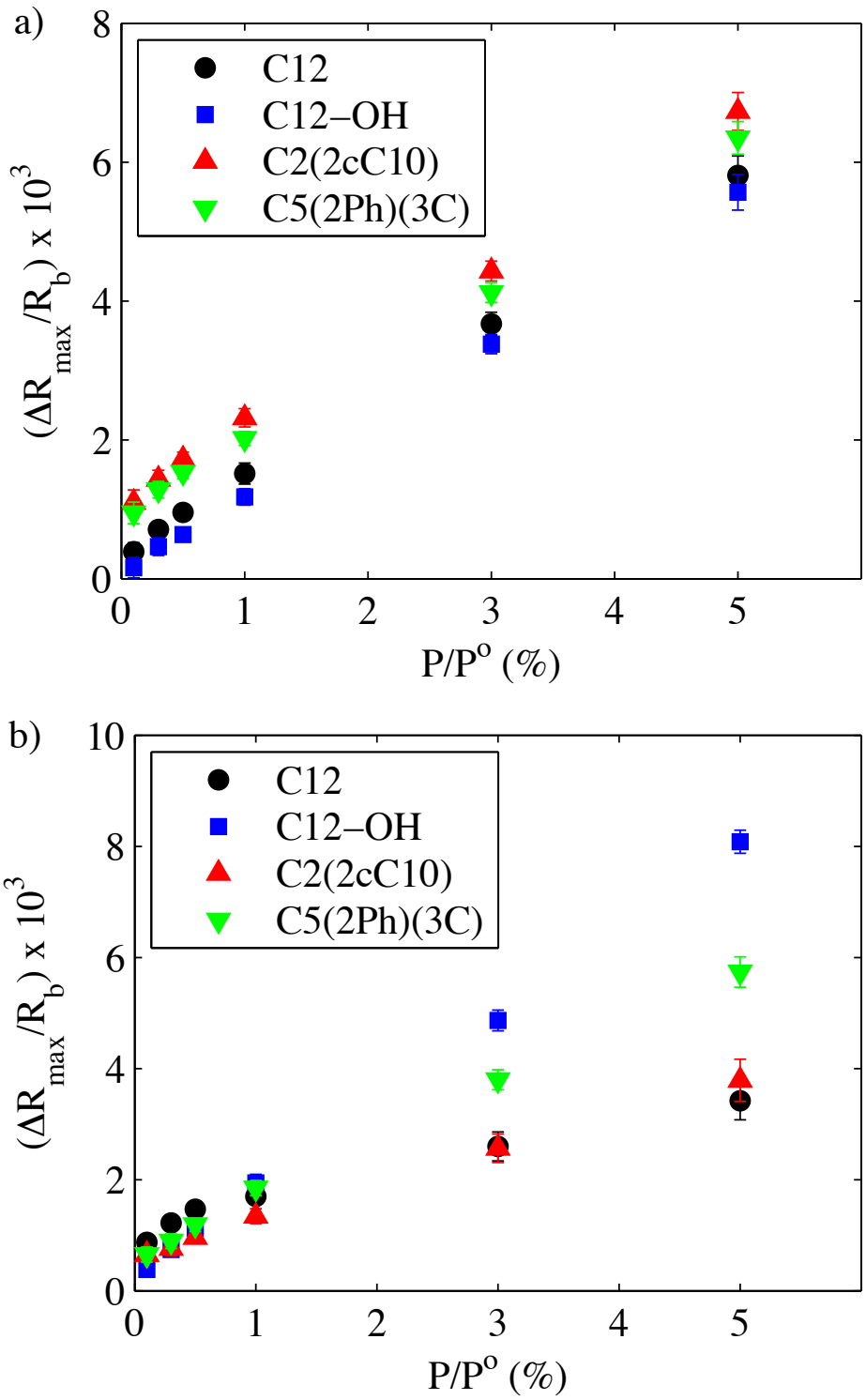

Figure 6.5: Maximum differential resistance change as a function of P/P° ($0.0010 \leq P/P^\circ \leq 0.0500$) for four different carboxylate-capped TiO_2-NP/CB chemiresistors upon exposure to a) hexane and b) ethanol.

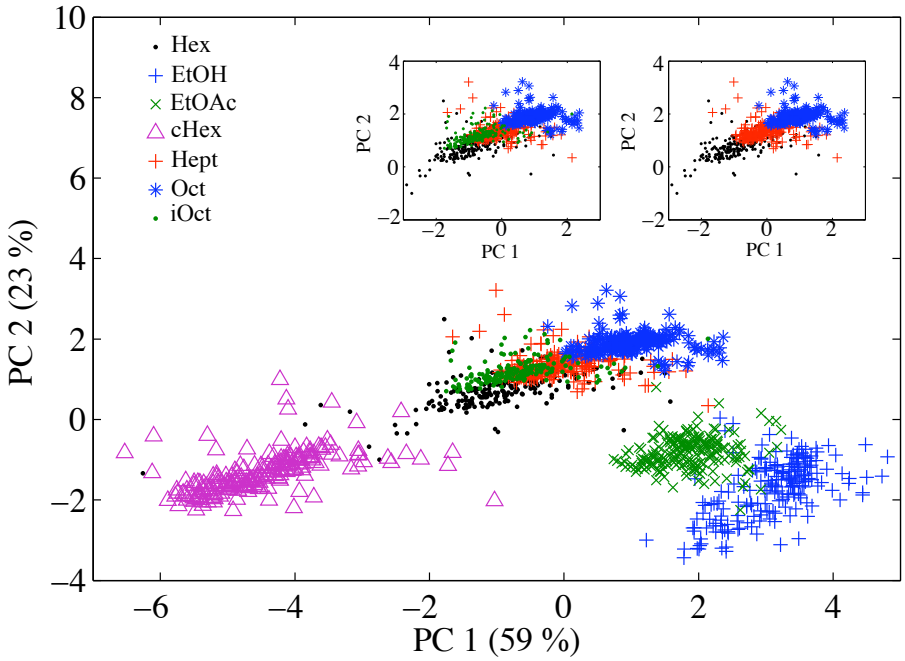

Figure 6.6: Principal components analysis projection of an array of the carboxylate-capped TiO_2-NP/CB chemiresistors upon exposure to seven analytes, each presented to P/P° = 0.0050. The left figure inset displays the PC projection of Hex, Hept, Oct and iOct, and the right figure inset displays the PC projection of Hex, Hept and Oct.

	Hex	Hept	Oct	*i*Oct	*c*Hex	EtOAc	EtOH
C8	93	130	190	99	34	230	86
C12	99	150	190	120	25	250	110
C24	65	89	140	48	18	200	76
C12-OH	88	110	130	120	47	120	120
C2(2cC10)	170	200	260	210	89	130	110
C10(C6)	130	200	220	190	66	120	83
C5(2Ph)(3C)	180	250	270	260	47	150	130

Table 6.2: Signal to noise ratios (SNR) of seven carboxylate-capped TiO_2-NP/CB composites in response to seven analytes over 200 exposures delivered in random order at P/P° = 0.0050.

composite sensors, such as CB composites with insulating polymers,[3] monomers,[1] or thiol-capped Au-NPs.[5] The small $\Delta R_{max}/R_b$ magnitude for the capped TiO_2-NP/CB composites is likely due to the lower surface ligand coverage of the NPs, which resulted in a lower mass of analyte sorbed into the sensing films. Consequently, the SNR values (SNR = $\Delta R_{max}/s_{baseline}$, $s_{baseline}$ is the standard deviation of R_b) obtained were lower than those observed for other chemiresistive sensing materials in response to the same set of test analytes (Table 6.2).[1,2]

The responses of sensors C8 and C12 were also larger, in general, than those of sensors that were made using C24 ligand caps. The C24 ligand has a low solubility, which prevents vapor analyte molecules from partitioning and separating C24-capped TiO_2-NPs. The hydroxy termination of the C12-OH film produced a higher sensitivity towards ethanol than was observed for the C12, C2(2*c*C10) and C5(2Ph)(3C) sensors. For P/P° = 0.0050, the C5(2Ph)(3C)-capped TiO_2-NP composite was the most sensitive material for the all vapors (Figure 6.4), and produced the highest SNR values (Table 6.2).

A percolative network of CB particles had to be incorporated into the sensing films to produce the required dc electrical conduction needed, for a chemiresistive sensor. For carboxylate-capped TiO_2-NP/CB composites, limited information could be obtained on the

mechanism of vapor-induced volume change that resulted from each of the film components. Both film components, the TiO_2-NPs and the CB particles, are able to sorb analyte and thus contribute to the overall observed film resistance change. Another limitation is that if TiO_2-NPs are functionalized with a specific chemistry, the effects on vapor sorption of such functionality will be reduced by the presence of CB, because only ~ 5 % by mass of the capped NP film contained the desired functional group.

6.5.2 Discrimination Performance

The PC projections for the first and second PCs (Figure 6.6) show that the TiO_2-NP sensor array was clearly able to separate the polar and nonpolar analytes. Both PCs differentiated analytes based on their polarity. Particularly for the alkanes, overlaps between the response clusters for Hex, and Hept and Oct were observed. Furthermore, the iOct cluster slightly overlapped with that of Hex, whereas high overlap was observed between the Hept and iOct clusters. The latter is a consequence of the similar vapor pressures of these two analytes ($P^{\circ}_{\text{Hept}} = 5.1 \times 10^4$ ppm, $P^{\circ}_{i\text{Oct}} = 5.6 \times 10^4$ ppm).

6.6 Conclusions

TiO_2 NPs capped by seven different carboxylate-functionalized ligands having variable chain lengths and polarities were synthesized by a sol-gel method, characterized by TEM and FTIR, and investigated as chemical vapor sensors. The capped NPs were mixed with CB and exposed to seven different analytes of varying polarity. The sensing materials responded uniquely to each analyte and responded in an approximately linear dependence

with vapor concentration for Hex and EtOH. The SNR value of each TiO_2 NP sensor varied with the ligand functionality for every analyte. PCA showed a fair clustering of the analytes tested, with the alkanes being the most difficult analytes to separate.

Bibliography

[1] Gao, T.; Woodka, M. D.; Brunschwig, B. S.; Lewis, N. S. *Chem. Mater.* **2006**, *18*(22), 5193–5202.

[2] Maldonado, S.; Garcia-Berrios, E.; Woodka, M. D.; Brunschwig, B. S.; Lewis, N. S. *Sens. Actuators B* **2008**, *134*(2), 521–531.

[3] Severin, E.; Doleman, B.; Lewis, N. *Anal. Chem.* **2000**, *72*(4), 658–668.

[4] Severin, E. J.; Lewis, N. S. *Anal. Chem.* **2000**, *72*(9), 2008–2015.

[5] Garcia-Berrios, E.; Gao, T.; Maldonado, S.; Woodka, M. D.; Ellsworth, M. W.; Brunschwig, B. S.; Lewis, N. S. *J. Phys. Chem. C* **2010**, *114*, 21914–21920.

[6] Garcia-Berrios, E.; Gao, T.; Theriot, J. C.; Brunschwig, B. S.; Lewis, N. S. *J. Phys. Chem. C* **2011**, *115*, 6208–6217.

[7] Grate, J. W.; Nelson, D. A.; Skaggs, R. *Anal. Chem.* **2003**, *75*(8), 1868–1879.

[8] Wohltjen, H.; Snow, A. W. *Anal. Chem.* **1998**, *70*(14), 2856–2859.

[9] Wuelfing, W. P.; Green, S. J.; Pietron, J. J.; Cliffel, D. E.; Murray, R. W. *J. Am. Chem. Soc.* **2000**, *122*, 11465–11472.

[10] Han, L.; Shi, X. J.; Wu, W.; Kirk, F. L.; Luo, J.; Wang, L. Y.; Mott, D.; Cousineau, L.; Lim, S. I. I.; Lu, S.; Zhong, C. J. *Sens. Actuators B* **2005**, *106*(1), 431–441.

[11] Wang, L. Y.; Kariuki, N. N.; Schadt, M.; Mott, D.; Luo, J.; Zhong, C. J.; Shi, X. J.; Zhang, C.; Hao, W. B.; Lu, S.; Kim, N.; Wang, J. Q. *Sensors* **2006**, *6*(6), 667–679.

[12] Wang, L. Y.; Shi, X. J.; Kariuki, N. N.; Schadt, M.; Wang, G. R.; Rendeng, Q.; Choi, J.; Luo, J.; Lu, S.; Zhong, C. J. *J. Am. Chem. Soc.* **2007**, *129*(7), 2161–2170.

[13] Burns, J.; Whitesides, G. *Chem. Rev.* **1993**, *93*(8), 2583–2601.

[14] Duda, R.; Hart, P. *Pattern Classification and Scene Analysis;* John Wiley Sons: New York, 1973.

[15] Geladi, P.; Kowalski, B. R. *Anal. Chim. Acta* **1986**, *185*, 1–17.

[16] Kowalski, B.; Bender, C. *Anal. Chem.* **1972**, *44*(8), 1405.

[17] Khoudiakov, M.; Parise, A. R.; Brunschwig, B. S. *J. Am. Chem. Soc.* **2003**, *125*(15), 4637–4642.

[18] Hug, S. J.; Sulzberger, B. *Langmuir* **1994**, *10*(10), 3587–3597.

[19] Kilsa, K.; Mayo, E. I.; Brunschwig, B. S.; Gray, H. B.; Lewis, N. S.; Winkler, J. R. *J. Phys. Chem. B* **2004**, *108*(40), 15640–15651.

[20] Weng, Y. X.; Li, L.; Liu, Y.; Wang, L.; Yang, G. Z. *J. Phys. Chem. B* **2003**, *107*(18), 4356–4363.

[21] Xagas, A. P.; Bernard, M. C.; Hugot-Le Goff, A.; Spyrellis, N.; Loizos, Z.; Falaras, P. *J. Photochem. Photobiol. A* **2000**, *132*(1-2), 115–120.

[22] Jeon, H. J.; Moon, S. D.; Kang, Y. S. *Colloid Surf. A* **2005**, *257-58*, 165–169.

[23] Wu, X.; Wang, D.; Yang, S. *J. Colloid Interface Sci.* **2000**, *222*, 37–40.

[24] Nakamoto, K. *Infrared and Raman Spectra of Inorganic and Coordination Compounds;* John Wiley Sons, Inc.: New York, 5th ed., 1997.

[25] Freund, M. S.; Lewis, N. S. *Proc. Natl. Acad. Sci. U.S.A.* **1995**, *92*(7), 2652–2656.

[26] Lonergan, M. C.; Severin, E. J.; Doleman, B. J.; Beaber, S. A.; Grubb, R. H.; Lewis, N. S. *Chem. Mater.* **1996**, *8*(9), 2298–2312.